

Furazan bis-ureas: a heterocyclic scaffold for anion binding and transport

William G. Ryder,^{a,b} Emilie G. Wu,^a Lijun Chen,^c Mohamed Fares,^{a,d} Daniel A. McNaughton,^{a,b} Karen Tran,^a Chengzhong Yu,^c and Philip A. Gale*^{a,b}

Table of Contents

General methods and materials	S1
Synthesis.....	S1
Characterisation data.....	S6
X-Ray crystallography	S24
¹ H NMR titration experiments.....	S27
Sample preparation.....	S27
Titration procedure.....	S27
Titration data fitting	S27
Transport studies.....	S41
General remarks and vesicle preparation	S41
ISE-based studies	S41
Fluorescence HPTS-based studies.....	S46
NMDG-Cl assay	S47
Cell culture	S52
MTT cell viability assay.....	S52
2D-NOESY ¹ H NMR Spectroscopic Analysis	S56
References	S62

^a School of Chemistry, The University of Sydney, Sydney, NSW, 2006, Australia.

^b School of Mathematical and Physical Sciences, Faculty of Science, University of Technology Sydney, Ultimo, NSW 2007, Australia.

^c Australian Institute for Bioengineering and Nanotechnology, The University of Queensland, Brisbane, QLD, 4072 Australia

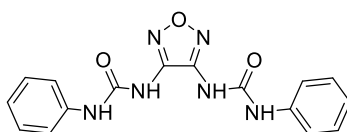
^d School of Pharmacy, The University of Sydney, Sydney, NSW 2006, Australia

General methods and materials

All chemicals and solvents were of reagent grade (>95%) and purchased from commercial supplies without further purification, unless otherwise noted. Deuterated solvents were purchased from Cambridge Isotope Laboratories and 1-Palmitoyl-2-oleoyl-sn-glycero-3-phosphocholine (POPC) was purchased from Corden Pharma. Anhydrous THF, CH₃CN, MeOH, and CH₂Cl₂ were collected from an Inert Corp PureSolv MD7 solvent purification system and deionised water was collected from a Merck Millipore Milli-Q™ reference ultrapure water purification system. Reactions were magnetically stirred and monitored *via* TLC using Merck aluminium silica gel 60 plates coated with fluorescent indicator F254 (60F-254), using short and long wave UV light, ninhydrin or potassium permanganate and heat as developing agents. ¹H and ¹³C NMR spectra were obtained at 300 K on a Bruker DRX 300, Bruker DPX 400, or Bruker AVANCE III 500 spectrometers equipped with a 5 mm BBFO probe with z-gradients. Chemical shifts are expressed as parts per million (ppm) and are referenced to solvent residual signals. The data are reported as chemical shift, multiplicity (br = broad, s = singlet, d = doublet, t = triplet, m = multiplet), coupling constant J in Hz and relative integral. Low resolution electrospray ionisation (ESI, positive or negative as indicated) and were performed on a Bruker AmaZon SL ion trap mass spectrometer. High resolution ESI and APCI mass spectrometry (HR-MS) were performed on a Bruker Solarix 2XR Fourier Transform Ion Cyclotron Resonance Mass Spectrometer with a 7.0 T magnet, fitted with an off-axis Analytic electrospray source with a quadrupole mass analyser, and are reported as m/z (relative intensity). The ISE assay experiments were conducted on the Fisherbrand™ Accumet™ Chloride Combination Electrode, and fluorescence-based transport data was recorded on an Agilent Cary Eclipse Fluorescence Spectrophotometer, equipped with a temperature-controlled multicell holder with temperature control enabled (25 °C).

Synthesis

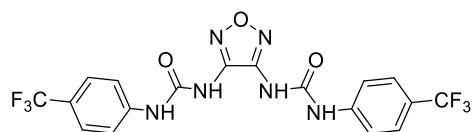
1,1'-(1,2,5-oxadiazole-3,4-diyl)bis(3-phenylurea) (1)



Diaminofurazan (100 mg, 100.08 mmol) was added to dry CH₃CN (10 mL) and stirred for 10 mins, phenyl isocyanate (0.33 mL, 3 mmol) was added dropwise, and the mixture was stirred vigorously at reflux for 17 h. The white precipitate was collected *via* vacuum filtration, washed with hexane (10 mL) and purified *via* flash chromatography (10 → 30% ethyl acetate in hexane) to afford the title compound as an amorphous white solid (250 mg, 0.74 mmol, 74%).

¹H NMR (500 MHz, DMSO-*d*₆) δ 9.40 (2 H, s), 9.24 (2 H, s), 7.51 – 7.45 (4 H, m), 7.35 – 7.27 (4 H, m), 7.07 – 7.00 (2 H, m); ¹³C NMR (126 MHz, DMSO-*d*₆) δ 151.1, 146.5, 138.5, 128.7, 122.7, 118.9; **LR-MS** (ESI⁻, *m/z*) 337.06 [M-H]⁻; **HR-MS** (ESI⁻, *m/z*) calcd for C₁₆H₁₃N₆O [M-H]⁻ 337.10546, found 337.10513

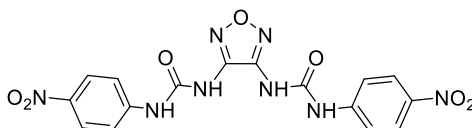
1,1'-(1,2,5-oxadiazole-3,4-diyl)bis(3-(4-(trifluoromethyl)phenyl)urea) (2)



Diaminofurazan (100 mg, 1 mmol) was added to dry CH₃CN (10 mL) and stirred for 10 mins, 4-(trifluoromethyl)phenyl isocyanate (0.43 mL, 3 mmol) was added dropwise, and the mixture was stirred vigorously at reflux for 17 h. The colourless solution was evaporated to dryness and purified *via* flash chromatography (10 → 80% ethyl acetate in hexane) to afford the title compound as an amorphous white solid (232 mg, 0.49 mmol, 49%).

¹H NMR (500 MHz, DMSO-*d*₆) δ 9.80 (2 H, s), 9.40 (2 H, s), 7.67 (8 H, t, *J* 6.4); ¹³C NMR (126 MHz, DMSO-*d*₆) δ 151.3, 146.7, 142.6, 126.2, 125.8, 122.8, 118.7; ¹⁹F NMR (471 MHz, DMSO-*d*₆) δ -60.26; LR-MS (ESI⁻, *m/z*) 473.05 [M-H]⁻; HR-MS (ESI⁻, *m/z*) calcd for C₁₈H₁₁F₆N₆O₃ [M-H]⁻ 473.08023, found 473.08002.

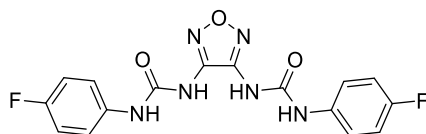
1,1'-(1,2,5-oxadiazole-3,4-diyl)bis(3-(4-nitrophenyl)urea) (3)



Diaminofurazan (100 mg, 1 mmol) was added to dry CH₃CN (10 mL) and stirred for 10 mins, 4-nitrophenyl isocyanate (492 mg, 3 mmol) was added dropwise, and the mixture was stirred vigorously at reflux for 17 h. The colourless solution was evaporated to dryness and recrystallised in DMF/water to afford the title compound as an amorphous pale-yellow solid (291 mg, 0.68 mmol, 68%).

¹H NMR (500 MHz, DMSO-*d*₆) δ 10.08 (2 H, s), 9.53 (2 H, s), 8.21 (4 H, d, *J* 8.7), 7.72 (4 H, d, *J* 8.8); ¹³C NMR (126 MHz, DMSO-*d*₆) δ 151.6, 151.1, 146.5, 145.6, 145.3, 141.8, 141.5, 125.1, 125.0, 118.3, 118.0; LR-MS (ESI⁻, *m/z*) 415.09 [M-H]⁻; HR-MS (ESI⁺, *m/z*) calcd for C₁₆H₁₂N₈NaO₇ [M+Na]⁺ 451.07212, found 451.07207.

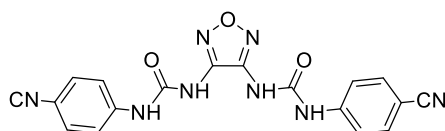
1,1'-(1,2,5-oxadiazole-3,4-diyl)bis(3-(4-fluorophenyl)urea) (4)



Diaminofurazan (100 mg, 1 mmol) was added to dry CH₃CN (10 mL) and stirred for 10 min. 4-fluorophenyl isocyanate (0.58 mL, 3 mmol) was added dropwise and the mixture was stirred vigorously at reflux for 17 h. The white precipitate was collected *via* filtration, washed with hexane (10 mL) and purified *via* flash chromatography (10 → 80% ethyl acetate in hexane) to afford the title compound as an amorphous white solid (281 mg, 0.75 mmol, 75%).

¹H NMR (500 MHz, DMSO-*d*₆) δ 9.42 (2 H, s), 9.30 (2 H, s), 7.54–7.42 (4 H, m), 7.14 (4 H, td, *J* 8.8, 1.4); ¹³C NMR (126 MHz, DMSO-*d*₆) δ 159.1, 157.2, 151.6, 146.8, 135.2, 121.2, 115.6; ¹⁹F NMR (471 MHz, DMSO-*d*₆) δ -120.46; LR-MS (ESI⁻, *m/z*) 373.02 [M-H]⁻; HR-MS (ESI⁻, *m/z*) calcd for C₁₆H₁₂F₆N₆O₃ [M-H]⁻ 373.08662, found 373.08631.

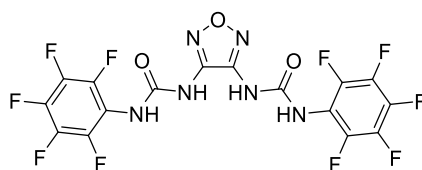
1,1'-(1,2,5-oxadiazole-3,4-diyl)bis(3-(4-cyanophenyl)urea) (5)



Diaminofurazan (100 mg, 1 mmol) was added to dry CH₃CN (10 mL) and stirred for 10 mins, 4-cyanophenyl isocyanate (432 mg, 3 mmol) was added dropwise, and the mixture was stirred vigorously at reflux for 17 h. The white precipitate was collected *via* vacuum filtration, washed with diethyl ether (20 mL) and sonicated in MeOH (50 mL) to afford the title compound as an amorphous white solid (295 mg, 0.76 mmol, 76%).

¹H NMR (500 MHz, DMSO-*d*₆) δ 9.87 (1 H, s), 9.45 (1 H, s), 7.79–7.73 (2 H, m), 7.66 (2 H, d, *J* 8.8); ¹³C NMR (126 MHz, DMSO-*d*₆) δ 151.1, 146.6, 143.2, 133.3, 119.1, 118.8, 104.4; LR-MS (ESI⁻, *m/z*) 387.12 [M-H]⁻; HR-MS (ESI⁻, *m/z*) calcd for C₁₈H₁₁N₈O₃ [M-H]⁻ 387.09596, found 387.09590.

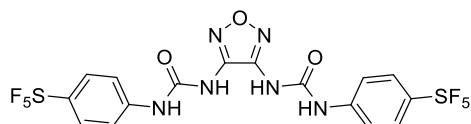
1,1'-(1,2,5-oxadiazole-3,4-diyl)bis(3-(perfluorophenyl)urea) (6)



Diaminofurazan (100 mg, 1 mmol) was added to dry CH₃CN (10 mL) and stirred for 10 mins, 2,3,4,5,6-pentafluorophenyl isocyanate (0.39 mL, 3 mmol) was then added dropwise and the mixture was stirred vigorously at reflux for 17 h. The white precipitate was collected *via* vacuum filtration, washed with hexane (10 mL), and purified *via* flash chromatography (10 → 80% ethyl acetate in hexane) and subsequently afford the title compound as an amorphous white solid (104 mg, 0.20 mmol, 20%).

¹H NMR (500 MHz, DMSO-*d*₆) δ 9.54 (4 H, s); ¹³C NMR (126 MHz, DMSO-*d*₆) δ 151.8, 146.9, 144.6, 142.6, 138.6, 136.7, 113.7; ¹⁹F NMR (471 MHz, DMSO-*d*₆) δ -61.71; LR-MS (ESI⁻, *m/z*) *m/z* 517.03 [M-H]⁻; HR-MS (ESI⁻, *m/z*) calcd for C₁₆H₁₃F₁₀N₆O₃ [M-H]⁻ 517.01124, found 517.01082

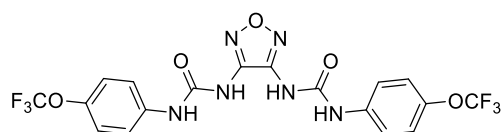
1,1'-(1,2,5-oxadiazole-3,4-diyl)bis(3-(4-(pentafluoro-*l*6-sulfanyl)phenyl)urea) (7)



Triphosgene (406, 1.37 mmol) was added slowly to a solution of 4-pentafluorosulfonyl aniline (439 mg, 2 mmol) in dry toluene (6 mL). Triethylamine (0.19 mL, 1.37 mmol) was immediately added, and the mixture was stirred at 70°C for 2 h. Pentane (1 mL) was added in one portion and the solution was filtered and concentrated under reduced pressure. Separately, diaminofurazan (91 mg, 0.91 mmol) was dissolved in a solution of dry CH₃CN (10 mL) and pyridine (0.5 mL) which was added in one portion to the isocyanate. The mixture was stirred vigorously at reflux for 18 h, concentrated under reduced pressure, and purified *via* flash chromatography (30 → 75% ethyl acetate in hexane) to afford the title compound as an amorphous ochre solid (313 mg, 0.531 mmol, 53%).

¹H NMR (500 MHz, DMSO-*d*₆) δ 9.87 (2 H, s), 9.42 (2 H, s), 7.86 – 7.80 (4 H, m), 7.67 (4 H, d, *J* 8.9); ¹³C NMR (126 MHz, DMSO-*d*₆) δ 151.2, 146.8 (m), 146.6, 142.2, 126.8 (m), 118.4; LR-MS (ESI⁺, *m/z*) 613.05 [M+H]⁺; HR-MS (ESI⁺, *m/z*) calcd for C₁₆H₁₂F₁₀N₆NaO₃S₂ [M+H]⁺ 613.01448, found 613.01372.

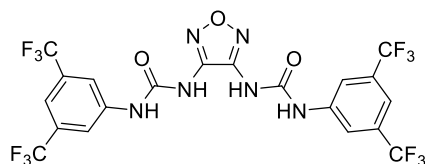
1,1'-(1,2,5-oxadiazole-3,4-diyl)bis(3-(4-(trifluoromethoxy)phenyl)urea) (8)



Triphosgene (593, 2 mmol) was added slowly to a solution of 4-(trifluoromethoxy)aniline (0.41 mL, 3 mmol) in dry toluene (6 mL). Triethylamine (0.19 mL, 1.37 mmol) was immediately added, and the mixture was stirred at 70°C for 2 h. Pentane (1 mL) was added in one portion and the solution was filtered and concentrated under reduced pressure. Separately, diaminofurazan (100 mg, 1 mmol) was dissolved in a solution of dry CH₃CN (10 mL) and pyridine (0.5 mL) which was added in one portion to the isocyanate. The mixture was stirred vigorously at reflux for 18 h, concentrated under reduced pressure, and purified *via* flash chromatography (20 → 100% ethyl acetate in hexane) to afford the title compound as an amorphous white solid (386 mg, 0.76 mmol, 76%).

¹H NMR (500 MHz, DMSO-*d*₆) δ 9.60 (2 H, s), 9.32 (2 H, s), 7.58 (4 H, m), 7.31 (4 H, m); ¹³C NMR (126 MHz, DMSO-*d*₆) δ 151.3, 146.6, 143.3, 138.0, 121.7, 120.4; ¹⁹F NMR (471 MHz, DMSO-*d*₆) δ -57.10; LR-MS (ESI⁻, *m/z*) 505.10 [M-H]⁻; HR-MS (ESI⁻, *m/z*) calcd for C₁₈H₁₁F₆N₆O₅ [M-H]⁻ 505.07006, found 505.07066.

1,1'-(1,2,5-oxadiazole-3,4-diyl)bis(3-(3,5-bis(trifluoromethyl)phenyl)urea) (9)



3,5-Bis(trifluoromethyl)phenyl isocyanate (0.33 mL, 3 mmol) was added dropwise to a solution of diaminofurazan (100 mg, 1 mmol) in DMSO (4 mL) and stirred for 5 h mins. The reaction mixture was poured into cold water and the white precipitate was collected *via* vacuum filtration, washed with hexane (10 mL) and purified *via* flash chromatography (10 → 30% ethyl acetate in hexane) and subjected to strong cation exchange (SCX-2) chromatography (CHCl₃ + 0.1% TFA) to afford the title compound as an amorphous white solid (189 mg, 0.31 mmol, 31%).

¹H NMR (500 MHz, DMSO-*d*₆) δ 10.00 (2 H, s), 9.81 (2 H, s), 8.10 (4 H, d, *J* 1.6), 7.66 (2 H, s); ¹³C NMR (126 MHz, DMSO-*d*₆) δ 151.3, 146.5, 140.6, 130.3 (q, *J* 32.8), 123.9, 121.7, 118.3, 115.0; LR-MS (ESI⁻, *m/z*) 609.02 [M-H]⁻; HR-MS (ESI⁻, *m/z*) calcd for C₂₀H₉F₁₂N₆O₃ [M-H]⁻ 609.05500, found 609.05498

Characterisation data

1,1'-(1,2,5-oxadiazole-3,4-diyl)bis(3-phenylurea) (1)

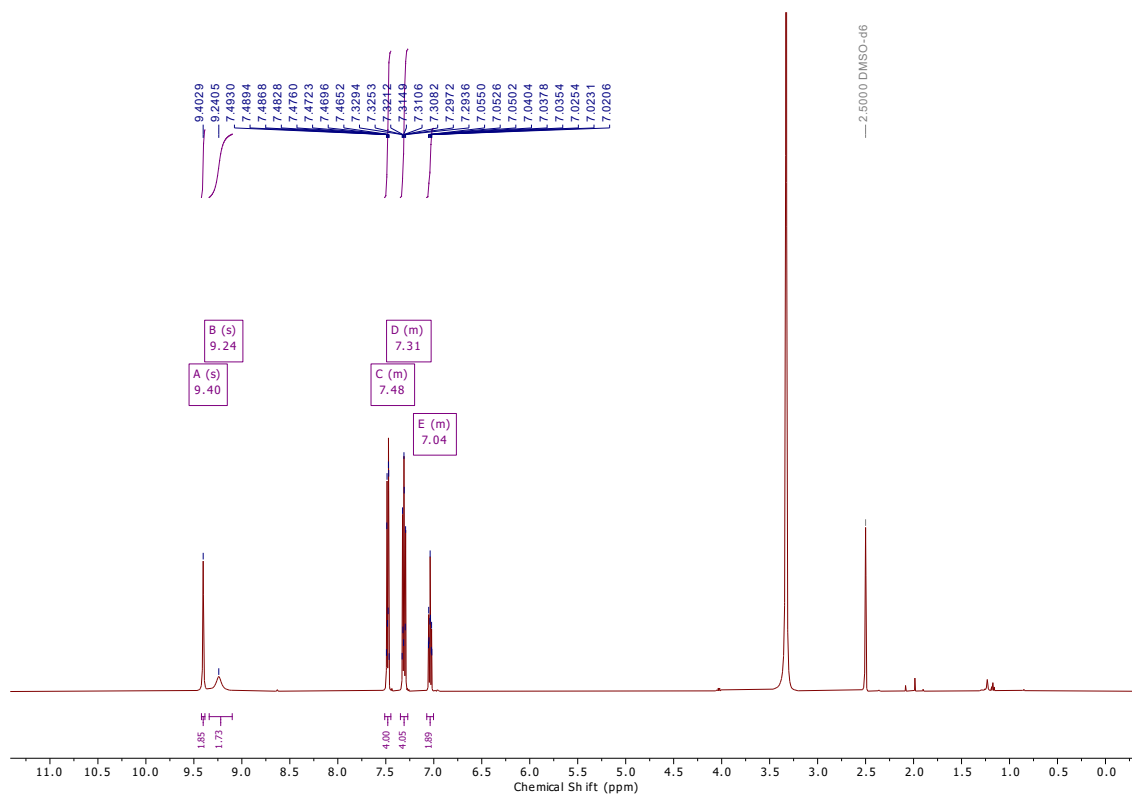
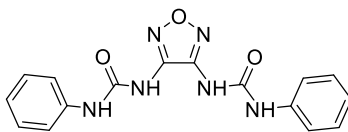


Figure S1. ^1H NMR (500 MHz) spectrum of **1** in $\text{DMSO-}d_6$ at 298 K.

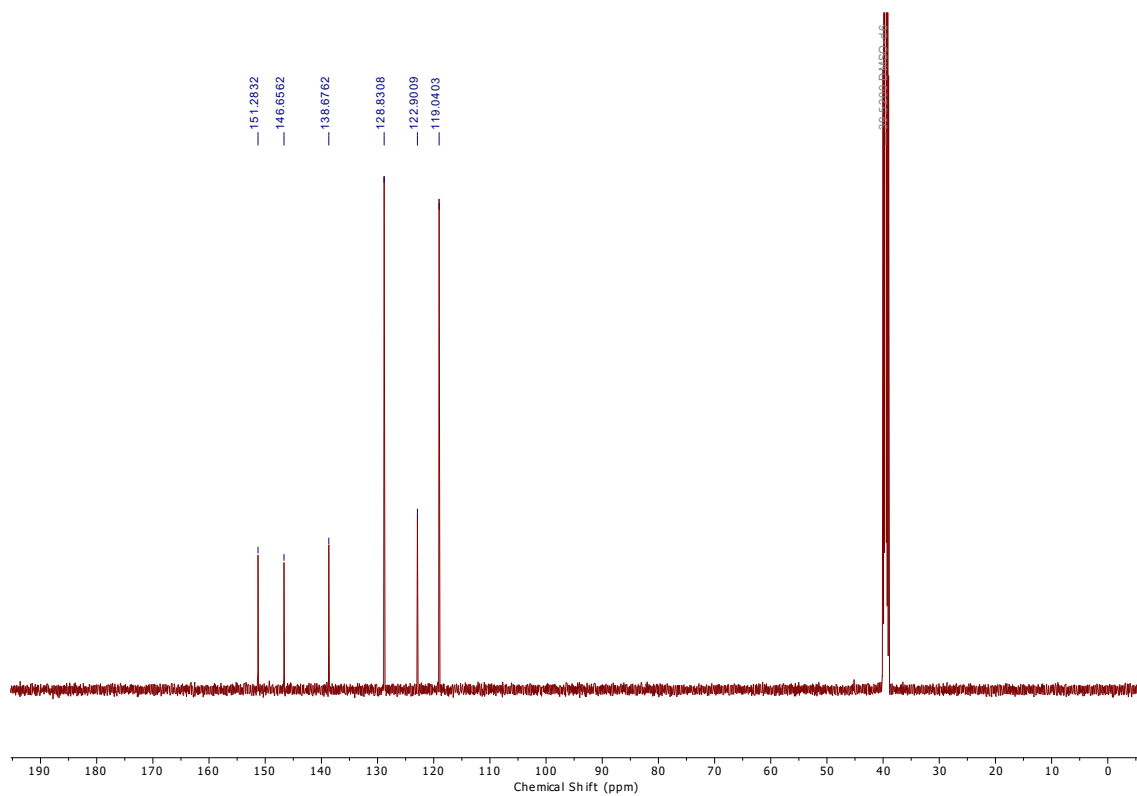


Figure S2. ^{13}C NMR (101 MHz) spectrum of **1** in $\text{DMSO-}d_6$ at 298 K.

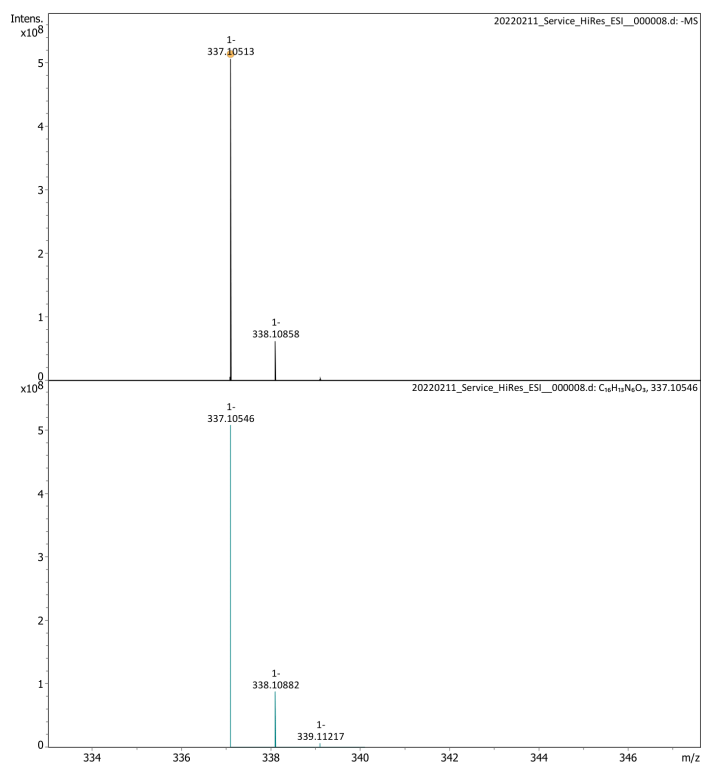


Figure S3. HR-MS (ESI $^-$) spectrum of **1**.

1,1'-(1,2,5-oxadiazole-3,4-diyl)bis(3-(4-(trifluoromethyl)phenyl)urea) (2)

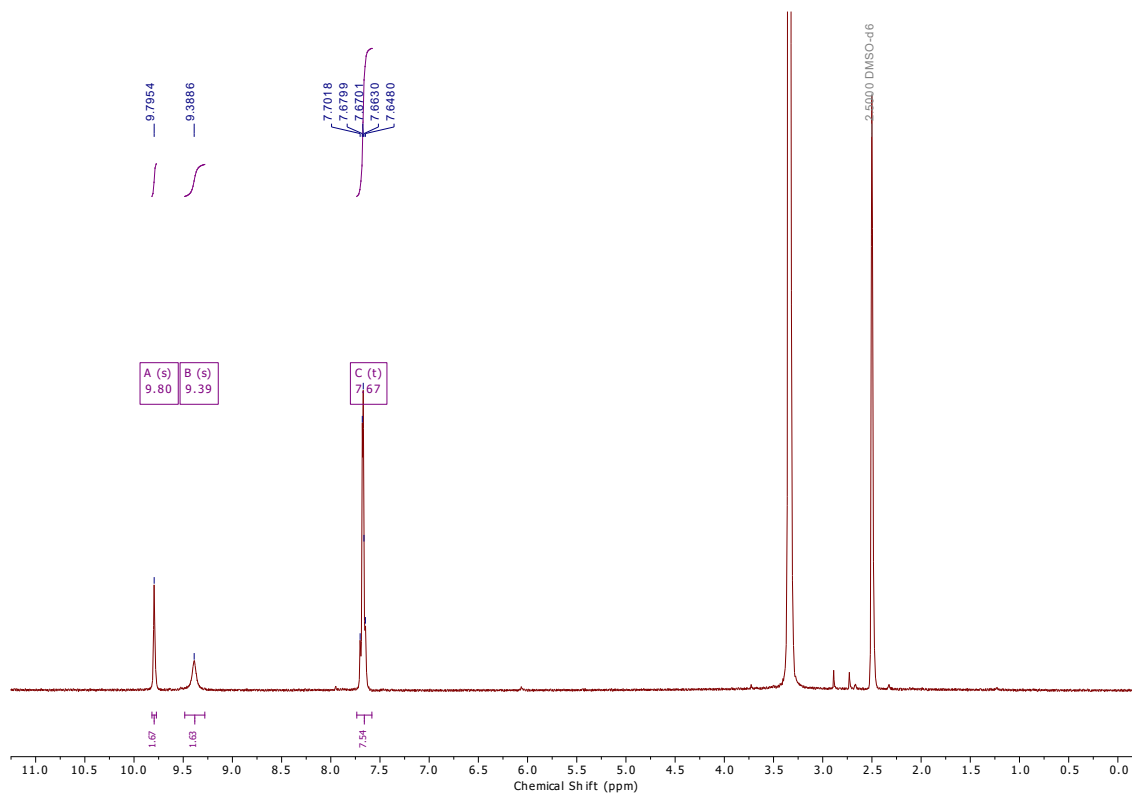
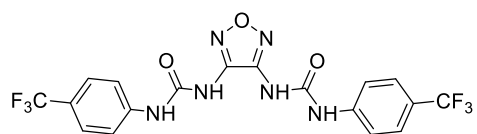


Figure S4. ^1H NMR (500 MHz) spectrum of **2** in $\text{DMSO-}d_6$ at 298 K.

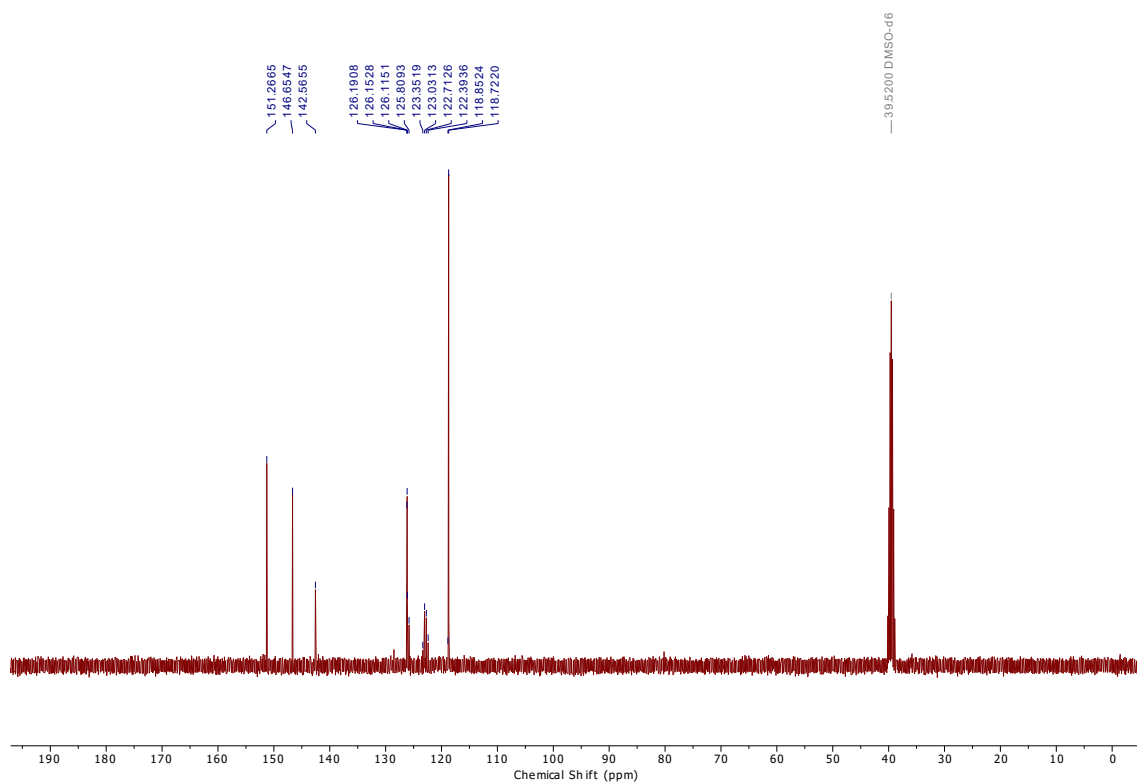


Figure S5. ^{13}C NMR (101 MHz) spectrum of **2** in $\text{DMSO-}d_6$ at 298 K.

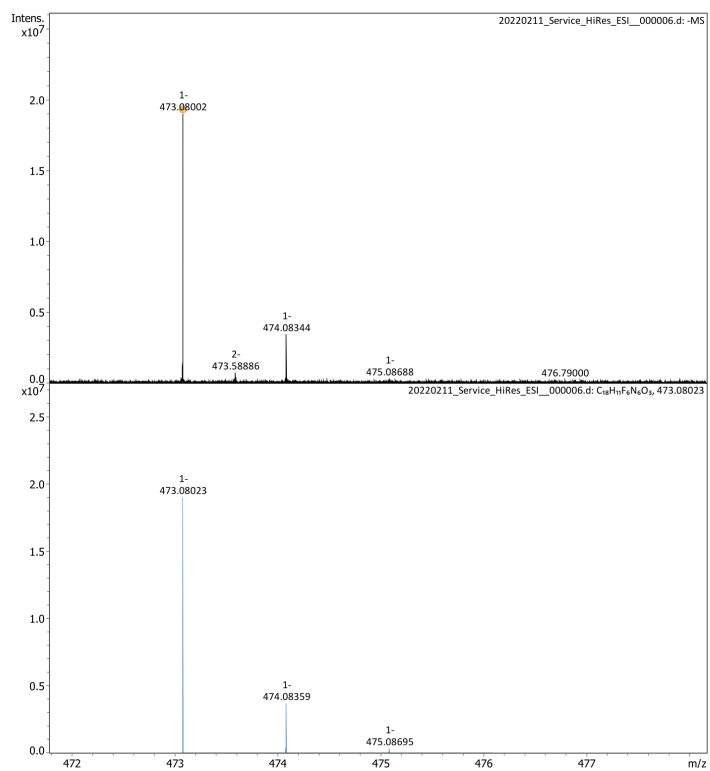


Figure S6. HR-MS (ESI $^-$) spectrum of **2**.

1,1'-(1,2,5-oxadiazole-3,4-diyl)bis(3-(4-(trifluoromethyl)phenyl)urea) (3)

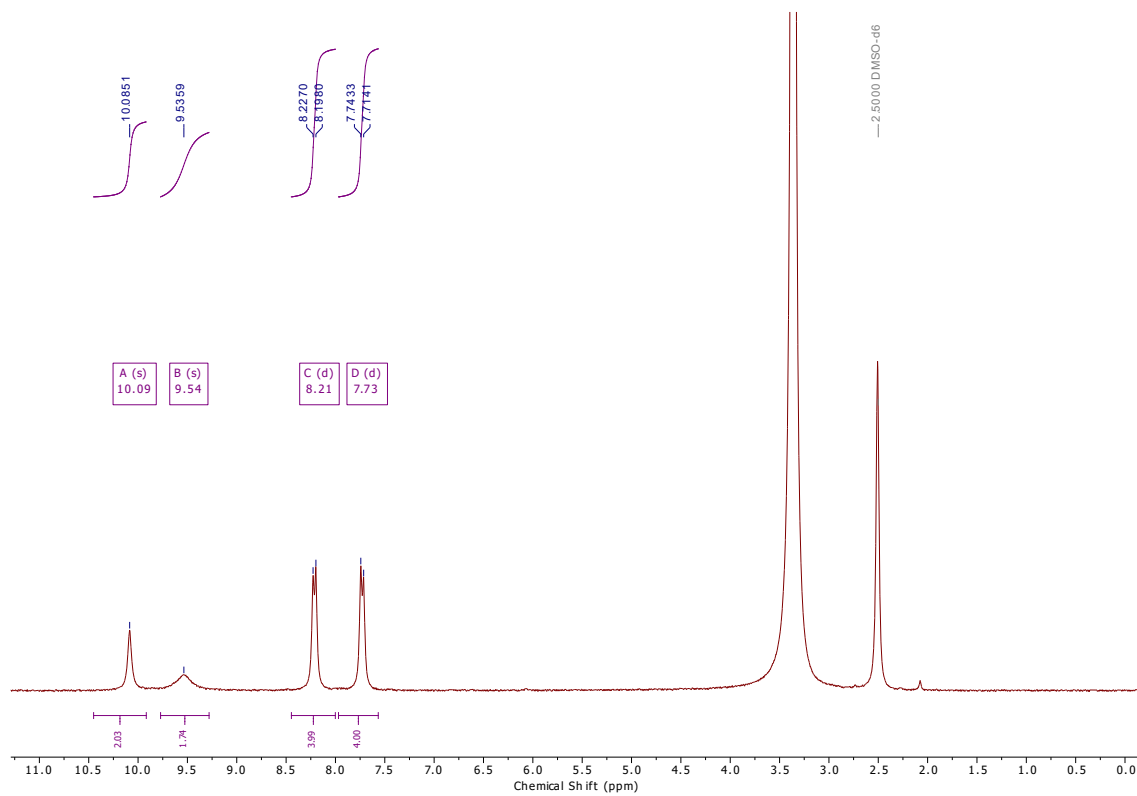
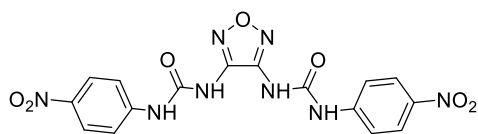


Figure S7. ^1H NMR (500 MHz) spectrum of **3** in $\text{DMSO-}d_6$ at 298 K.

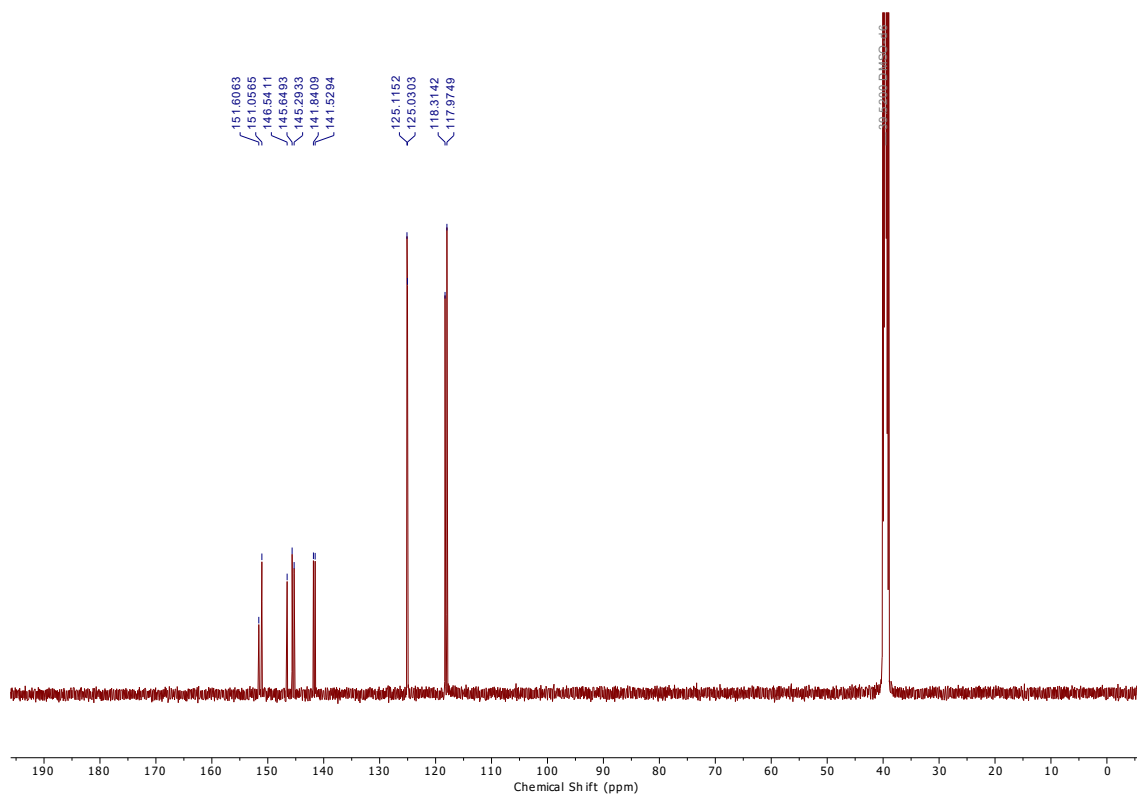


Figure S8. ^{13}C NMR (101 MHz) spectrum of **3** in $\text{DMSO-}d_6$ at 298.

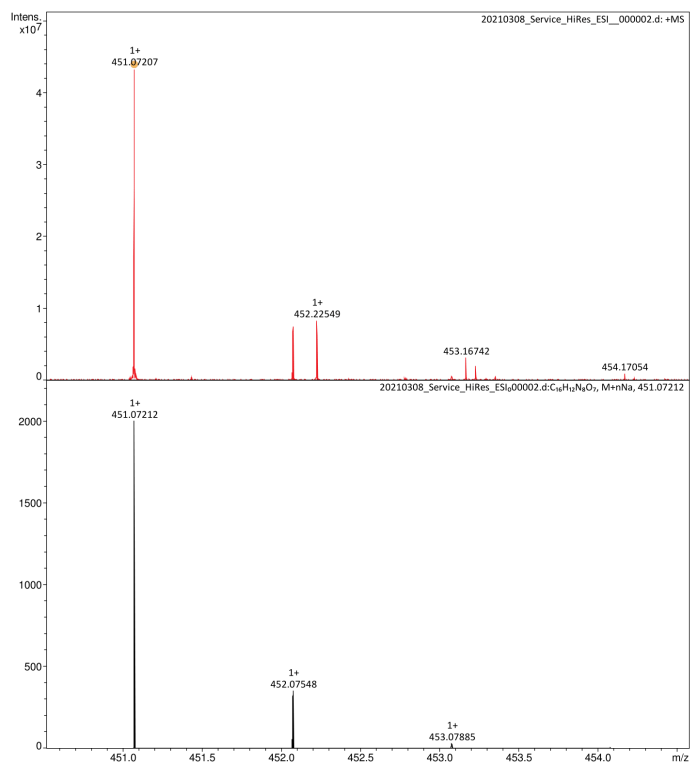


Figure S9. HR-MS (ESI^+) spectrum of **3**.

1,1'-(1,2,5-oxadiazole-3,4-diyl)bis(3-(4-fluorophenyl)urea) (4)

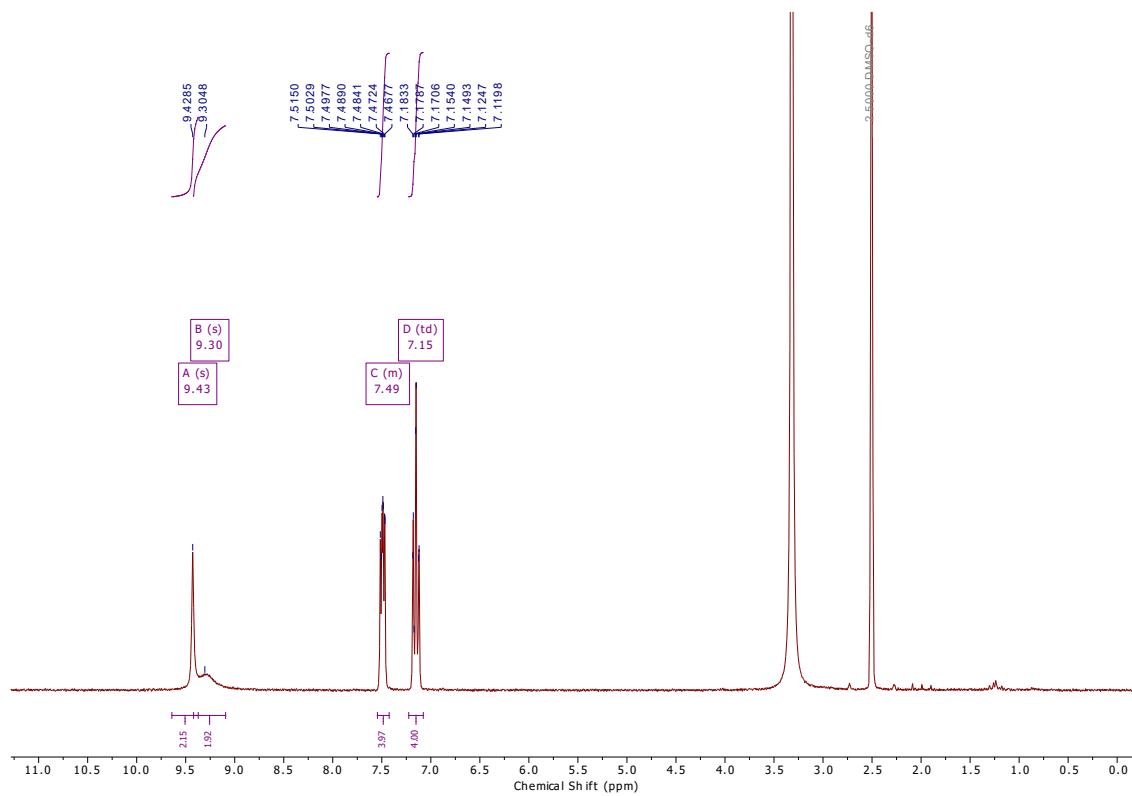
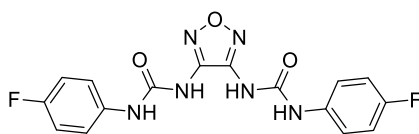


Figure S10. ^1H NMR (500 MHz) spectrum of 4 in $\text{DMSO-}d_6$ at 298 K.

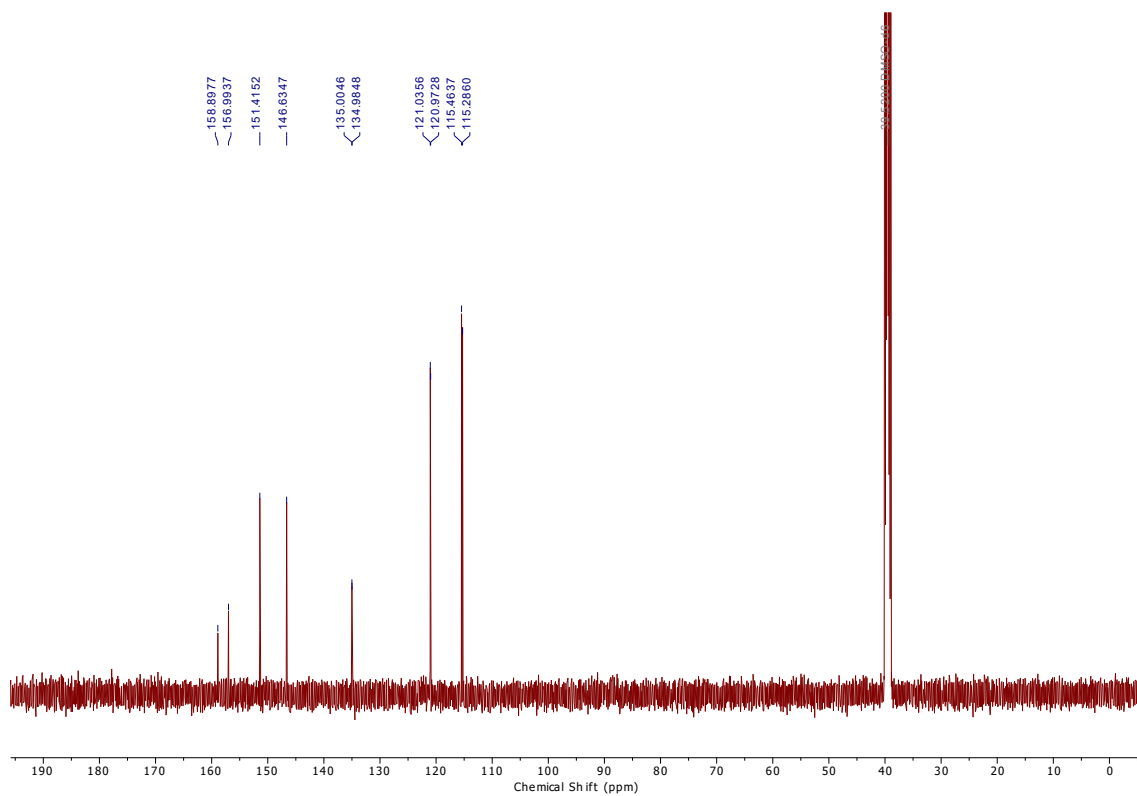


Figure S11. ^{13}C NMR (101 MHz) spectrum of **4** in $\text{DMSO-}d_6$ at 298 K.

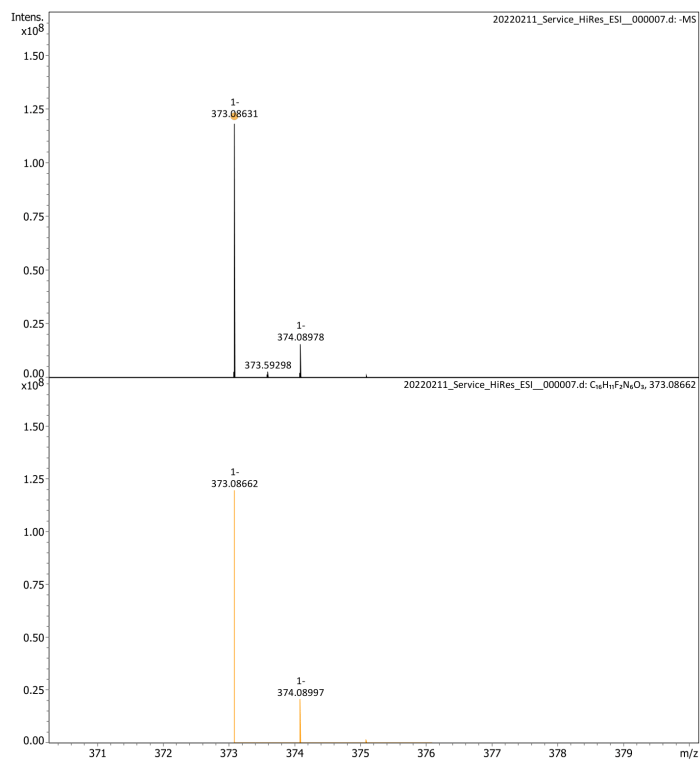


Figure S12. HR-MS (ESI) spectrum of **4**.

1,1'-(1,2,5-oxadiazole-3,4-diyl)bis(3-(4-cyanophenyl)urea) (5)

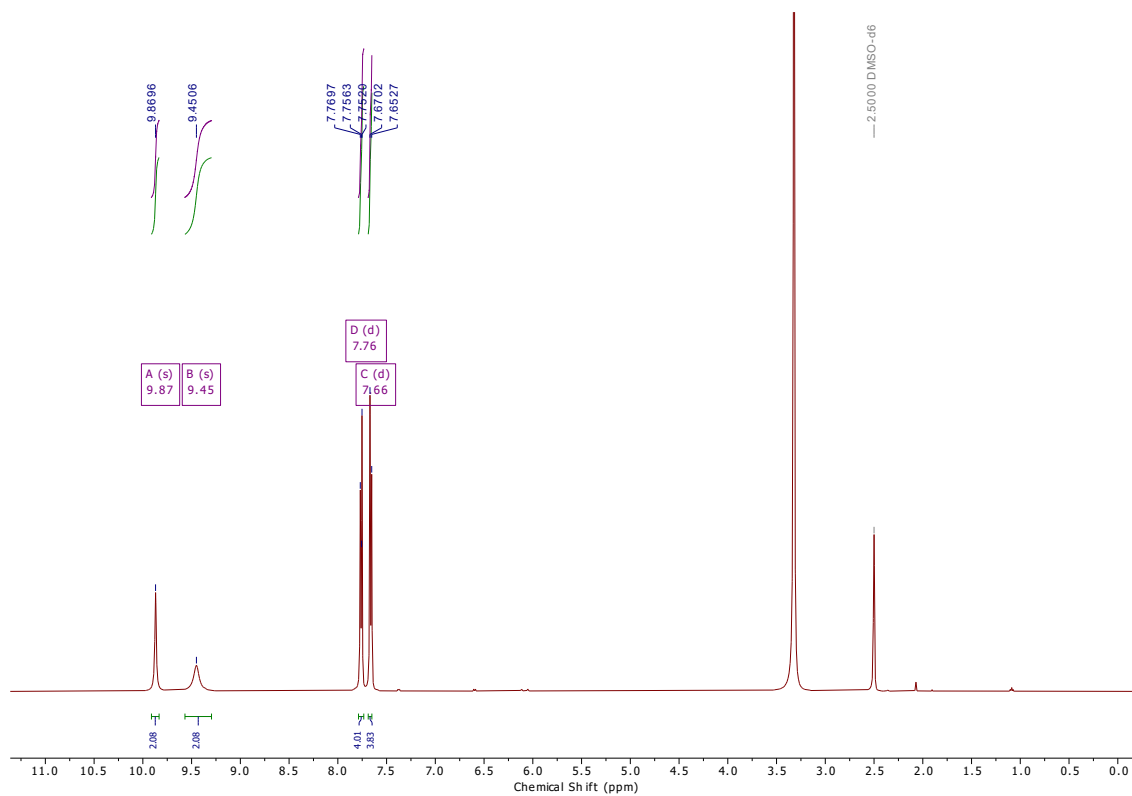
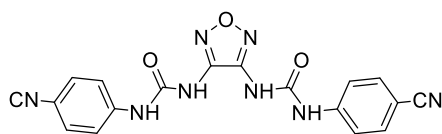


Figure S13. ^1H NMR (500 MHz) spectrum of **5** in $\text{DMSO-}d_6$ at 298 K.

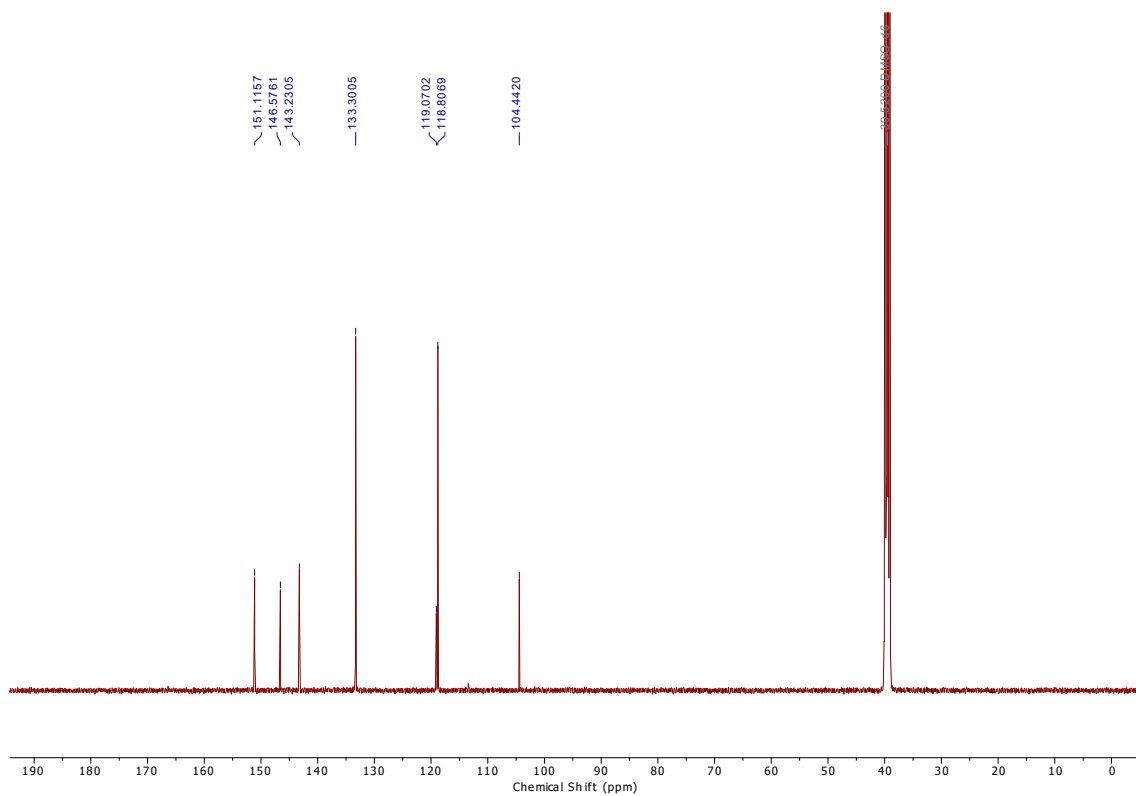


Figure S14. ^{13}C NMR (101 MHz) spectrum of **5** in $\text{DMSO-}d_6$ at 298 K.

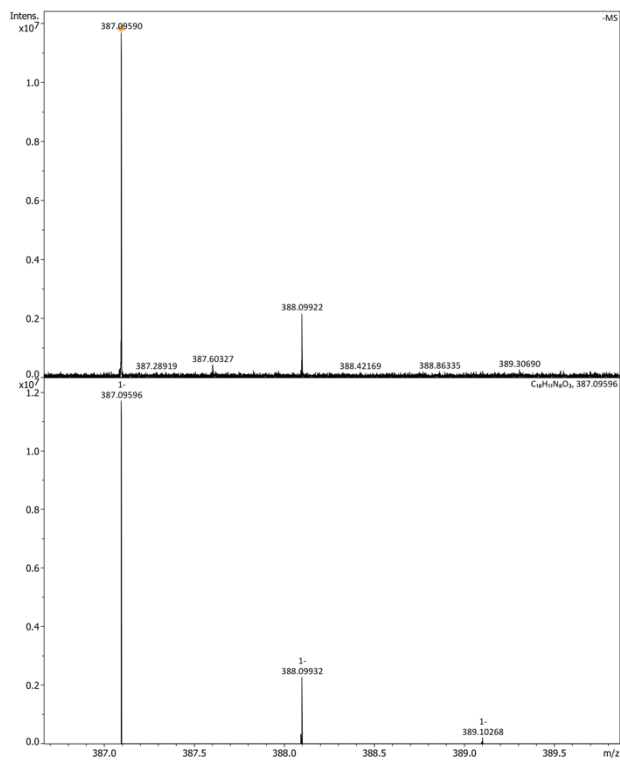


Figure S15. HR-MS (ESI) spectrum of **5**.

1,1'-(1,2,5-oxadiazole-3,4-diyl)bis(3-(perfluorophenyl)urea) (6)

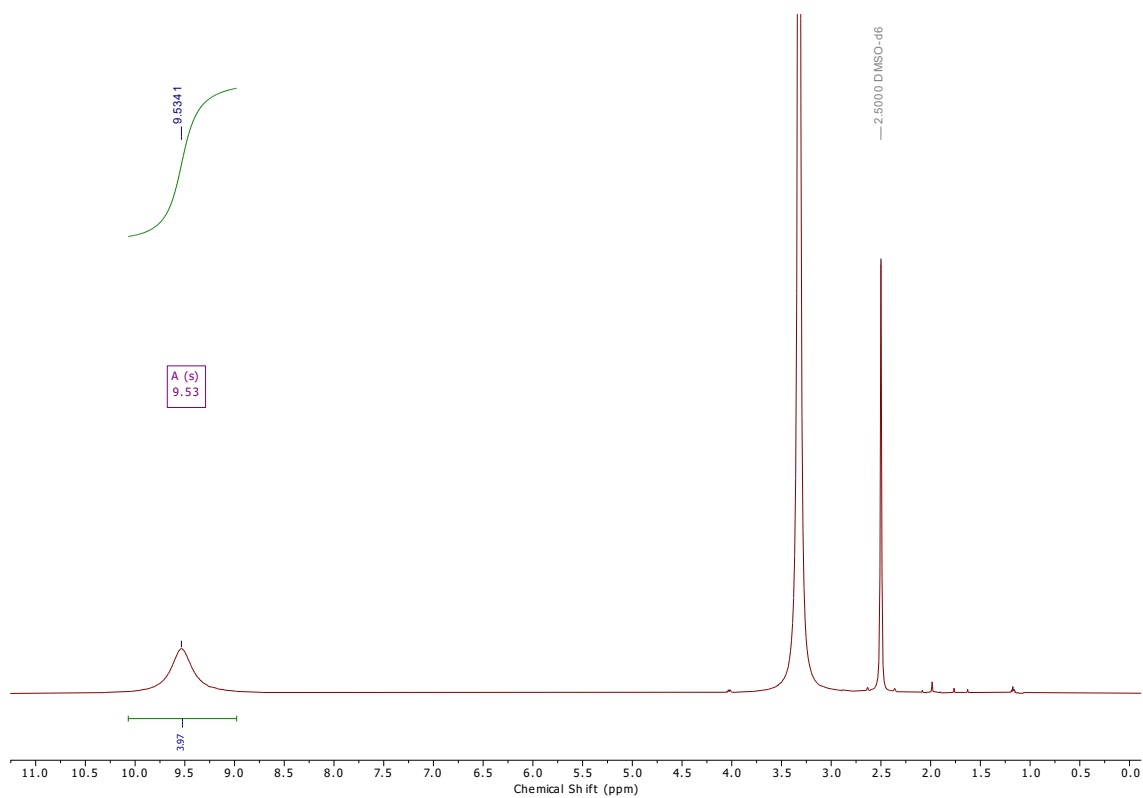
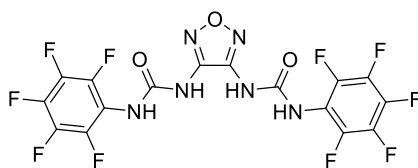


Figure S16. ^1H NMR (500 MHz) spectrum of **6** in $\text{DMSO-}d_6$ at 298 K.

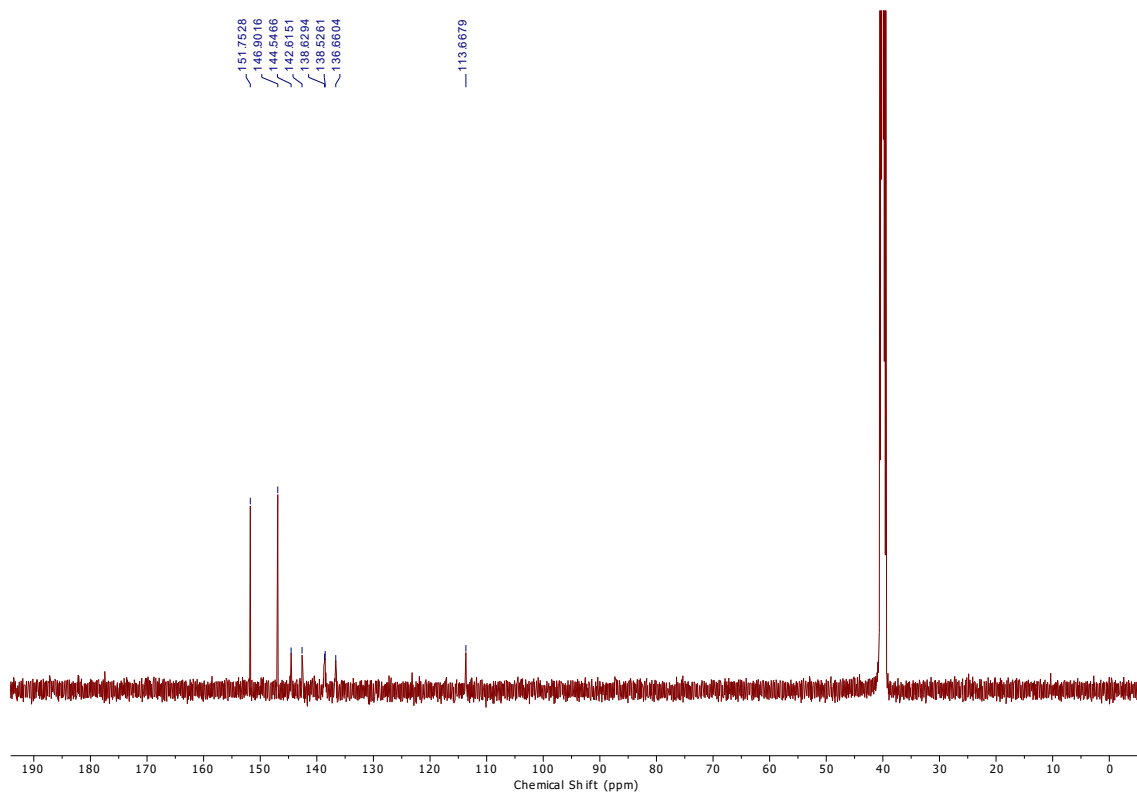


Figure S17. ^{13}C NMR (101 MHz) spectrum of **6** in $\text{DMSO-}d_6$ at 298 K.

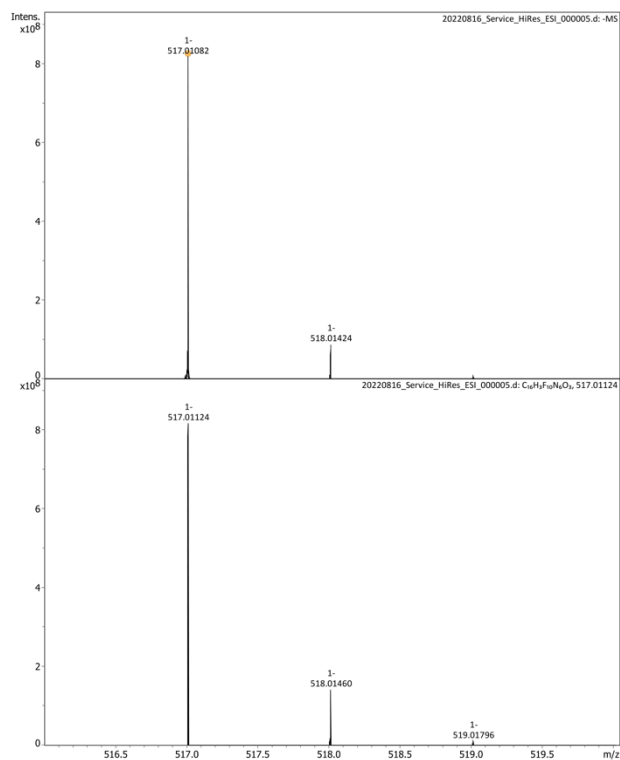


Figure S18. HR-MS (ESI) spectrum of **6**.

1,1'-(1,2,5-oxadiazole-3,4-diyl)bis(3-(4-(pentafluoro-16-sulfanyl)phenyl)urea) (7)

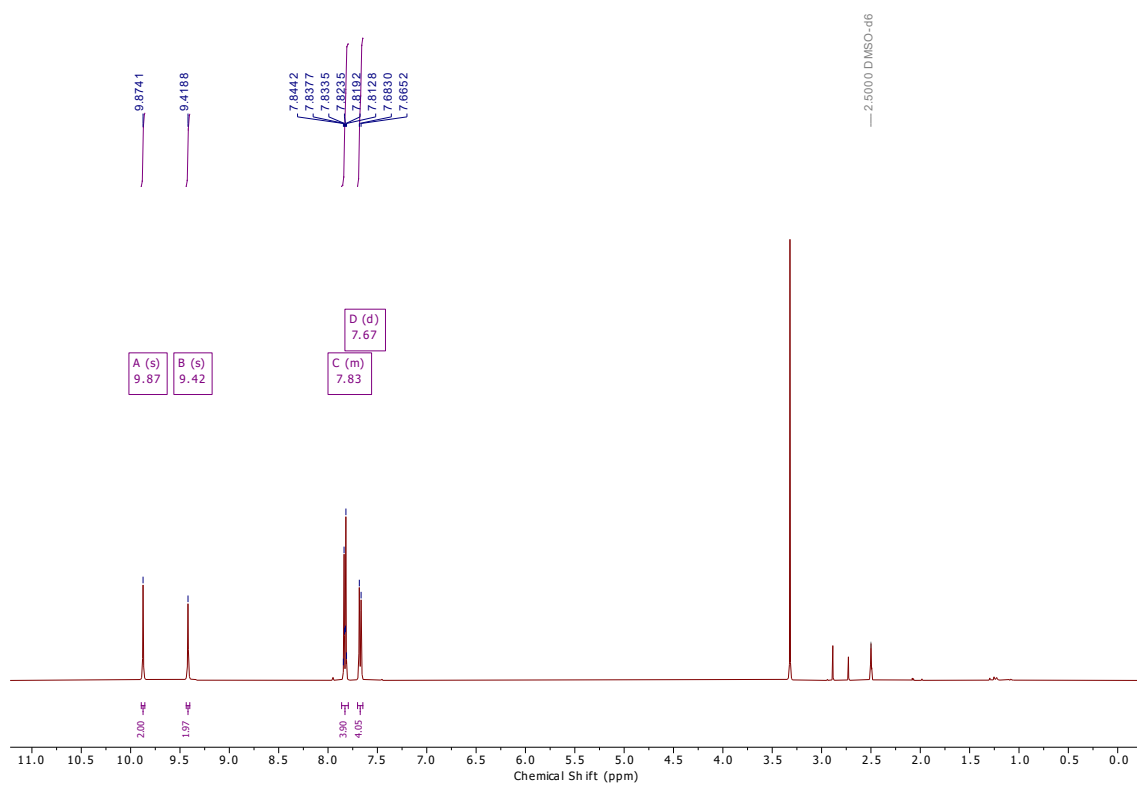
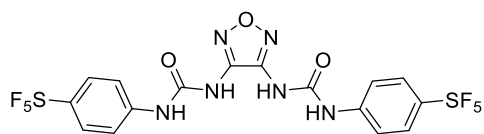


Figure S19. ^1H NMR (500 MHz) spectrum of **7** in $\text{DMSO-}d_6$ at 298 K.

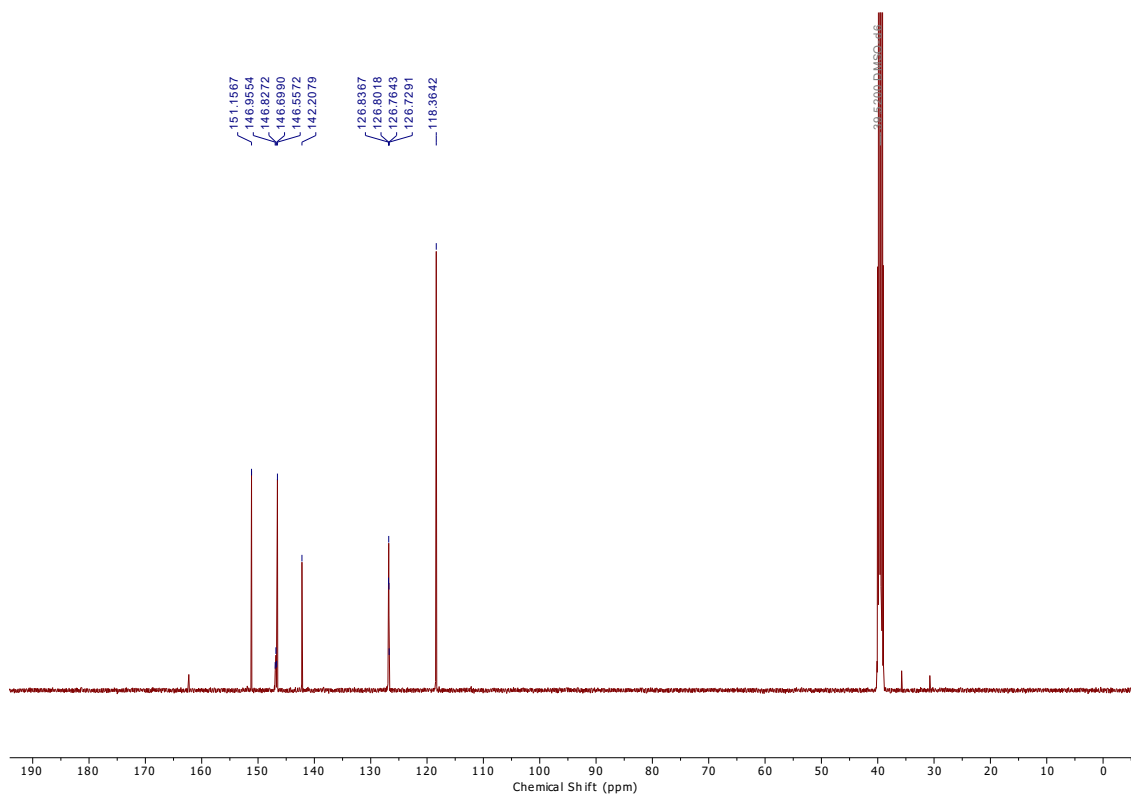


Figure S20. ^{13}C NMR (101 MHz) spectrum of **7** in $\text{DMSO-}d_6$ at 298 K.

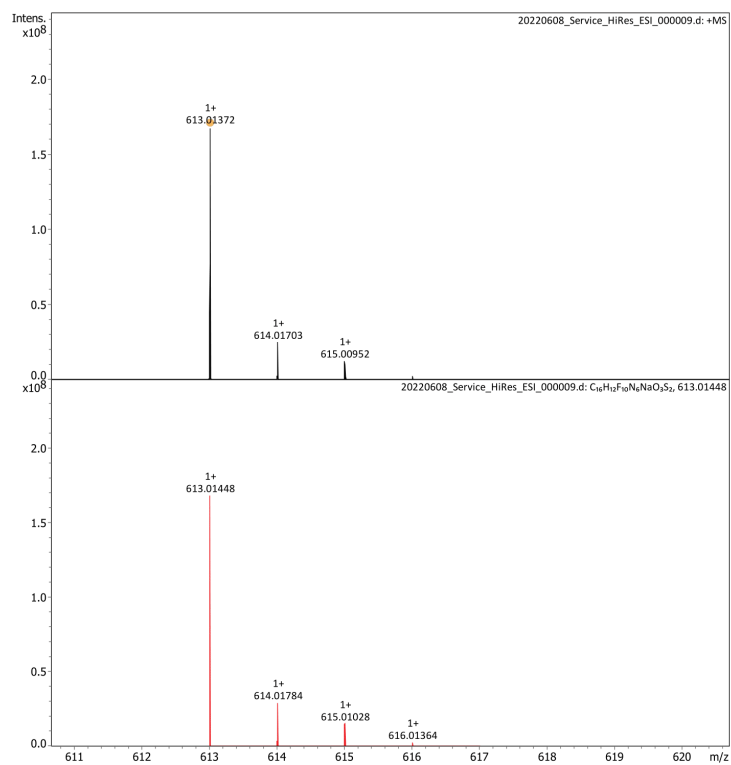


Figure S21. HR-MS (ESI^+) spectrum of **7**.

1,1'-(1,2,5-oxadiazole-3,4-diyl)bis(3-(4-(trifluoromethoxy)phenyl)urea) (8)

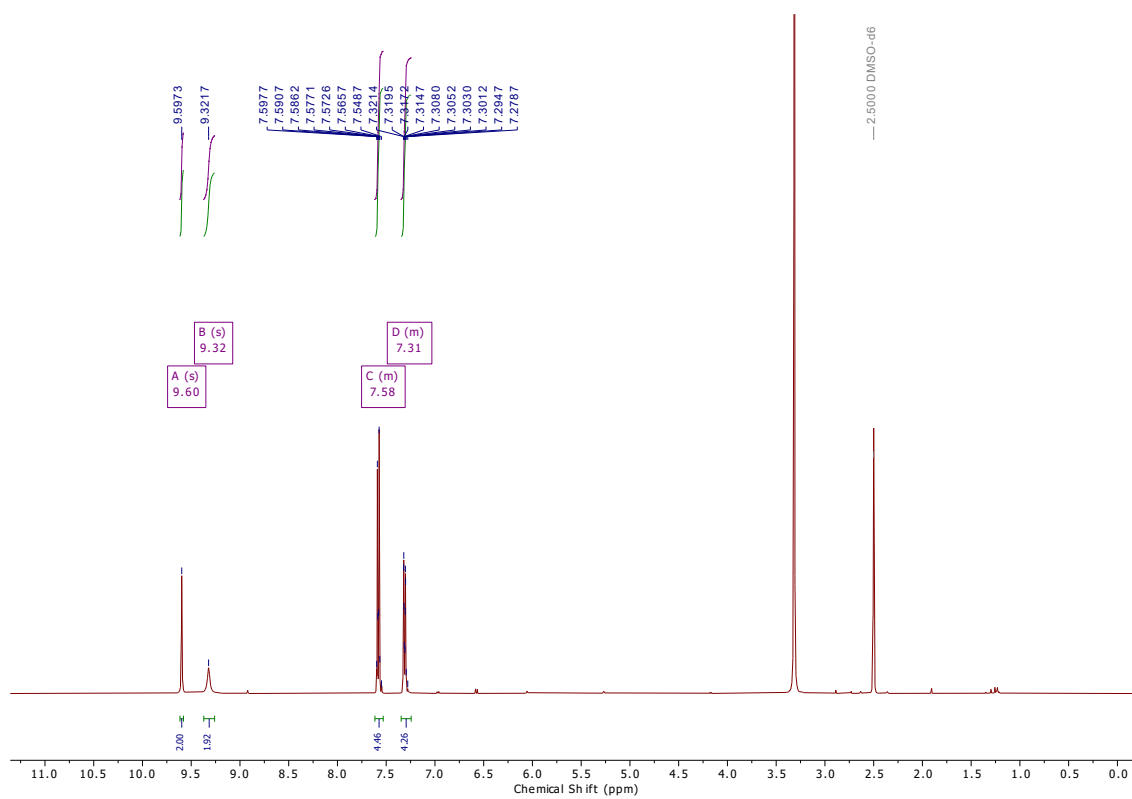
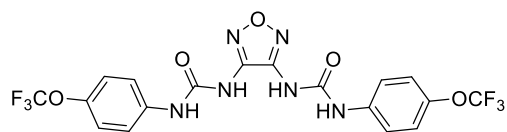


Figure S22. ¹H NMR (500 MHz) spectrum of **8** in DMSO-*d*₆ at 298 K.

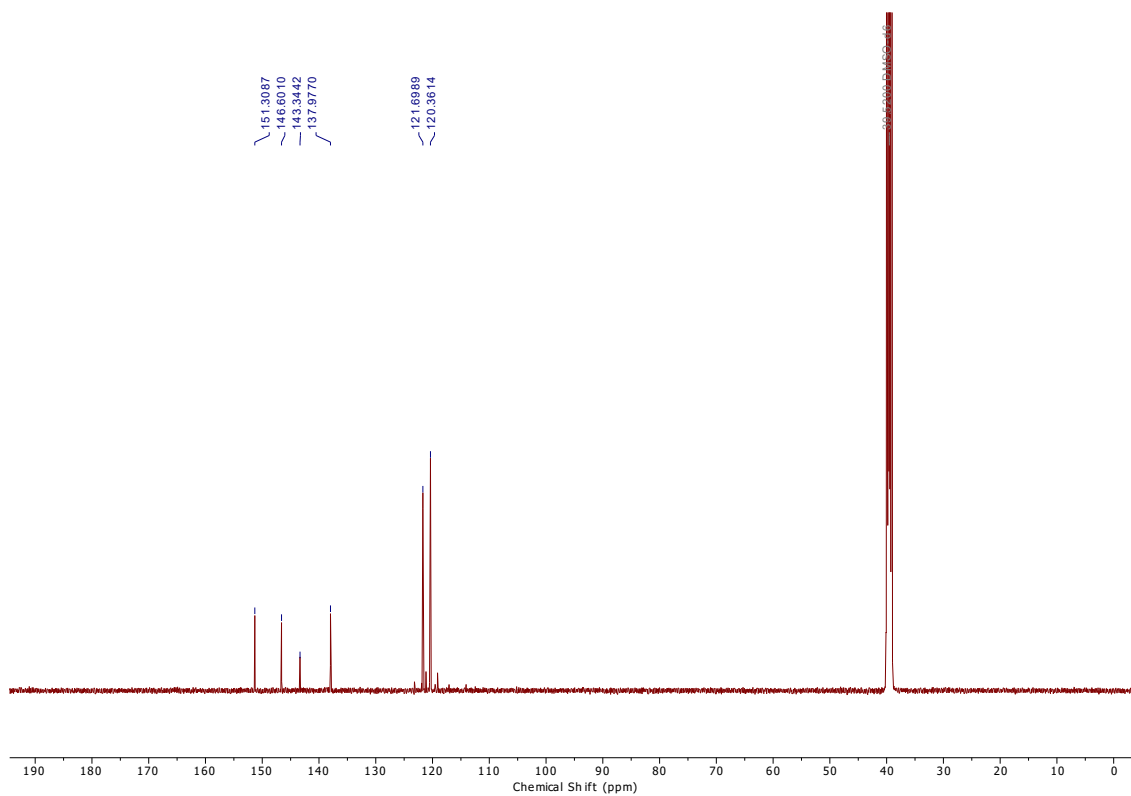


Figure S23. ^{13}C NMR (101 MHz) spectrum of **8** in $\text{DMSO-}d_6$ at 298 K.

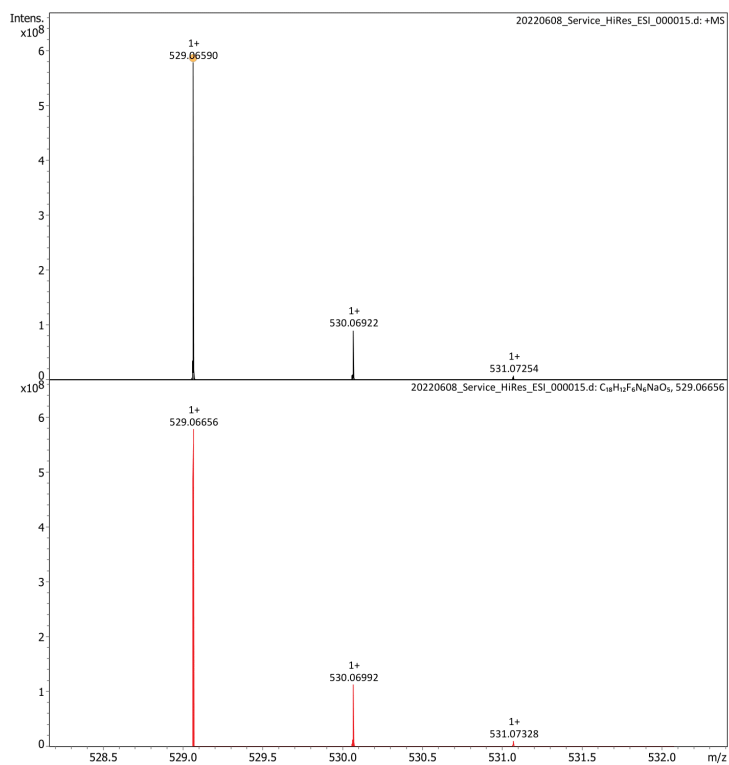


Figure S24. HR-MS (ESI $^-$) spectrum of **8**.

1,1'-(1,2,5-oxadiazole-3,4-diyl)bis(3-(3,5-bis(trifluoromethyl)phenyl)urea) (9)

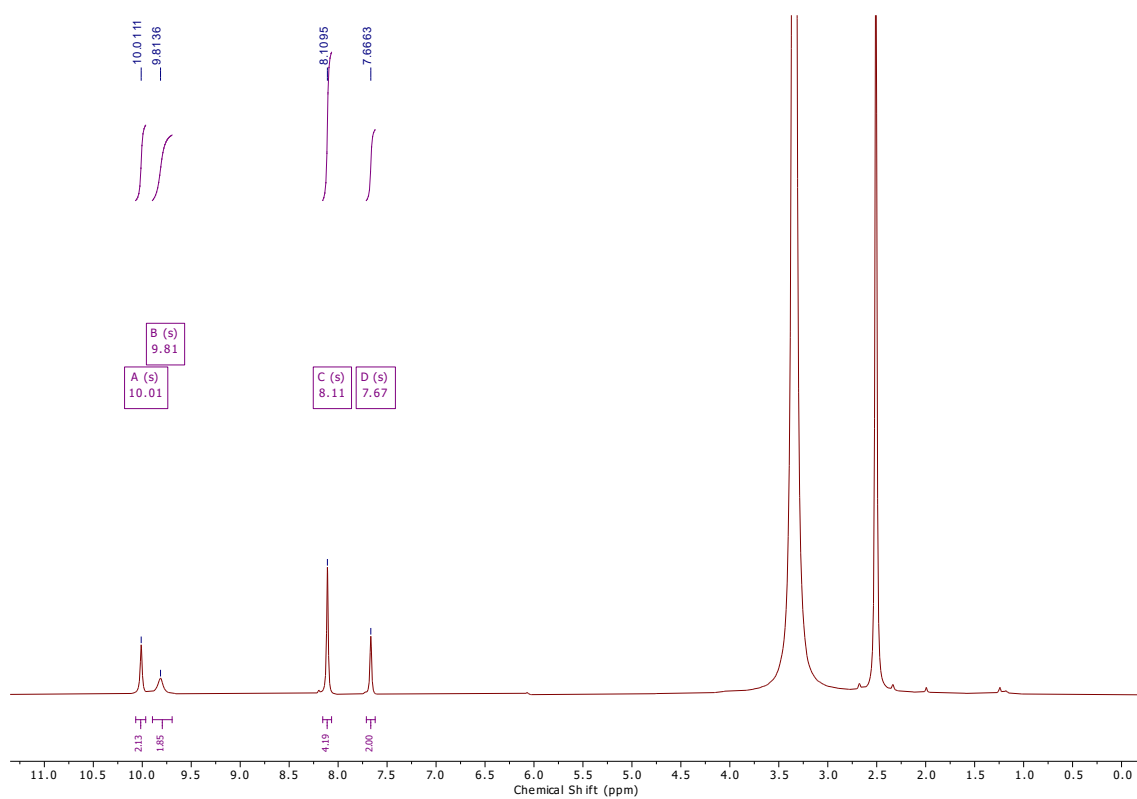
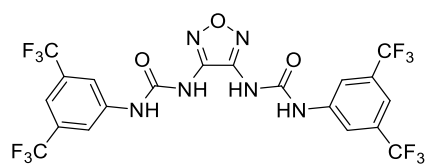


Figure S25. ^1H NMR (500 MHz) spectrum of **9** in $\text{DMSO-}d_6$ at 298 K.

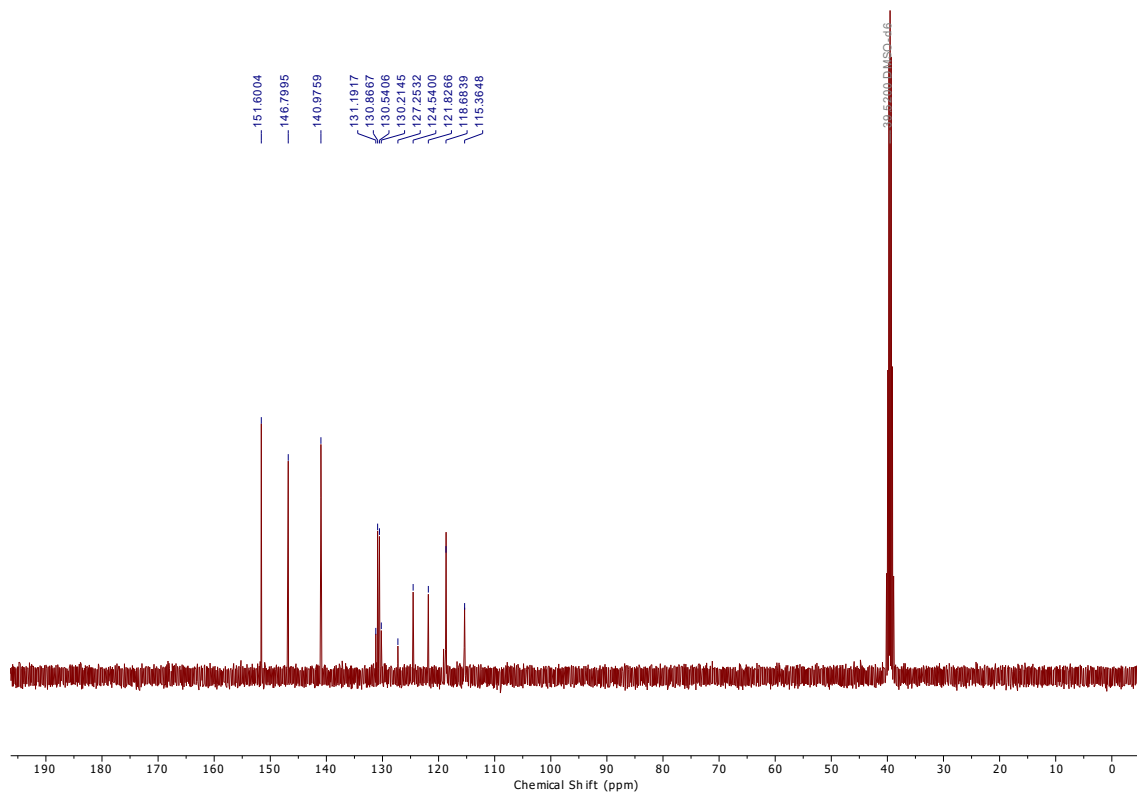


Figure S26. ^{13}C NMR (101 MHz) spectrum of **9** in $\text{DMSO-}d_6$ at 298 K.

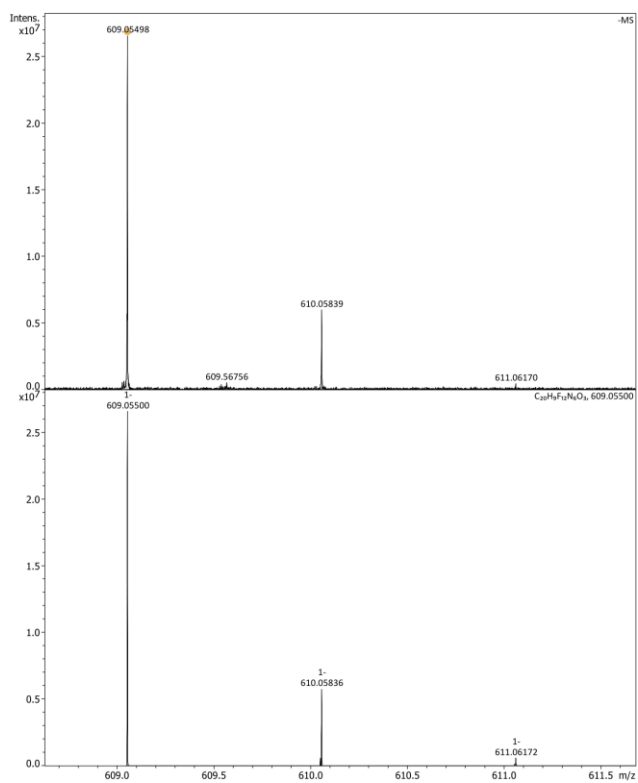


Figure S27. HR-MS (ESI) spectrum of **9**.

X-Ray crystallography

Single crystals suitable for X-ray diffraction were obtained through the slow evaporation of a concentrated solution of compound **1** in DMSO or CH₃CN. A suitable crystal was selected and in Paratone on a micromount on a SuperNova, Dual, Cu at home/near, Atlas diffractometer. The crystal was kept at 100 K during data collection. Using Olex2^[1], the structure was solved with the ShelXS^[2] structure solution program using Direct Methods and refined with the ShelXL^[3] refinement package using Least Squares minimization.

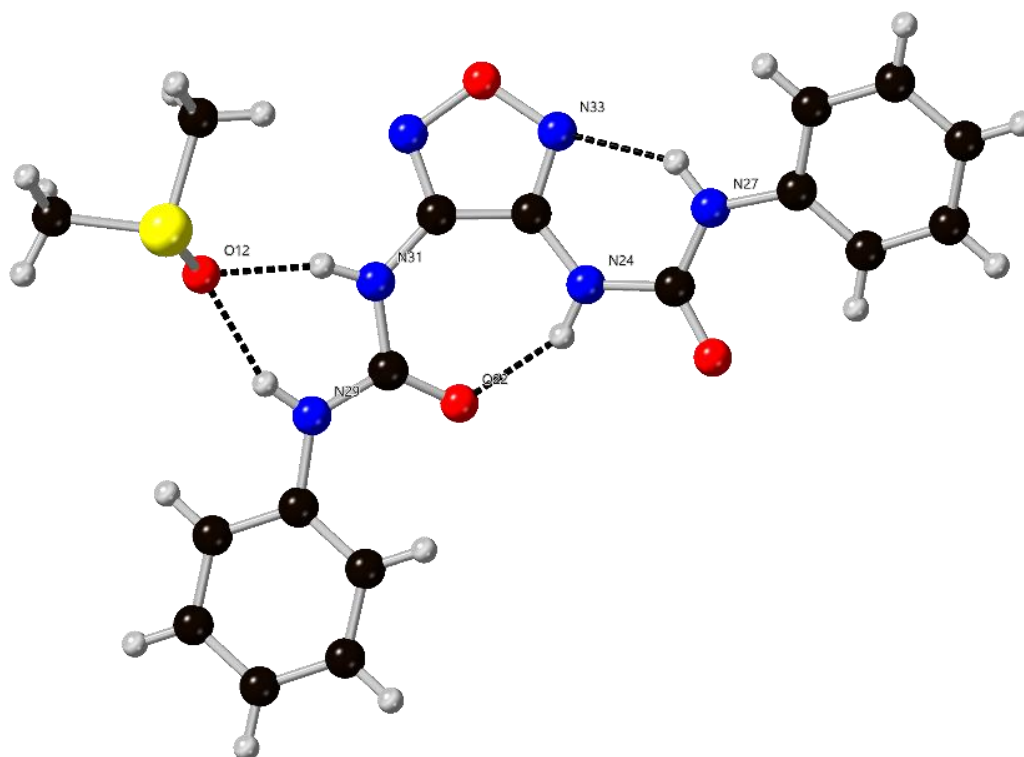


Figure S28. Crystal structure of **1** as a DMSO solvate. The dashed line represents a hydrogen bond.

Table S1. Crystal and data refinement parameters for the X-ray studies.

CCDC	2279691
Identification code	pag22_s2551_fr259
Empirical formula	C ₁₈ H ₂₀ N ₆ O ₄ S
Formula weight	416.46
Temperature/K	100.00
Crystal system	triclinic
Space group	P-1
a/Å	10.0029(9)
b/Å	13.1480(11)
c/Å	16.1305(15)

$\alpha/^\circ$	104.952(2)
$\beta/^\circ$	106.869(2)
$\gamma/^\circ$	96.165(2)
Volume/ \AA^3	1922.9(3)
Z	4
$\rho_{\text{calc}}/\text{cm}^3$	1.439
μ/mm^{-1}	0.208
F(000)	872.0
Crystal size/ mm^3	0.39 × 0.33 × 0.235
Radiation	MoK α ($\lambda = 0.71073$)
2 θ range for data collection/ $^\circ$	2.77 to 59.68
Index ranges	-13 ≤ h ≤ 13, -17 ≤ k ≤ 14, -22 ≤ l ≤ 22
Reflections collected	43991
Independent reflections	9951 [$R_{\text{int}} = 0.0242$, $R_{\text{sigma}} = 0.0193$]
Data/restraints/parameters	9951/0/527
Goodness-of-fit on F^2	1.024
Final R indexes [$I \geq 2\sigma(I)$]	$R_1 = 0.0326$, $wR_2 = 0.0862$
Final R indexes [all data]	$R_1 = 0.0366$, $wR_2 = 0.0893$
Largest diff. peak/hole / $e \text{\AA}^{-3}$	0.40/-0.36

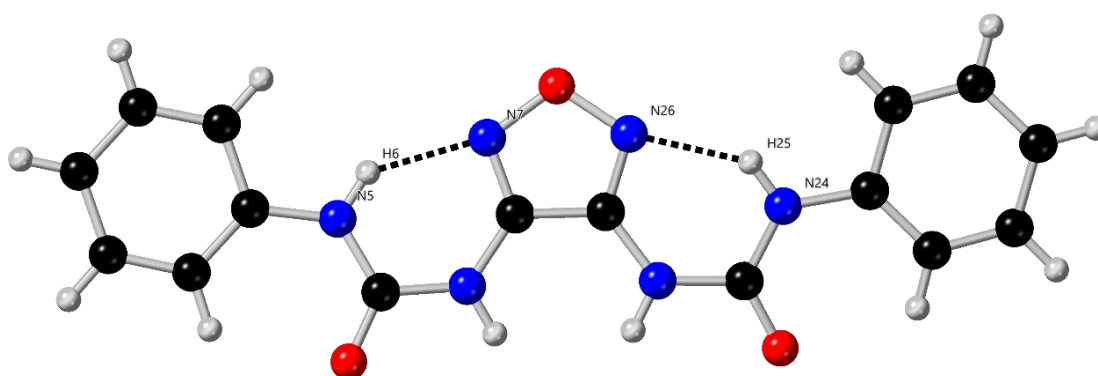


Figure S29. X-ray crystal structure of **1** in CH_3CN

Table S2. Crystal and data refinement parameters for the X-ray studies.

CCDC	2279693
Identification code	pag22_s2547_fr255
Empirical formula	$\text{C}_{16}\text{H}_{14}\text{N}_6\text{O}_3$
Formula weight	338.33

Temperature/K	99.93
Crystal system	monoclinic
Space group	C2/c
a/Å	16.93(3)
b/Å	11.502(16)
c/Å	8.484(13)
α/°	90
β/°	118.36(4)
γ/°	90
Volume/Å³	1453(4)
Z	4
ρ_{calc}/cm³	1.546
μ/mm⁻¹	0.112
F(000)	704.0
Crystal size/mm³	0.44 × 0.025 × 0.02
Radiation	MoKα (λ = 0.71073)
2θ range for data collection/°	4.474 to 53.222
Index ranges	-20 ≤ h ≤ 20, -14 ≤ k ≤ 13, -10 ≤ l ≤ 8
Reflections collected	5177
Independent reflections	1469 [R _{int} = 0.1620, R _{sigma} = 0.2083]
Data/restraints/parameters	1469/0/114
Goodness-of-fit on F²	1.084
Final R indexes [I ≥ 2σ (I)]	R1 = 0.1229, wR2 = 0.3316
Final R indexes [all data]	R1 = 0.2244, wR2 = 0.3930
Largest diff. peak/hole / e Å⁻³	0.47/-0.60

¹H NMR titration experiments

Sample preparation

¹H NMR spectra were recorded on a Bruker DPX 400, or Bruker AVANCE III 500 spectrometer and calibrated to the DMSO-*d*₆ residual solvent peak ($\delta = 2.50$ ppm) at 300 K. Stack plots were made using MestReNova Version 14.1.2. The TBA (or TEA for HCO₃⁻) anion salts were purchased from Merck. The salts and receptors were dried under high vacuum for a minimum of 17 h to remove residual solvents and water, respectively. A general stock solution of the host (~5 mM) was prepared using the deuterated solvent mixture DMSO-*d*₆/0.5 % H₂O. The same stock solution was used to prepare the guest titrant solutions containing either 1.0 or 0.1 M of the respective anion as their TBA or TEA salt, which ensured the host concentration was maintained throughout the experiment (**Chapter 2** = 5 mM; **Chapter 3** = 2.5 mM; and **Chapter 4** = 2.5 mM). The host solution (600 μ L) was added to a NMR sample tube (5 mm) with an air-tight screwcap lid to minimise spillage.

Titration procedure

The ¹H NMR spectra of the host solution was collected at the start of the experiment. Aliquots (1-200 μ L) of the guest solutions were transferred to the NMR tube *via* Hamiltonian microlitre syringes, inverted 5 times to ensure homogenous distribution, and equilibrated for up to 2 min in the NMR probe before the ¹H NMR spectra was collected. For the anion screen, 5 or 10 equiv. of the respective anion salt was added as described above, and the ¹H NMR spectra was collected. During a titration experiment, 16-20 spectra with increasing concentration of guest were recorded, resulting in a range from 0-100 equiv. of guest to host. The parameters of the NMR spectrometer remained constant for each experiment.

Titration data fitting

For all receptors the proton resonances were monitored for changes in their chemical shift, indicative of anion:receptor hydrogen bonding. Wherever possible, two or more resonances were monitored, enabling the utilisation of multiple data sets for the calculation of the association constant (K_a). The implementation of global fitting considered all the data sets simultaneously, enhancing the quality of the non-linear fitting process. The web applet (supramolecular.org) was employed to analyse the titration data using either a 1:1 or 2:1 host-guest binding model. The preference for a 2:1 model was determined if covariance of fit ($Fcov_{fit}$) was at least five times superior to the covariance of fit for the 1:1 model. Additionally, the binding constant, isotherm fit, and residuals were compared to assess the quality of fit of the data to each binding model. Both models were applied to the data for comparison purposes.

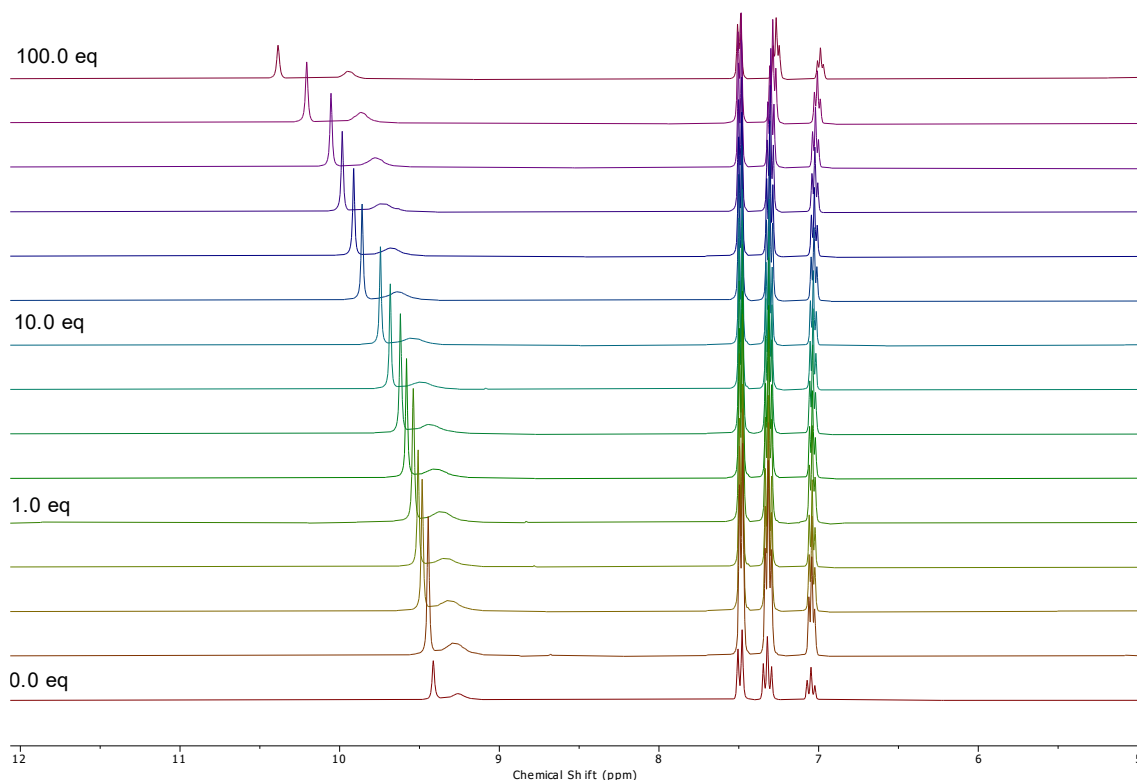


Figure S30. ^1H NMR (400 MHz) titration spectra as a stack plot for **1** (5 mM) + TBACl in $\text{DMSO-}d_6/0.5\%$ H_2O at 298 K.

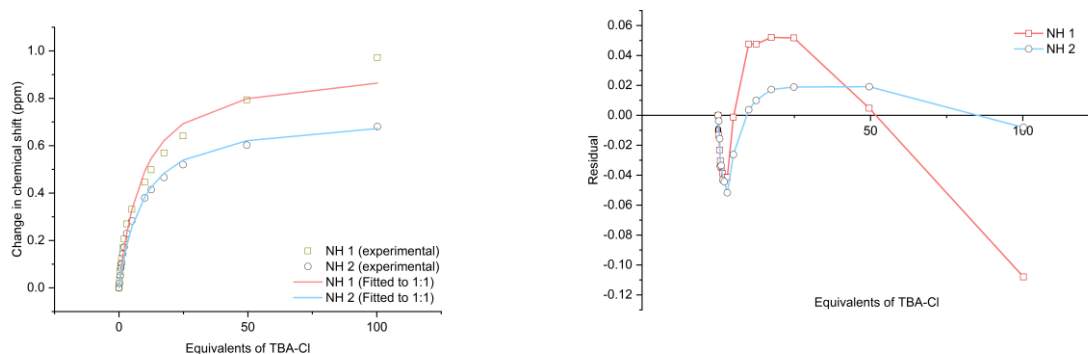


Figure S31. Fitted binding isotherm of **1** + TBACl showing the change in chemical shift of the NH protons fitted to the 1:1 binding model (left), $K_a = 15.1 \text{ M}^{-1}$. Residual plot showing the random error obtained from the binding isotherm fitting (right).

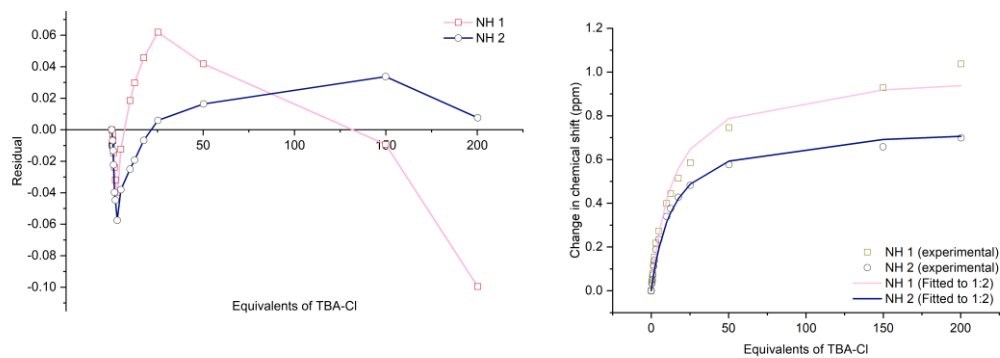


Figure S32. Fitted binding isotherm of **1** + TBACl showing the change in chemical shift of the NH protons fitted to the 1:2 binding model (left), $K_{11} = 41.7 \text{ M}^{-1}$, $K_{12} = 2.1 \text{ M}^{-1}$. Residual plot showing the random error obtained from the binding isotherm fitting (right).

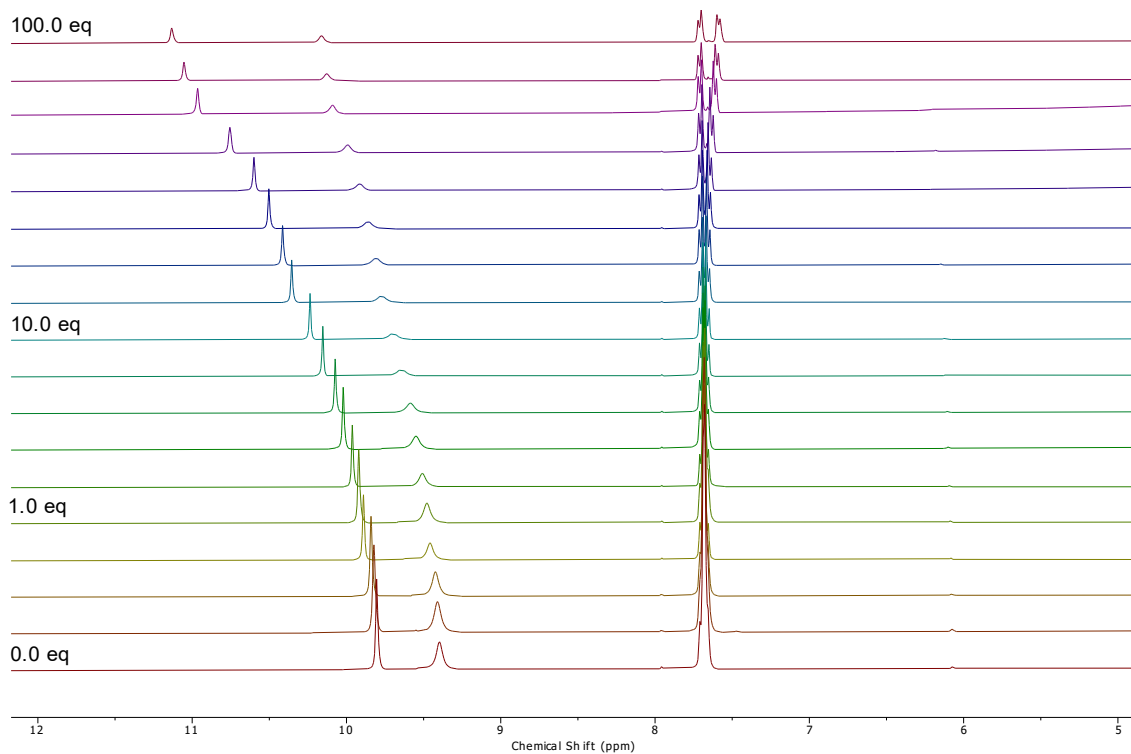


Figure S33. ¹H NMR (400 MHz) titration spectra as a stack plot for **2** (5 mM) + TBACl in DMSO-*d*₆/0.5% H₂O at 298 K.

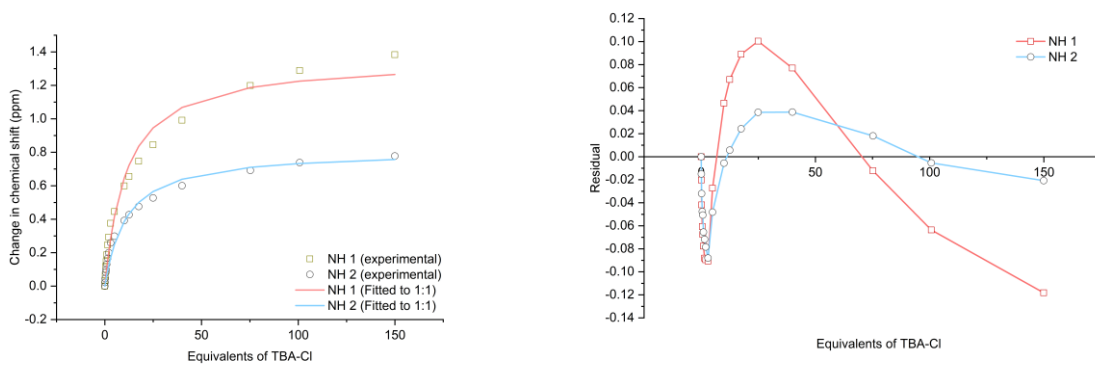


Figure S34. Fitted binding isotherm of **2** + TBACl showing the change in chemical shift of the NH protons fitted to the 1:1 binding model (left), $K_a = 18.4 \text{ M}^{-1}$. Residual plot showing the random error obtained from the binding isotherm fitting (right).

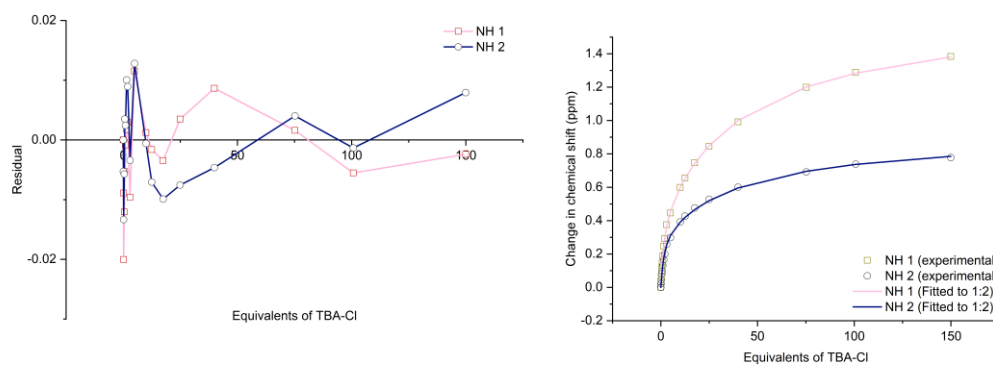


Figure S35. Fitted binding isotherm of **2** + TBACl showing the change in chemical shift of the NH protons fitted to the 1:2 binding model (left), $K_{11} = 219.7 \text{ M}^{-1}$, $K_{12} = 4.4 \text{ M}^{-1}$. Residual plot showing the random error obtained from the binding isotherm fitting (right).

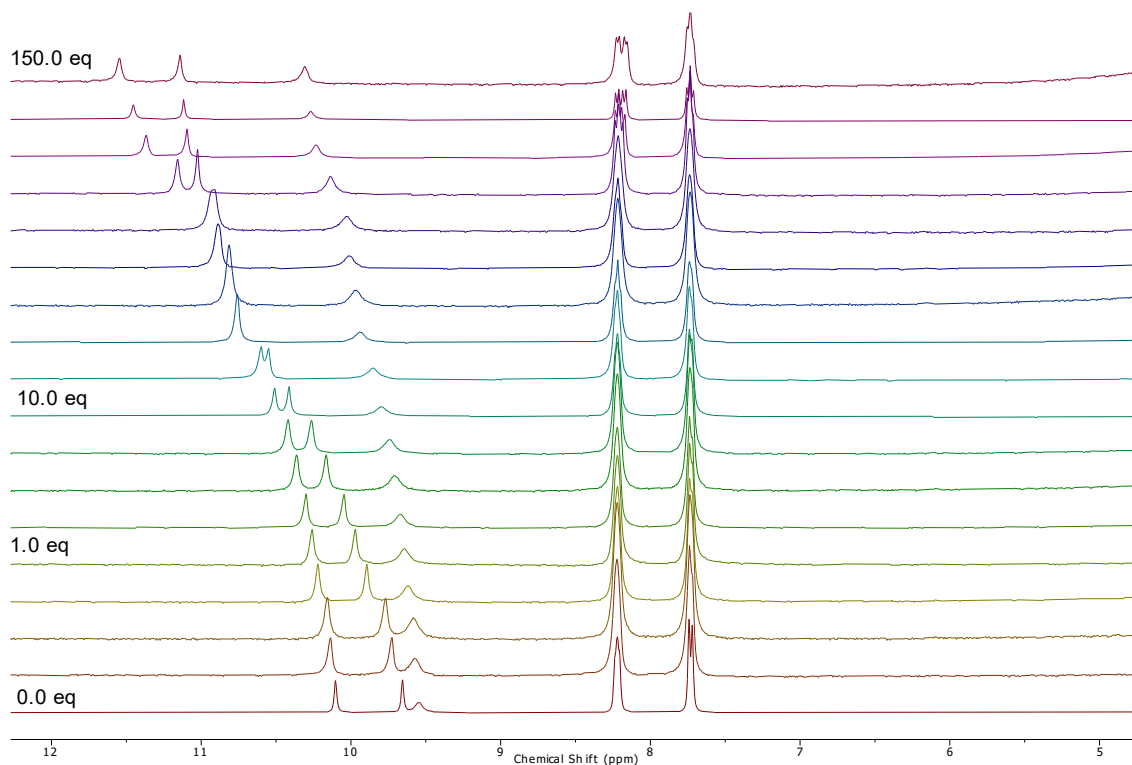


Figure S36. ^1H NMR (400 MHz) titration spectra as a stack plot for **3** (5 mM) + TBACl in $\text{DMSO-}d_6/0.5\%$ H_2O at 298 K.

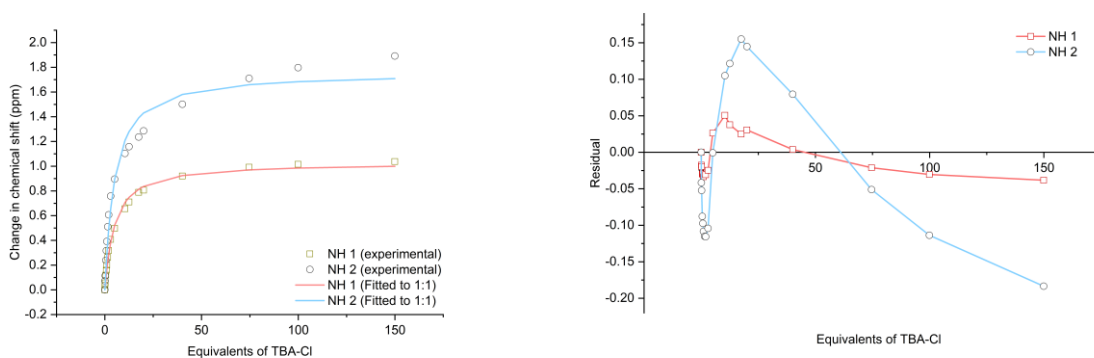


Figure S37. Fitted binding isotherm of **3** + TBACl showing the change in chemical shift of the NH protons fitted to the 1:1 binding model (left), $K_a = 46.9 \text{ M}^{-1}$. Residual plot showing the random error obtained from the binding isotherm fitting (right).

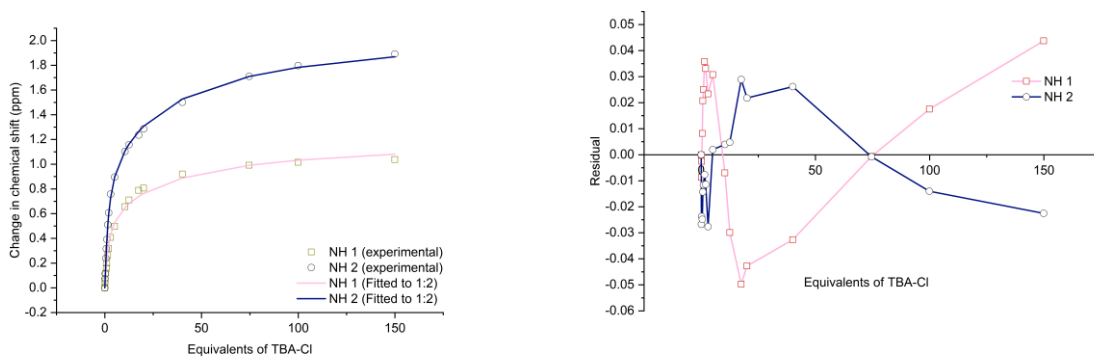


Figure S38. Fitted binding isotherm of **3** + TBACl showing the change in chemical shift of the NH protons fitted to the 1:2 binding model (left), $K_{11} = 196.0 \text{ M}^{-1}$, $K_{12} = 5.4 \text{ M}^{-1}$. Residual plot showing the random error obtained from the binding isotherm fitting (right).

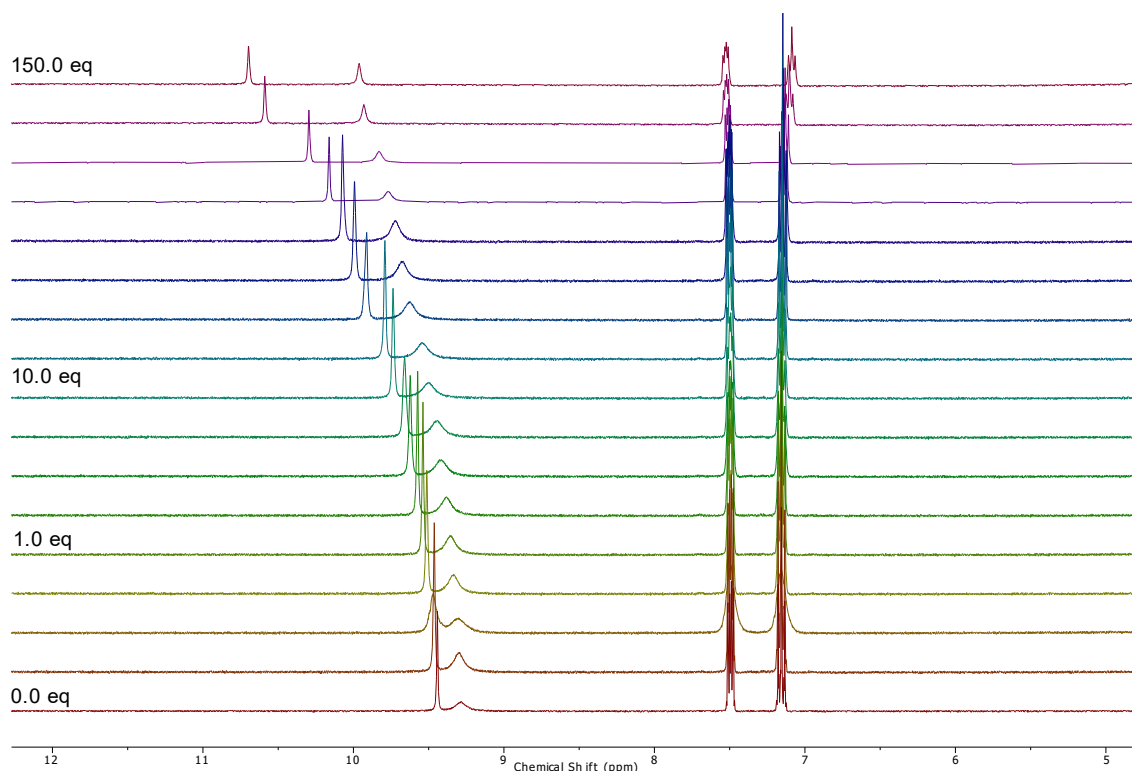


Figure S39. ^1H NMR (400 MHz) titration spectra as a stack plot for **4** (5 mM) + TBACl in $\text{DMSO-}d_6/0.5\% \text{ H}_2\text{O}$ at 298 K.

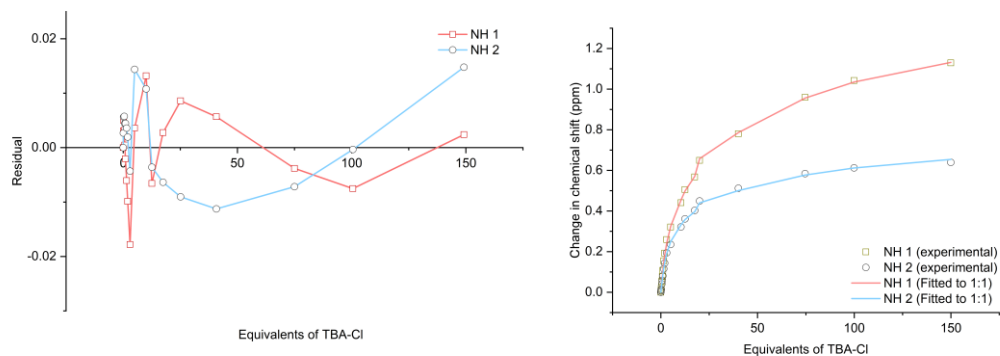


Figure S40. Fitted binding isotherm of **4** + TBACl showing the change in chemical shift of the NH protons fitted to the 1:1 binding model (left), $K_a = 15.8 \text{ M}^{-1}$. Residual plot showing the random error obtained from the binding isotherm fitting (right).

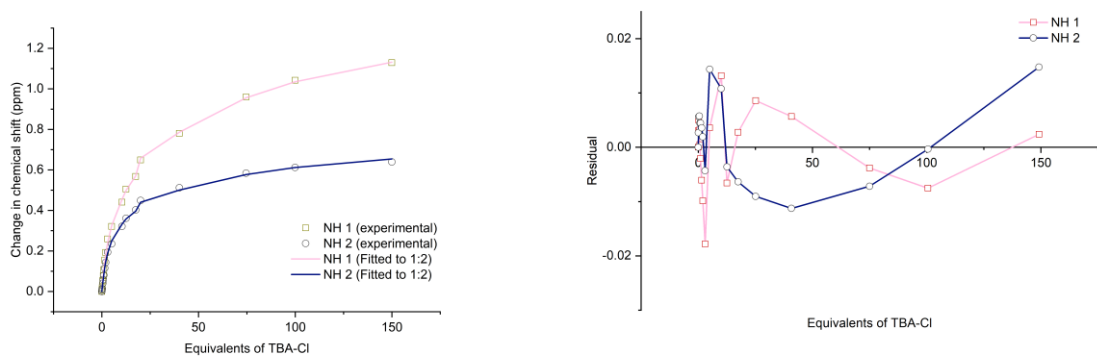


Figure S41. Fitted binding isotherm of **4** + TBACl showing the change in chemical shift of the NH protons fitted to the 1:2 binding model (left), $K_{11} = 86.4 \text{ M}^{-1}$, $K_{12} = 3.2 \text{ M}^{-1}$. Residual plot showing the random error obtained from the binding isotherm fitting (right).

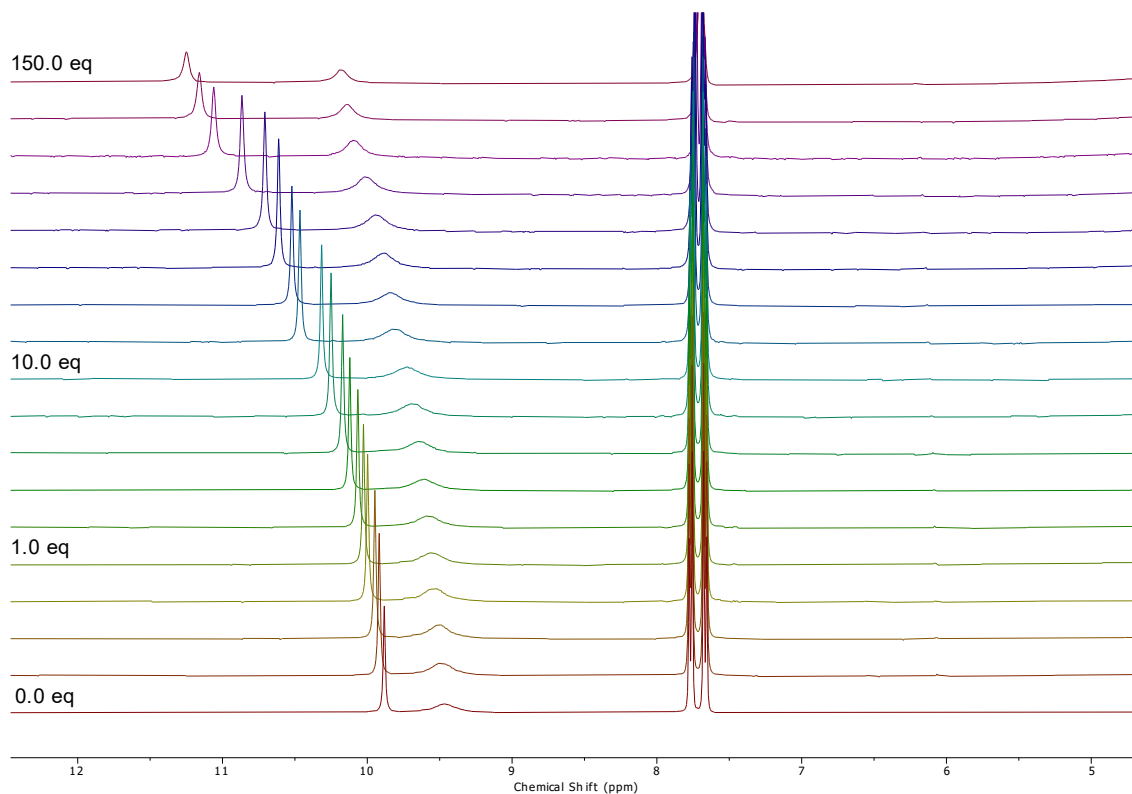


Figure S42. ^1H NMR (400 MHz) titration spectra as a stack plot for **5** (5 mM) + TBACl in $\text{DMSO-}d_6/0.5\%$ H_2O at 298 K.

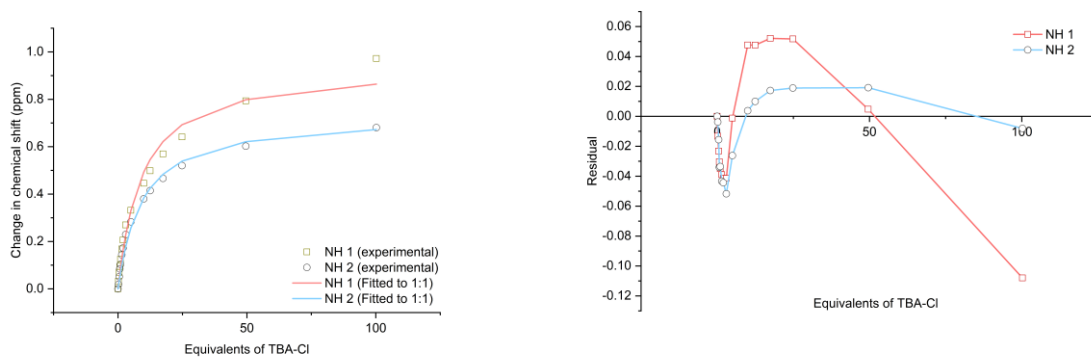


Figure S43. Fitted binding isotherm of **5** + TBACl showing the change in chemical shift of the NH protons fitted to the 1:1 binding model (left), $K_a = 25.9 \text{ M}^{-1}$. Residual plot showing the random error obtained from the binding isotherm fitting (right).

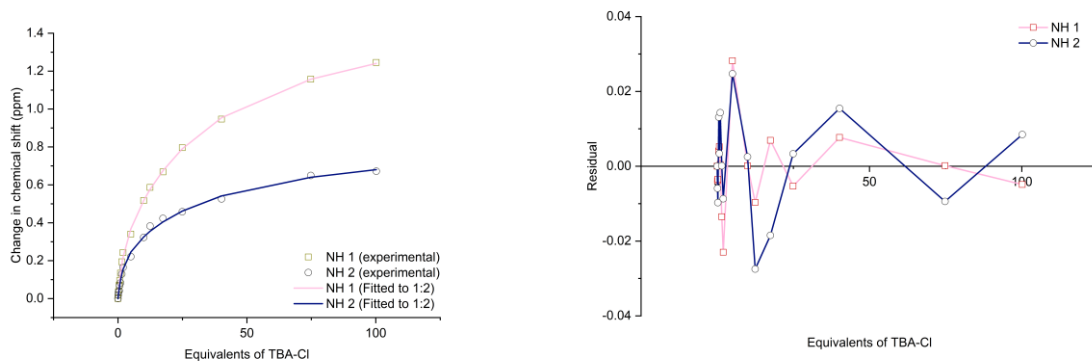


Figure S44. Fitted binding isotherm of **5** + TBACl showing the change in chemical shift of the NH protons fitted to the 1:2 binding model (left), $K_{11} = 206.2 \text{ M}^{-1}$, $K_{12} = 7.2 \text{ M}^{-1}$. Residual plot showing the random error obtained from the binding isotherm fitting (right).

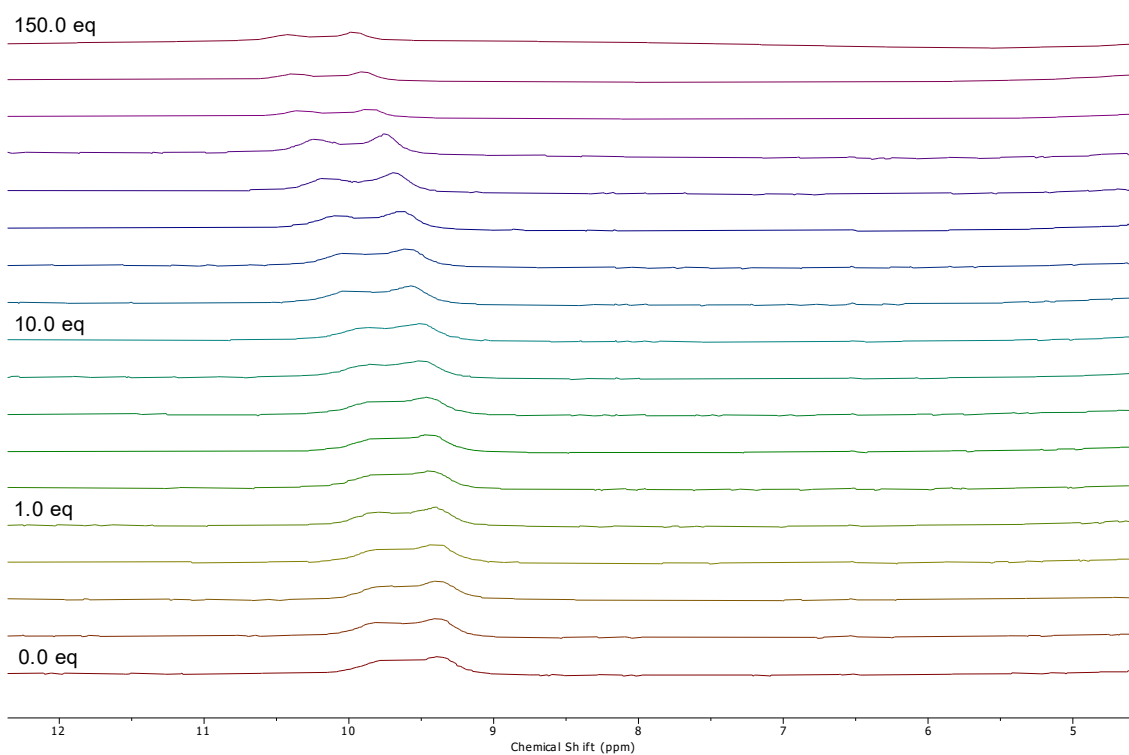


Figure S45. ^1H NMR (400 MHz) titration spectra as a stack plot for **6** (5 mM) + TBACl in $\text{DMSO-}d_6/0.5\%$ H_2O at 298 K.

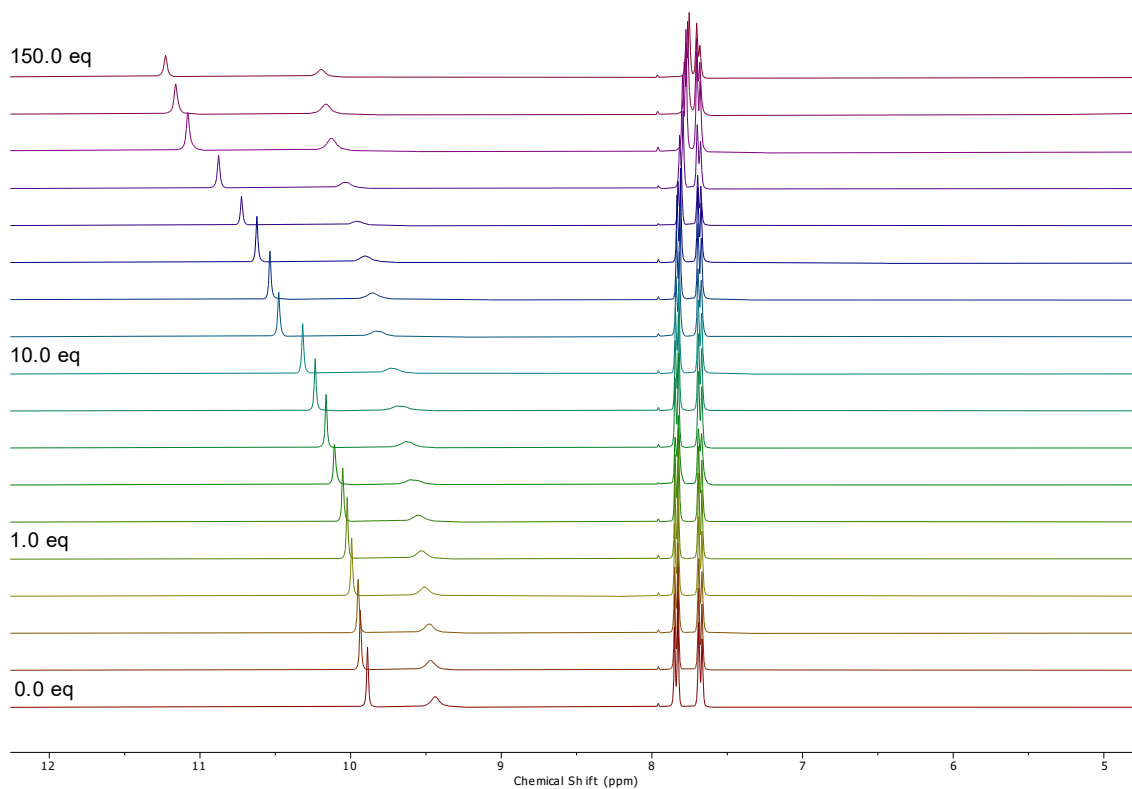


Figure S46. ^1H NMR (400 MHz) titration spectra as a stack plot for **7** (5 mM) + TBACl in $\text{DMSO-}d_6/0.5\%$ H_2O at 298 K.

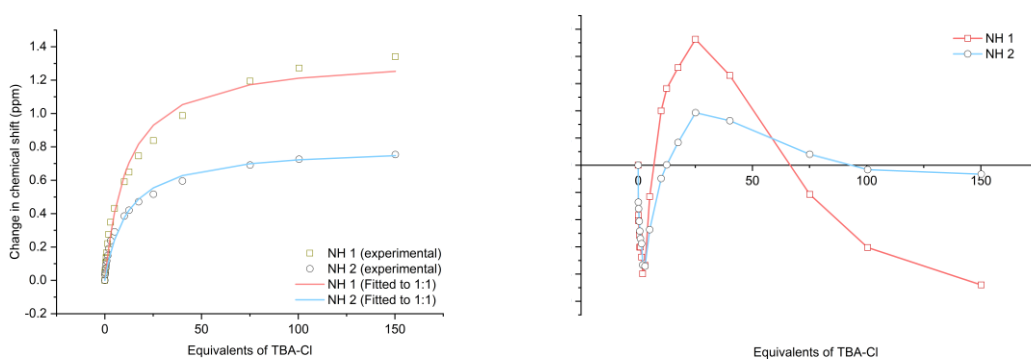


Figure S47. Fitted binding isotherm of **7** + TBACl showing the change in chemical shift of the NH protons fitted to the 1:1 binding model (left), $K_a = 18.3 \text{ M}^{-1}$. Residual plot showing the random error obtained from the binding isotherm fitting (right).

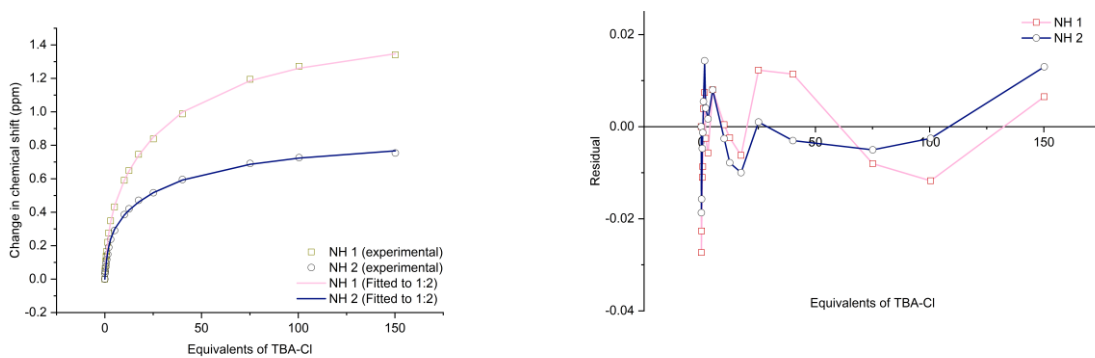


Figure S48. Fitted binding isotherm of **7** + TBACl showing the change in chemical shift of the NH protons fitted to the 1:2 binding model (left), $K_{11} = 211.1 \text{ M}^{-1}$, $K_{12} = 5.4 \text{ M}^{-1}$. Residual plot showing the random error obtained from the binding isotherm fitting (right).

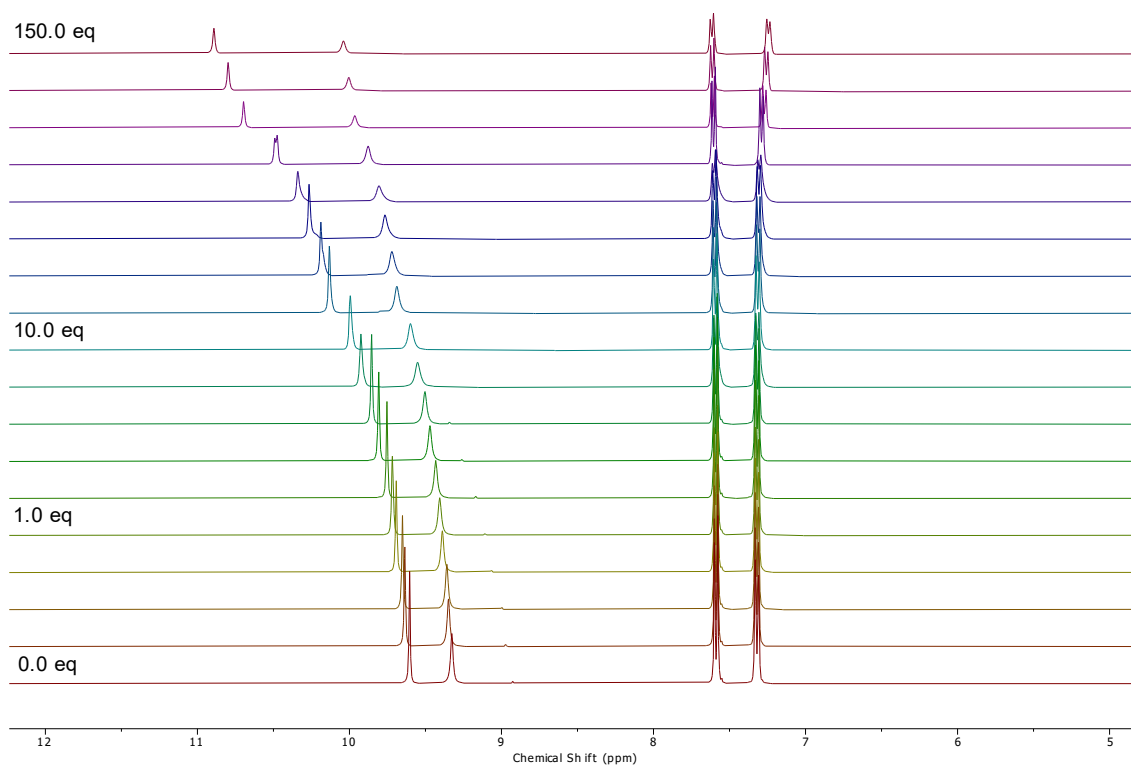


Figure S49. ^1H NMR (400 MHz) titration spectra as a stack plot for **8** (5 mM) + TBACl in $\text{DMSO-}d_6/0.5\% \text{ H}_2\text{O}$ at 298 K.

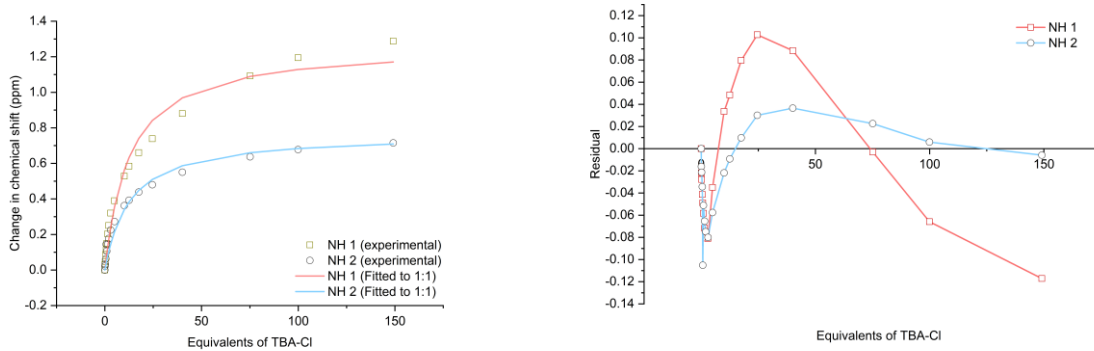


Figure S50. Fitted binding isotherm of **8** + TBACl showing the change in chemical shift of the NH protons fitted to the 1:1 binding model (left), $K_a = 16.4 \text{ M}^{-1}$. Residual plot showing the random error obtained from the binding isotherm fitting (right).

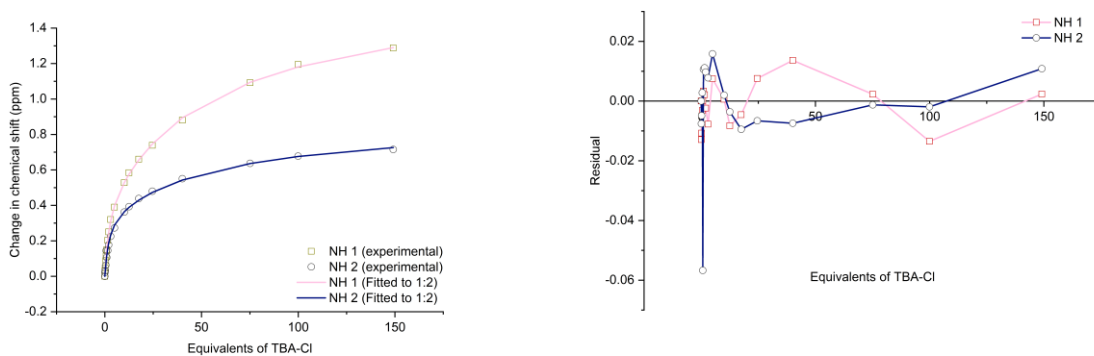


Figure S51. Fitted binding isotherm of **8** + TBACl showing the change in chemical shift of the NH protons fitted to the 1:2 binding model (left), $K_{11} = 155.7 \text{ M}^{-1}$, $K_{12} = 3.4 \text{ M}^{-1}$. Residual plot showing the random error obtained from the binding isotherm fitting (right).

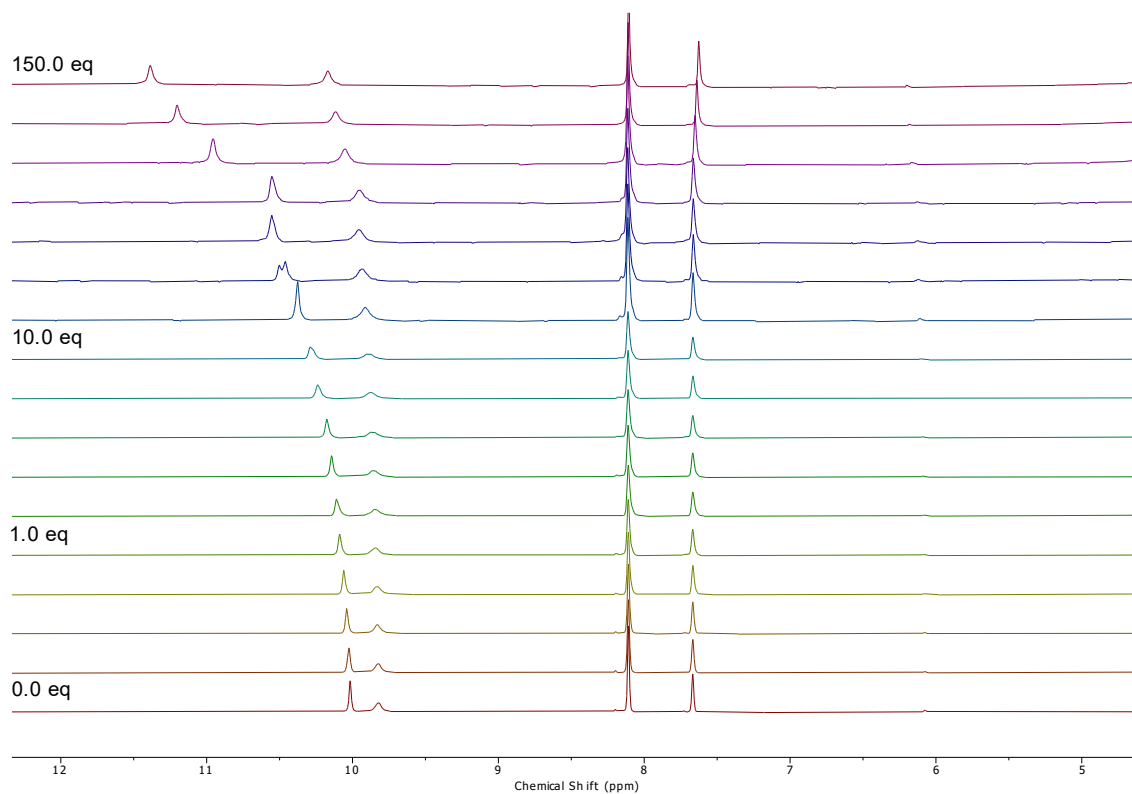


Figure S52. ^1H NMR (400 MHz) titration spectra as a stack plot for **9** (5 mM) + TBACl in $\text{DMSO-}d_6/0.5\%$ H_2O at 298 K.

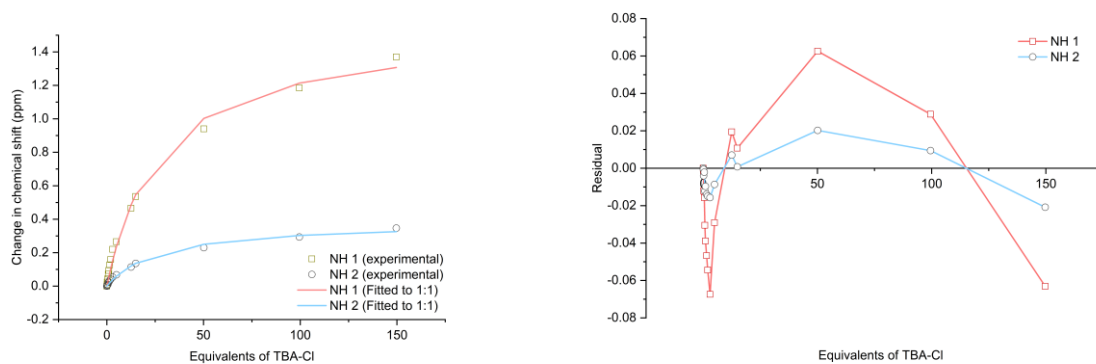


Figure S53. Fitted binding isotherm of **9** + TBACl showing the change in chemical shift of the NH protons fitted to the 1:1 binding model (left), $K_a = 20.2 \text{ M}^{-1}$. Residual plot showing the random error obtained from the binding isotherm fitting (right).

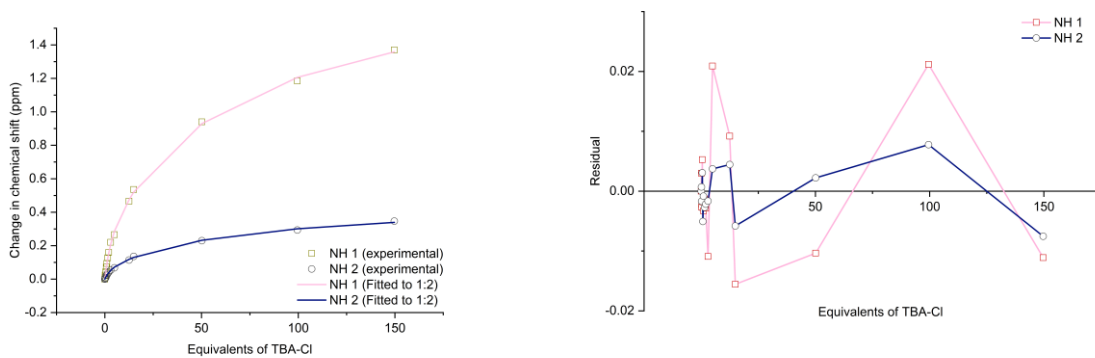


Figure S54. Fitted binding isotherm of **9** + TBACl showing the change in chemical shift of the NH protons fitted to the 1:2 binding model (left), $K_{11} = 220.4 \text{ M}^{-1}$, $K_{12} = 7.2 \text{ M}^{-1}$. Residual plot showing the random error obtained from the binding isotherm fitting (right).

Transport studies

General remarks and vesicle preparation

POPC (1- palmitoyl-2-oleoyl-sn-glycero-3-phosphocholine) was stored at -20°C as a solution in chloroform (1 g POPC in 35 mL chloroform) and was supplied by Corden Pharma Switzerland LLC. Triton X-100 was used as detergent and was supplied by Sigma-Aldrich.

Unilamellar vesicles were prepared following literature procedure.^[4] A lipid film of POPC (1-palmitoyl-2-oleoyl-sn-glycero-3-phosphocholine) was prepared from a chloroform solution evaporated under reduced pressure and dried under high vacuum for 8 or more h. The lipid film was rehydrated by vortexing with an aqueous metal chloride (MCl) salt solution until the lipids were removed from the sides. The suspension was subjected to nine freeze-thaw cycles by freezing in a liquid nitrogen bath and thawing in room temperature water bath. The lipid suspension was allowed to rest at room temperature for 30 min and was subsequently extruded 25 times through a 200nm polycarbonate membrane (Nucleopore TM) using an extruder set (Avanti Polar Lipids Inc) to form monodisperse vesicles. The resulting unilamellar vesicles were dialysed (Spectra/Por[®] 2 Membrane MWCO 12-14kD) against the external solution to remove unencapsulated MCl salts.

ISE-based studies

Cl^- concentrations during the transport experiments for the $\text{Cl}^-/\text{NO}_3^-$ exchange and cationophore couple assay were determined using an Accumet Cl^- ion selective electrode (ISE). The electrode was calibrated against NaCl solutions of known concentrations prior to each experiment in accordance with the supplier's manual. The electrode potential, y , was plotted against the respective concentration of NaCl, x , and fit to a simplified version of the Nernst equation (**Equation 3**) in *Origin2022* to afford the calibration parameters P_1 and P_2

$$y = (P_1 \log_{10} x) + P_2$$

Equation 1. The simplified Nernst Equation.

Using **Equation 3**, the Cl^- concentration can be calculated at any point during the experiments by using the calculated parameters, P_1 , P_2 , and the raw electrode value, y , to solve for x . Subtracting the Cl^- concentration at $t = 0$ from the Cl^- concentration at any time point within the experiment ($t \geq 0$) provided the total Cl^- concentration released from the vesicles at any given time. The data was subsequently converted to percentage Cl^- efflux to allow for a simpler comparison. This conversion involved normalising that data using the 100% Cl^- efflux value recorded at the end of the experiment, $t = 420$ s, upon treatment of Triton X-100 (11 wt%) in $\text{H}_2\text{O}:\text{DMSO}$ (7:1 v/v). The Cl^- efflux (%) was plotted as a function of the receptor concentration (mol%) and were fit to the Hill equation using *Origin2022*:

$$y = y_0 + (y_1 - y_0) \frac{x^n}{k^n + x^n}$$

Equation 2. The Hill equation

$$y = V_{max} \frac{x^n}{k^n + x^n} = 100\% \frac{x^n}{(EC_{50})^n + x^n}$$

Equation 3. The Hill equation with substituted values for anion transport assays.

Where y is the Cl⁻ efflux at 270 s (%) and x is the carrier concentration (mol%, carrier to lipid). V_{max} is the maximum efflux possible (often fixed to 100% (hence, $y_0 = 0$ and $y_1 = 100$), as this is physically the maximum Cl⁻ efflux possible), and k is the carrier concentration needed to reach $V_{max}/2$ (when V_{max} is fixed to 100%, k equals EC_{50}). The sigmoidicity of the curve is represented by the Hill coefficient, n .

Initial rate calculations

$k_{initial}$ values were calculated by fitting the obtained Cl⁻ efflux to a non-linear exponential decay function (**Equation 4**).

$$y = A_1 e^{\left(\frac{-x}{t_1}\right)} + A_2 e^{\left(\frac{-x}{t_2}\right)} + y_0$$

Equation 4. A non-linear exponential decay function

Where y represents the percentage of Cl⁻ efflux (%), x is the receptor concentration (mol%), y_0 is the percentage Cl⁻ efflux at $t = 0$ s, and A_1 , A_2 , t_1 , and t_2 are the derived parameters. The initial rate was obtained by calculating the first derivative at $x = 0$ (**Equation 5**), which is given as:

$$k_{initial} = \frac{-A_1}{t_1} - \frac{A_2}{t_2}$$

Equation 5. First derivative of the decay function used to calculate the initial rate given in % s⁻¹.

Where appropriate, $k_{initial}$ values were calculated by fitting to the initial linear range of the obtained Cl⁻ efflux to **Equation 6**.

$$y = a + bx,$$

Equation 6. Linear equation used to calculate the initial rate given in % s⁻¹.

Where y represents the percentage the Cl⁻ efflux (%), x is time (s) and $k_{initial}$ is given by the slope b . In case of a sigmoidal time dependence, the first two or three data points were omitted from the fit. In order to obtain standard deviations on the initial rate of transport, the fits were performed for each individual repeat and subsequently averaged.

Cationophore coupled assay

Vesicles were prepared as described above with an internal solution of KCl (300 mM) adjusted to pH 7.2 with phosphate buffer (5 mM). The lipids were suspended in an external solution of KGlu (300 mM) buffered to pH 7.2 with phosphate buffer (5 mM). Following the extrusion of the lipids, the solution was subject to size exclusion chromatography using G-25 Sephadex[®] pre equilibrated with the KGlu external solution. The same solution was used to elute the lipids which were subsequently diluted to a 1 mM concentration.

Each experiment was prepared by adding 0.5 mL of the 1 mM lipid solution to a 4.5 mL solution of KGlu. The transporter was added as a solution of DMSO (10 μ L) to initiate the start of the experiment, efflux of Cl⁻ out of the vesicles was monitored by an ISE. After 300 s, the vesicles were lysed using a solution of Triton X-100 in H₂O/DMSO (7:1, v/v) (50 μ L) and then 100% Cl⁻ efflux reading was taken after 420 s. The electrode voltages were converted to Cl⁻ concentration using a standard calibration, the final 700 s value was used as 100% Cl⁻ efflux and the initial 0 s value was set to 0% Cl⁻ efflux. The data points were converted to percentages and plotted as a function of transporter concentration (mol%, transporter:lipid molar concentration).

Two solutions of ionophores valinomycin and monensin were prepared as a DMSO solution (0.1 mol%, transporter:lipid molar concentration). Either the valinomycin or the monensin solution was added (10 μ L) to the test solution -30 s before the start of the experiment and the Cl⁻ efflux was recorded as described above. DMSO control experiments were performed in the absence of the transporter, and experiments were repeated in duplicate.

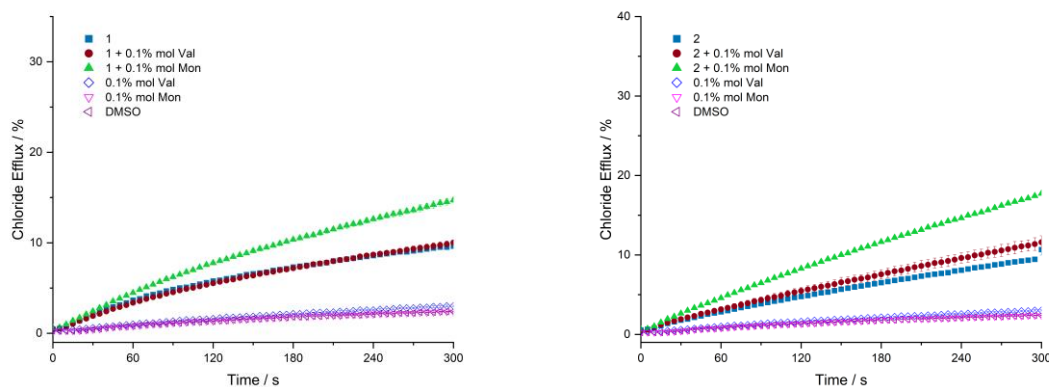


Figure S55. Chloride efflux facilitated by **1** (left, 10 mol%) and **2** (right, 10 mol%) in POPC vesicles loaded with 300 mM KCl and suspended in an isotonic external solution of KGlu in the presence of 0.1 mol% monensin (green), 0.1 mol% valinomycin (red), and alone (blue). Each data point is the average of two repeats, with the error bars showing the standard deviation.

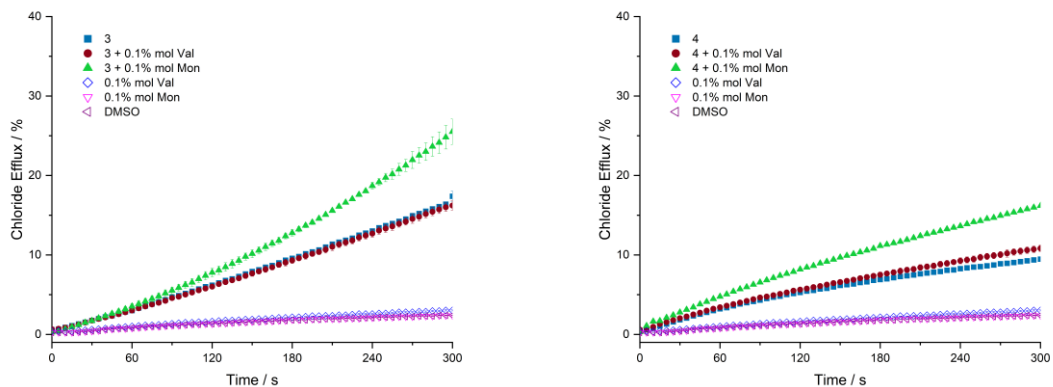


Figure S56. Chloride efflux facilitated by **3** (left, 10 mol%) and **4** (right, 10 mol%) in POPC vesicles loaded with 300 mM KCl and suspended in an isotonic external solution of KGluc in the presence of 0.1 mol% monensin (green), 0.1 mol% valinomycin (red), and alone (blue). Each data point is the average of two repeats, with the error bars showing the standard deviation.

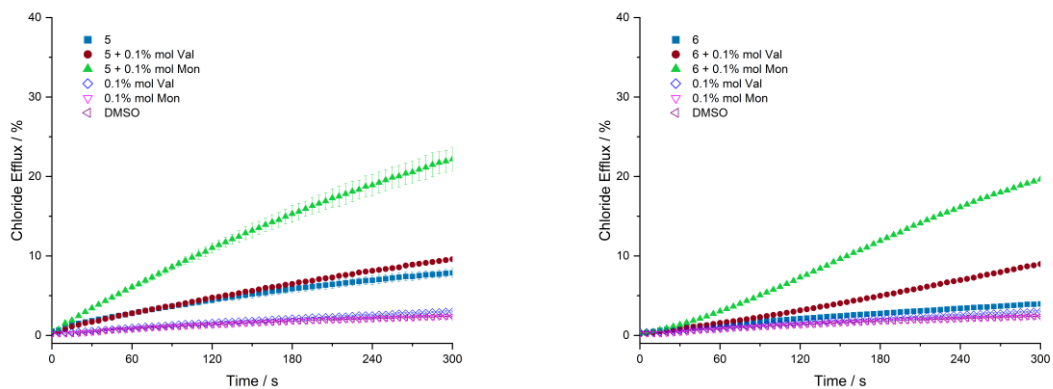


Figure S57. Chloride efflux facilitated by **5** (left, 10 mol%) and **6** (right, 10 mol%) in POPC vesicles loaded with 300 mM KCl and suspended in an isotonic external solution of KGluc in the presence of 0.1 mol% monensin (green), 0.1 mol% valinomycin (red), and alone (blue). Each data point is the average of two repeats, with the error bars showing the standard deviation.

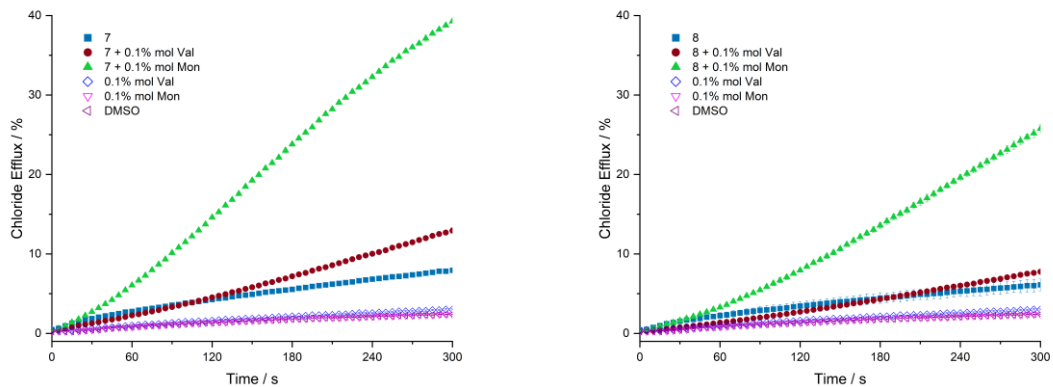


Figure S58. Chloride efflux facilitated by **7** (left, 10 mol%) and **8** (right, 10 mol%) in POPC vesicles loaded with 300 mM KCl and suspended in an isotonic external solution of K₂Glu in the presence of 0.1 mol% monensin (green), 0.1 mol% valinomycin (red), and alone (blue). Each data point is the average of two repeats, with the error bars showing the standard deviation.

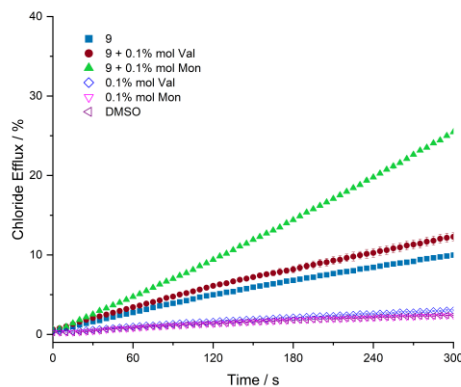


Figure S59. Chloride efflux facilitated by **9** (10 mol%) in POPC vesicles loaded with 300 mM KCl and suspended in an isotonic external solution of K₂Glu in the presence of 0.1 mol% monensin (green), 0.1 mol% valinomycin (red), and alone (blue). Each data point is the average of two repeats, with the error bars showing the standard deviation.

Fluorescence HPTS-based studies

NMDG-Cl assay

Vesicles were prepared as described above with an internal solution of HPTS (1 mM) in NMDG-Cl (100 mM) buffered to pH 7.0 with HEPES (10 mM). The lipids were suspended in an external solution of NMDG-Cl (100 mM) similarly buffered to pH 7.0 with HEPES (10 mM). Following the extrusion of the lipids, the solution was subject to size exclusion chromatography using G-25 Sephadex® pre equilibrated with the NMDG-Cl external solution. The same solution was used to elute the lipids which were subsequently diluted to 10 mL of a known concentration.

The lipid stock was diluted with external solution in a 2.5 mL cuvette to give the test solution (0.1 mM, 2.5 mL). An NMDG base pulse (25 µL, 0.5 M) was added to basify the external solution to pH 8.0 and the transporters were added as a solution of DMSO (5 µL) to initiate the start of the experiment. The fluorescence emission of the intravesicular HPTS was recorded using a fluorometer. After $t = 210$ s a solution of Triton X-100 (11 w%) in DMSO:H₂O (1:7, v/v) (25 µL) was added to lyse the vesicles to fully dissipate the pH gradient and a final fluorescence reading was $t = 300$ s. Experiments that included the use of Gramicidin (Gra, 0.1 mol%) or oleic acid (OA, 2 mol%) were added as a DMSO solution (5 µL) prior to the addition of the transporter.

Fatty acid sequestered vesicles were prepared by the addition of bovine serum albumin (BSA, 1 mol%) to a portion of the vesicles and agitated for a minimum of 2 h. The experimental procedure was performed as described above using the BSA treated vesicles. DMSO control experiments were performed in the absence of the transporter, and experiments were repeated in triplicate.

HPTS was used as a ratiometric probe to measure the H⁺/Cl⁻ symport (or equivalent OH⁻/Cl⁻ antiport) through the intravesicular pH change during the experiment. The acidic and basic forms of HPTS were excited at $\lambda_{\text{ex}} = 403$ nm and $\lambda_{\text{ex}} = 460$ nm respectively, and the fluorescence emission of both forms was collected at $\lambda_{\text{em}} = 510$ nm. The fluorescence intensity ratio (R) of the basic form and the acidic form of HPTS was calculated, which allowed the calculation of the fractional fluorescence intensity (I_f) using **Equation 7**.

$$I_f = \frac{R_t - R_0}{R_d - R_0}$$

Equation 7. Calculation of the fractional fluorescence intensity (I_f) from the raw HPTS data.

Where R_t is the ratiometric fluorescence value at a given time (t), R_0 is the ratiometric fluorescence value at $t = 0$ s and R_d is the fluorescence ratiometric value recorded at $t = 300$ s following vesicular lysis.

Dose response experiments were performed with at least six different receptor concentrations providing varying percentage Cl⁻ efflux values at 200 s. The fractional fluorescence (I_f) was plotted as a function of the receptor concentration (mol %) and were fit to the Hill equation using *Origin2022*:

$$y = y_0 + (y_{\text{max}} - y_0) \frac{x^n}{k^n + x^n}$$

Equation 2. The Hill equation

Where y is the I_f at 200 s, y_0 is the I_f value at 200 s for the DMSO blank run, y_{max} is the maximum I_f value, x is the receptor concentration (mol %, with respect to lipid), n is the Hill coefficient and k is the concentration of transporter required to facilitate 0.5 I_f (EC_{50}).

NMDG-Cl assay

Fluorometer vesicle-based assay results and Hill analysis are shown for furazan bis-ureas **1–8**.

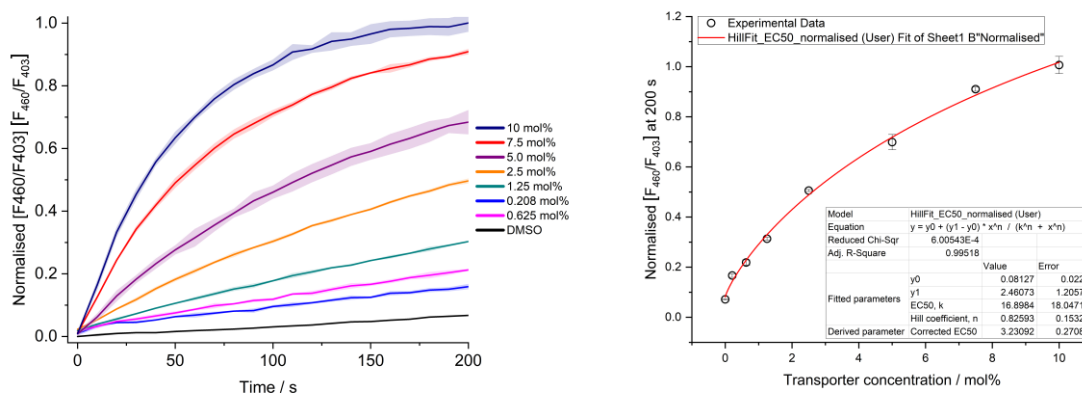


Figure S60. Hill analysis of H^+/Cl^- symport (or Cl^-/OH^- antiport) facilitated by **1** in the NMDG-Cl assay. Each data point is the average of three repeats, with the error bars showing the standard deviation and DMSO was used as a control.

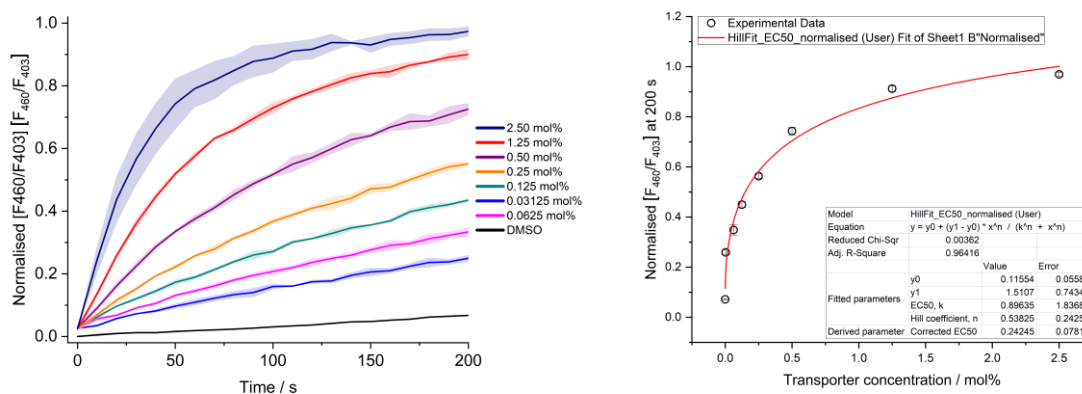


Figure S61. Hill analysis of H^+/Cl^- symport (or Cl^-/OH^- antiport) facilitated by **2** in the NMDG-Cl assay. Each data point is the average of three repeats, with the error bars showing the standard deviation and DMSO was used as a control.

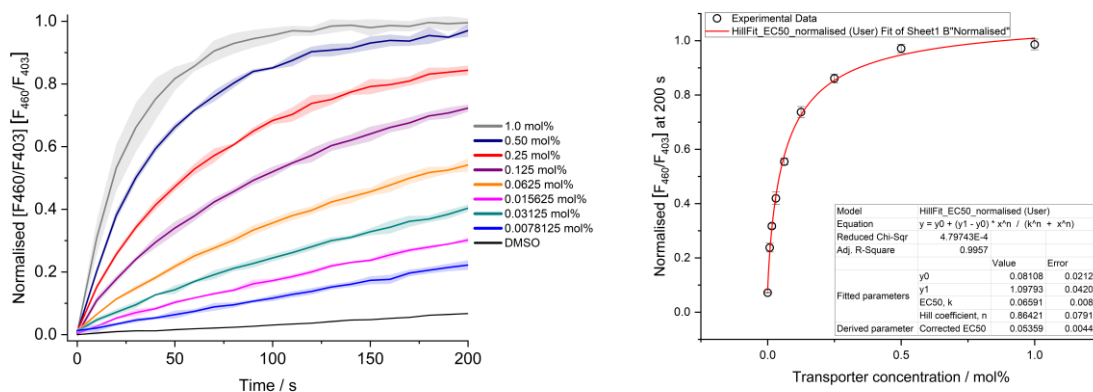


Figure S62. Hill analysis of H⁺/Cl⁻ symport (or Cl⁻/OH⁻ antiport) facilitated by **3** in the NMDG-Cl assay. Each data point is the average of three repeats, with the error bars showing the standard deviation and DMSO was used as a control.

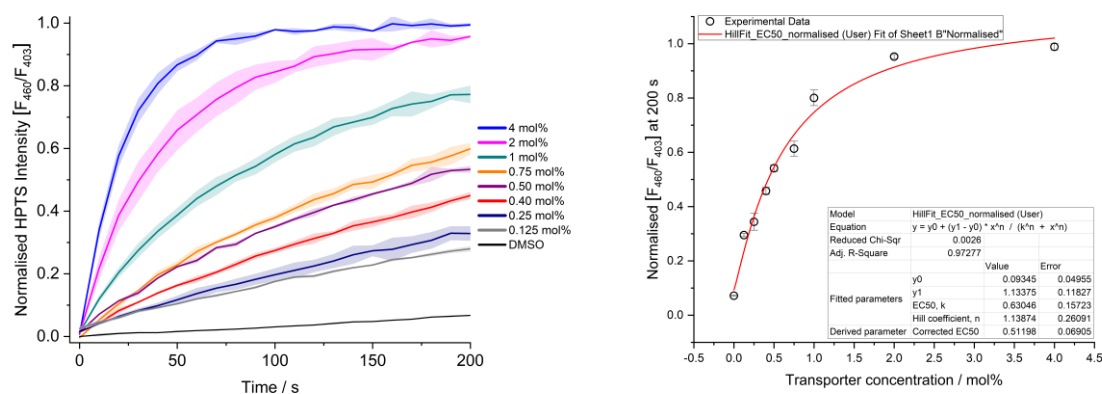


Figure S63. Hill analysis of H⁺/Cl⁻ symport (or Cl⁻/OH⁻ antiport) facilitated by **4** in the NMDG-Cl assay. Each data point is the average of three repeats, with the error bars showing the standard deviation and DMSO was used as a control.

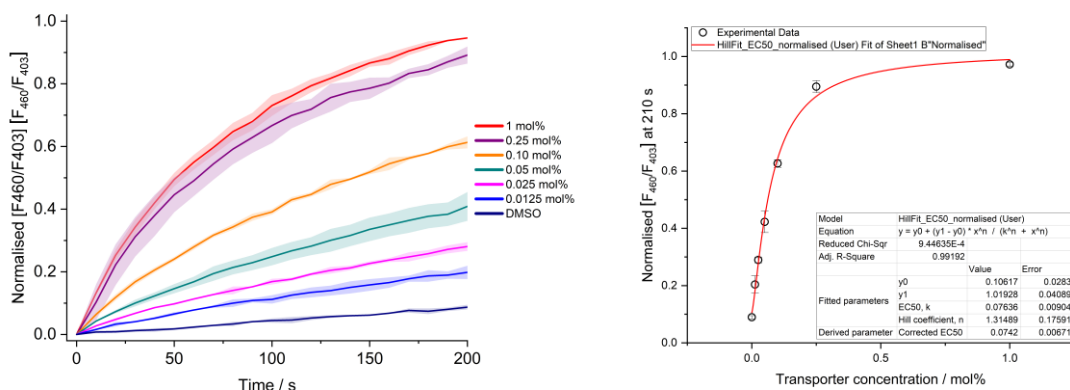


Figure S64. Hill analysis of H⁺/Cl⁻ symport (or Cl⁻/OH⁻ antiport) facilitated by **5** in the NMDG-Cl assay. Each data point is the average of three repeats, with the error bars showing the standard deviation and DMSO was used as a control.

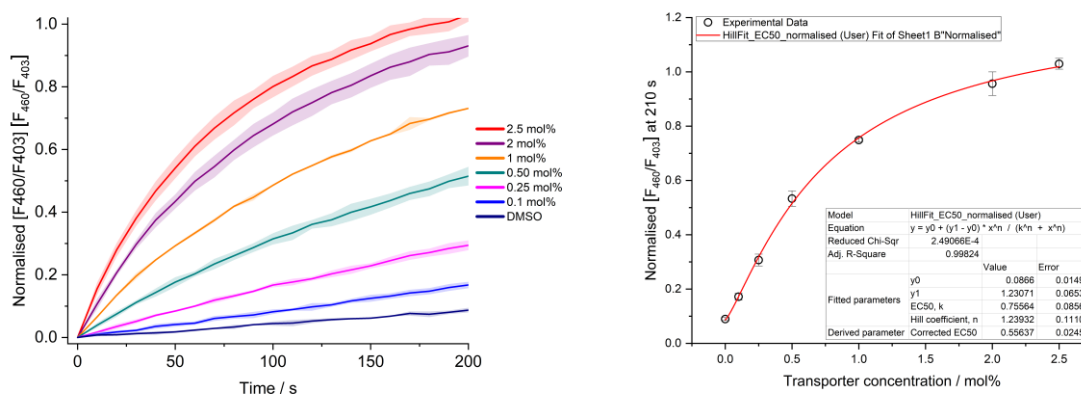


Figure S65. Hill analysis of H⁺/Cl⁻ symport (or Cl⁻/OH⁻ antiport) facilitated by **6** in the NMDG-Cl assay. Each data point is the average of three repeats, with the error bars showing the standard deviation and DMSO was used as a control.

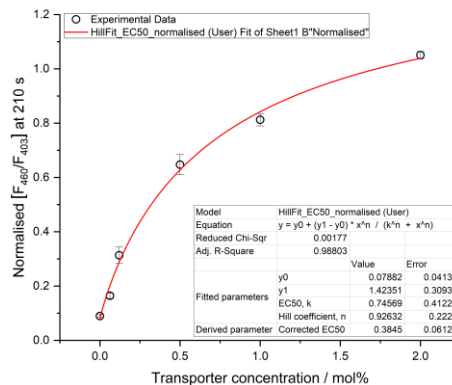
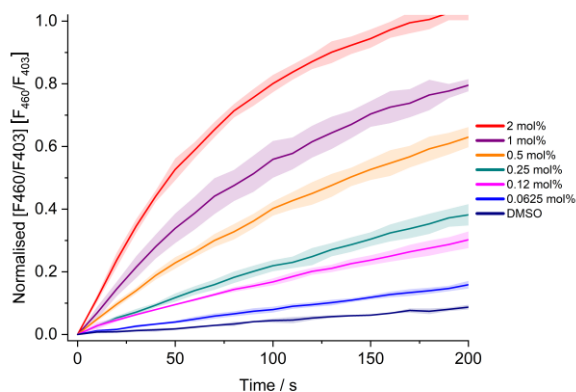


Figure S66. Hill analysis of H⁺/Cl⁻ symport (or Cl⁻/OH⁻ antiport) facilitated by **7** in the NMDG-Cl assay. Each data point is the average of three repeats, with the error bars showing the standard deviation and DMSO was used as a control.

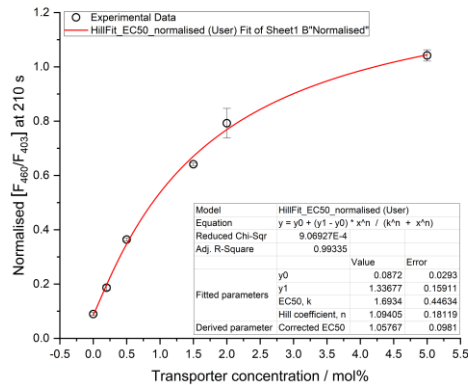
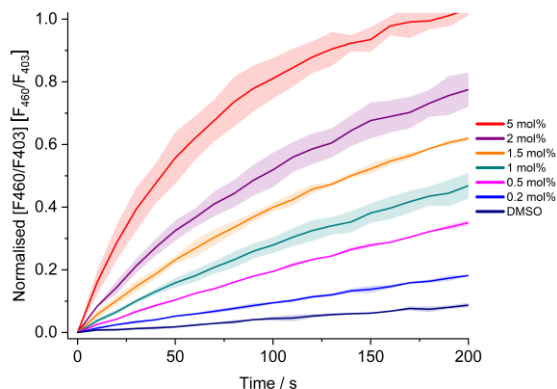


Figure S67. Hill analysis of H⁺/Cl⁻ symport (or Cl⁻/OH⁻ antiport) facilitated by **8** in the NMDG-Cl assay. Each data point is the average of three repeats, with the error bars showing the standard deviation and DMSO was used as a control.

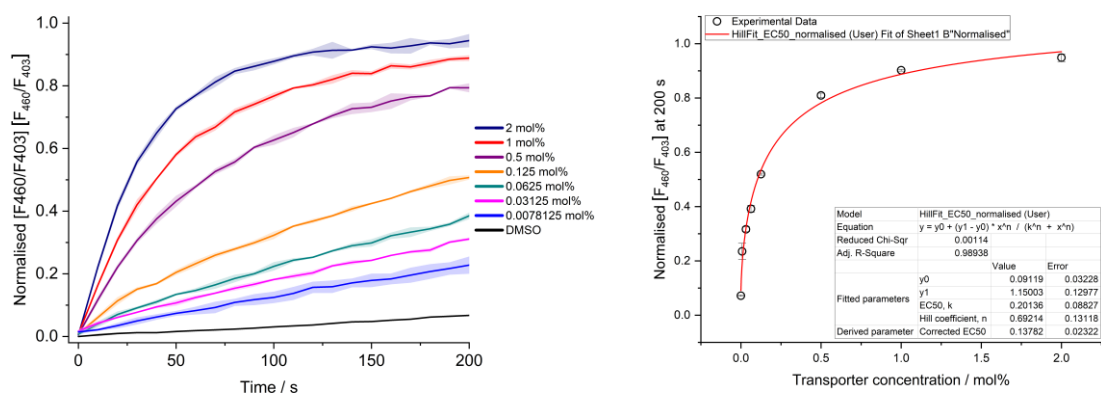


Figure S68. Hill analysis of H⁺/Cl⁻ symport (or Cl⁻/OH⁻ antiport) facilitated by **9** in the NMDG-Cl assay. Each data point is the average of three repeats, with the error bars showing the standard deviation and DMSO was used as a control.

Cell culture

A549 cell lines were cultured in T25 or T75 flasks and maintained in the exponential growth phase as monolayers in Advanced Dulbecco's Modified Eagle Medium (ADMEM), supplemented with 10% FBS, and 1% glutamine. Cells were incubated under standard culturing conditions at 37 °C with 5% CO₂ under humidified conditions. The cell lines were sub-cultured using 0.25% trypsin to facilitate cellular detachments from the flask. Cells were passaged every 3-4 days.

MTT cell viability assay

4T1 and HEK293 cells were seeded in 96 well plates in ADMEM (100 µL) at a density of 2.5×10^4 cells per well and allowed to adhere for 16 h. Stock solutions of the transporters were diluted to 400 µM in ADMEM, containing 1% DMSO. 100 µL of either ADMEM and PBS (for controls), ADMEM containing 1% DMSO and ADMEM containing the transporters were added to wells in triplicate. The cells were incubated for 24 h, before the addition of MTT. After a further 3 h incubation, the absorbance of each well was measured at 565 nm. Values were normalised to controls containing ADMEM and PBS and the data is presented as the average percentage viability of at least triplicate values from a single experiment.

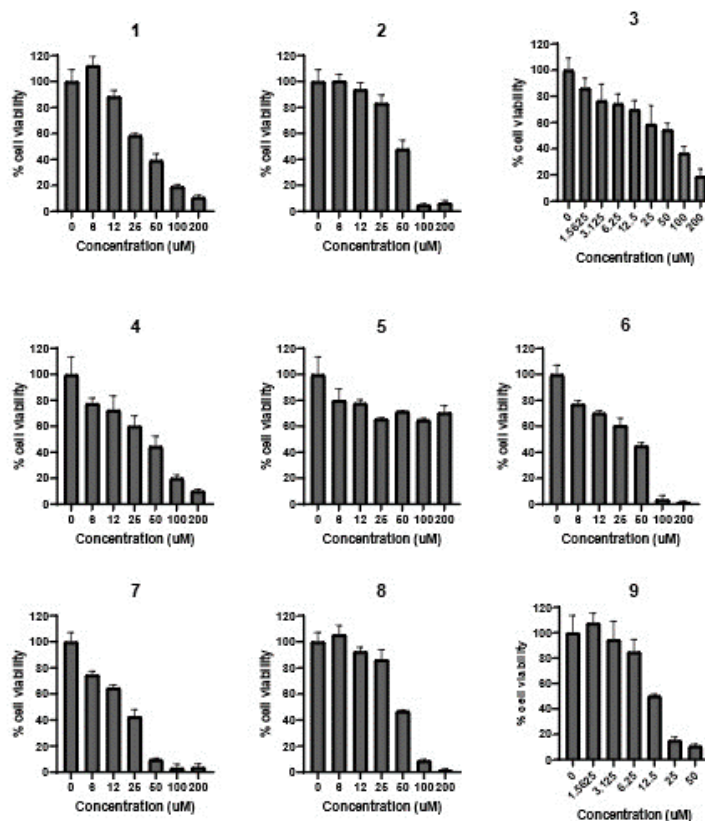


Figure S69. Dose-response cell viability results in the MTT assay from the HEK cell line when treated with varying doses of receptors 1–8 for 24 h. Experiments were performed in triplicate with the error bars showing the standard deviation.

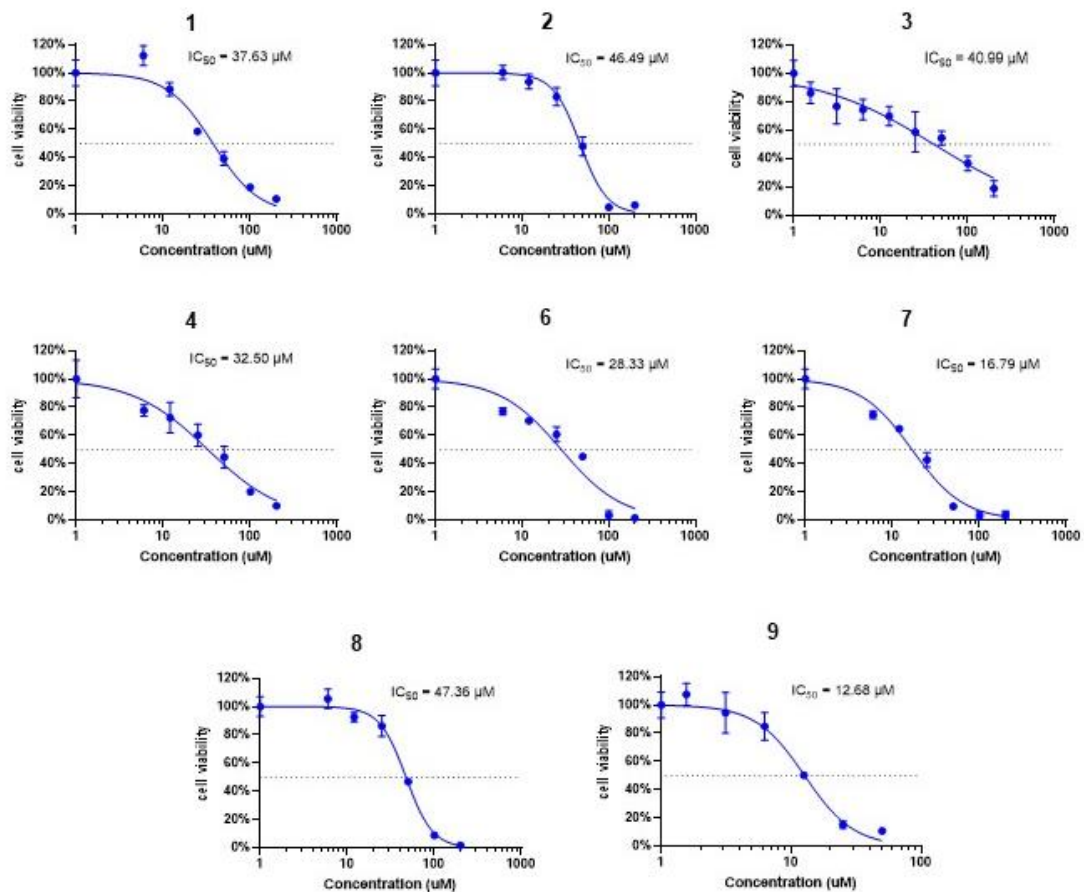


Figure S70. Dose-response cell viability curves in the MTT assay from the HEK cell line when treated with varying doses of receptors 1–8 for 24 h. Experiments were performed in triplicate with the error bars showing the standard deviation.

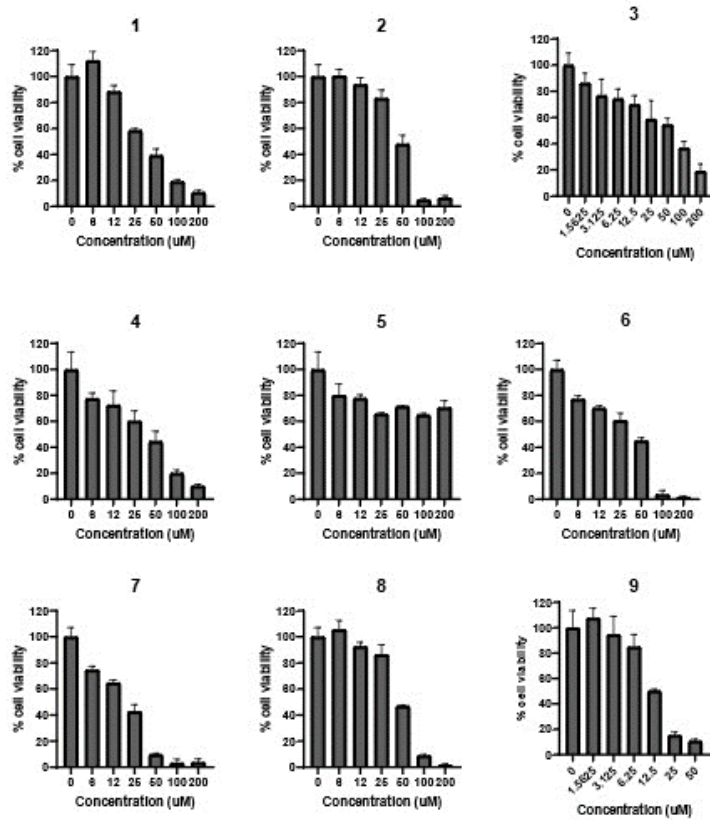


Figure S71. Dose-response cell viability results in the MTT assay from the 4T1 cell line when treated with varying doses of receptors 1–8 for 24 h. Experiments were performed in triplicate with the error bars showing the standard deviation.

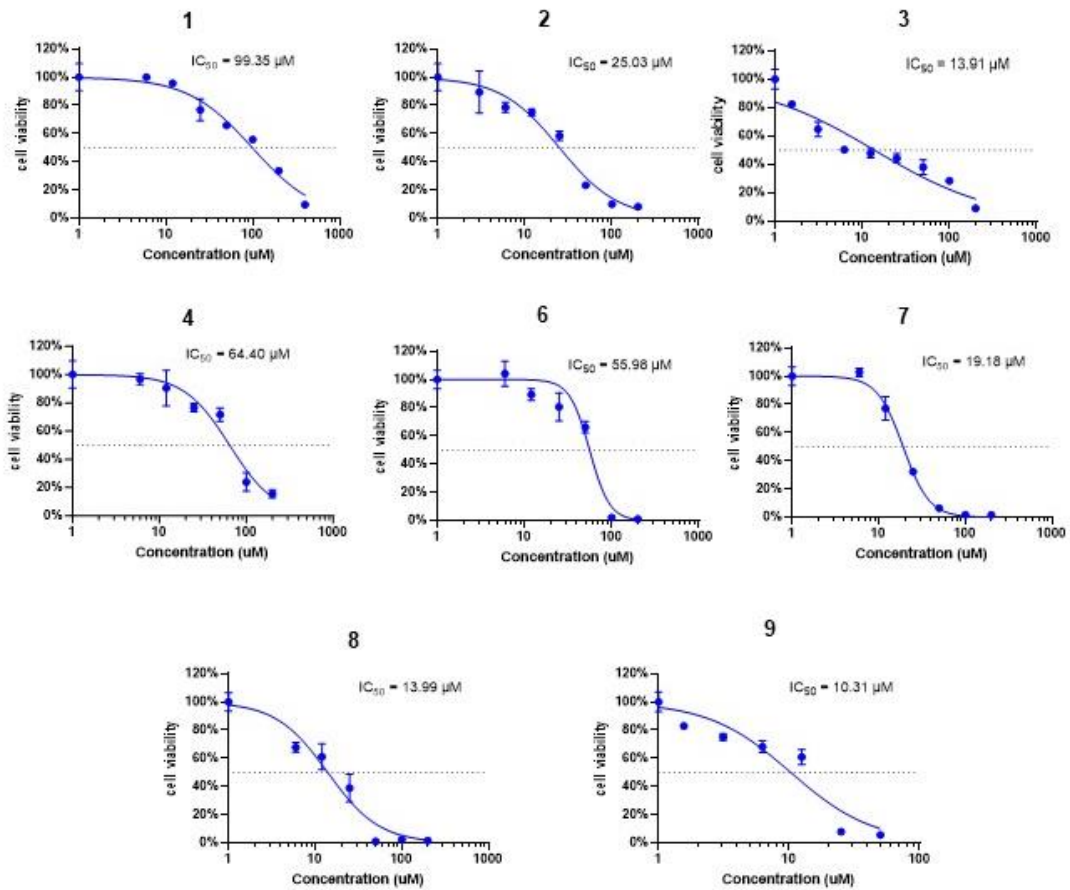


Figure S72. Dose-response cell viability curves in the MTT assay from the 4T1 cell line when treated with varying doses of receptors 1–8 for 24 h. Experiments were performed in triplicate with the error bars showing the standard deviation.

2D-NOESY ^1H NMR Spectroscopic Analysis

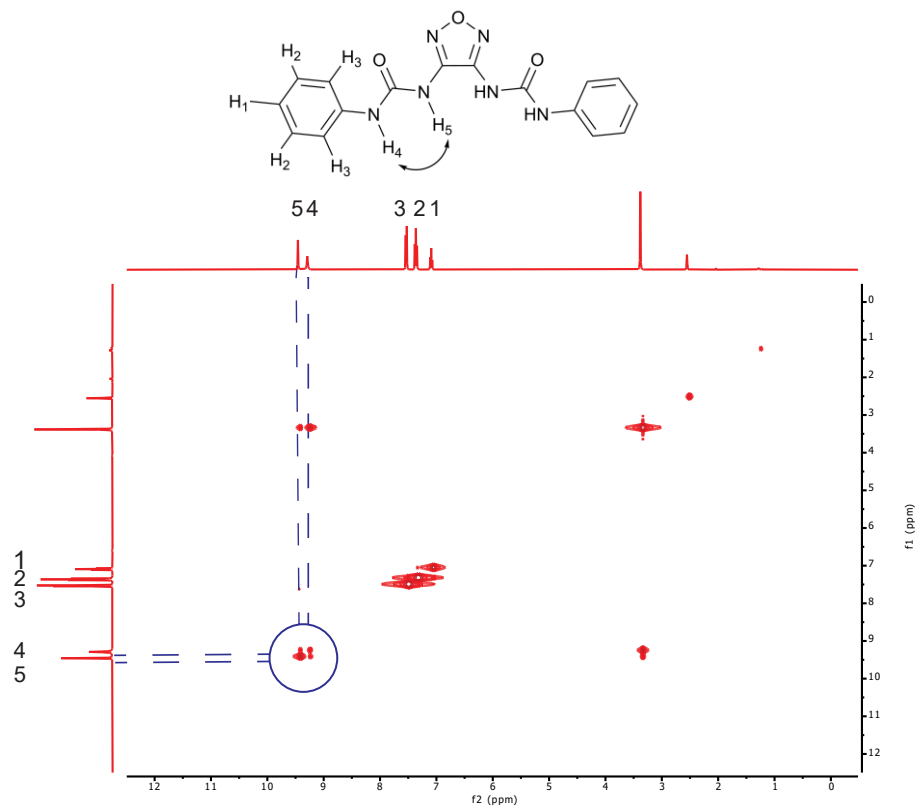


Figure S73. The 2D NOESY ^1H -NMR spectrum of **1** in d_6 -DMSO.

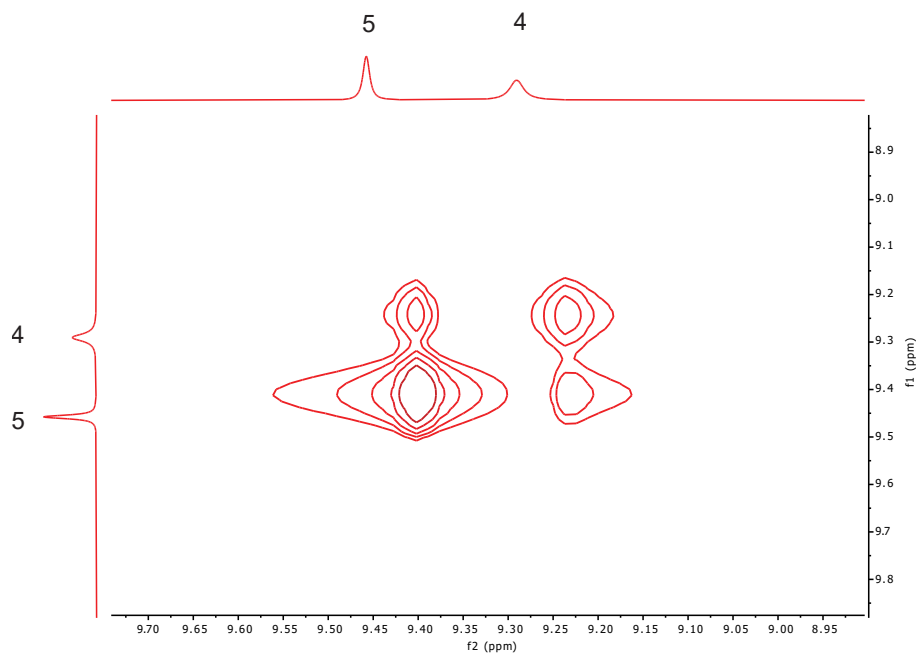


Figure S74. A magnified segment of the 2D NOESY ^1H -NMR spectrum of **1** in d_6 -DMSO, showing the cross-peak interactions between the signals of the two NH urea protons, H4 and H5 ($\delta = 9.40$ ppm and $\delta = 9.24$ ppm, respectively).

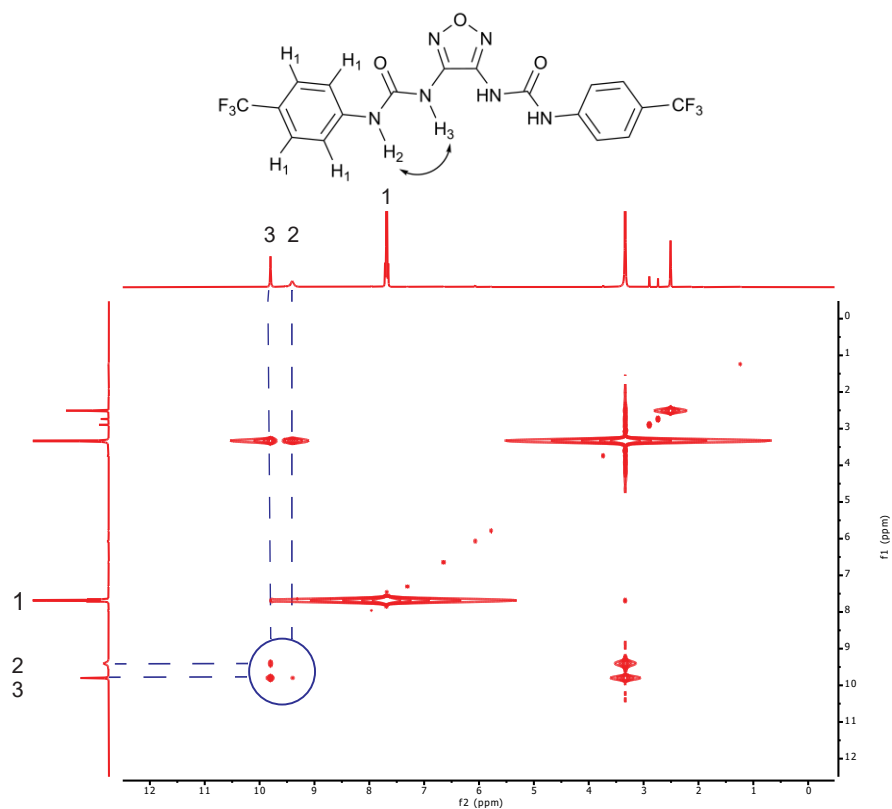


Figure S75. The 2D NOESY ^1H -NMR spectrum of **2** in d_6 -DMSO.

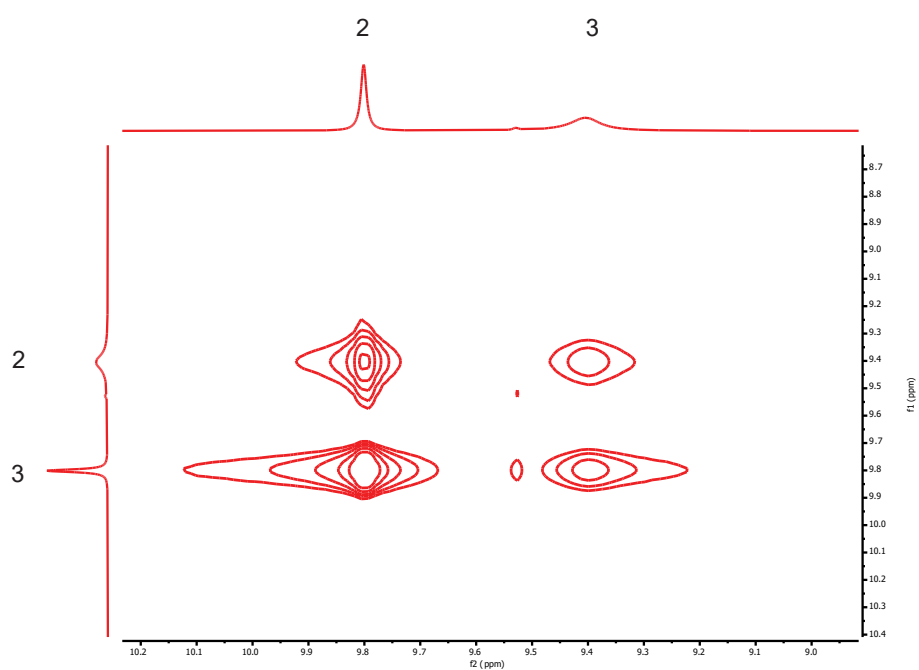


Figure S76. A magnified segment of the 2D NOESY ^1H -NMR spectrum of **2** in d_6 -DMSO, showing the cross-peak interactions between the signals of the two NH urea protons, H2 and H3 ($\delta = 9.80$ ppm and $\delta = 9.40$ ppm, respectively).

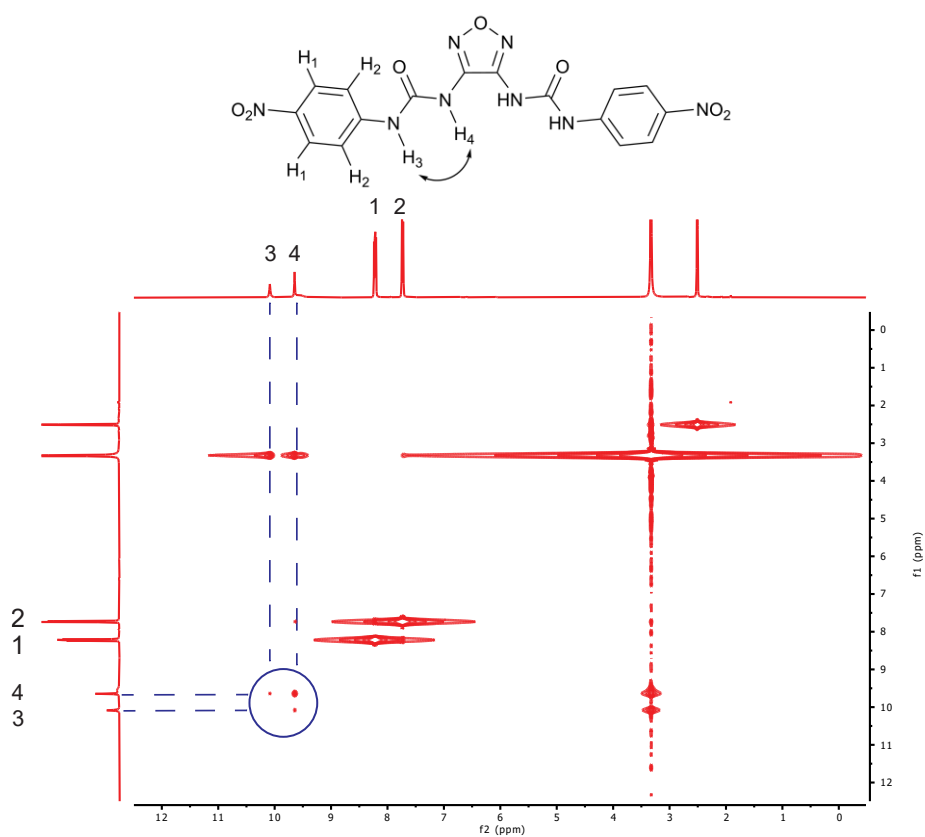


Figure S77. The 2D NOESY ^1H -NMR spectrum of **3** in d_6 -DMSO.

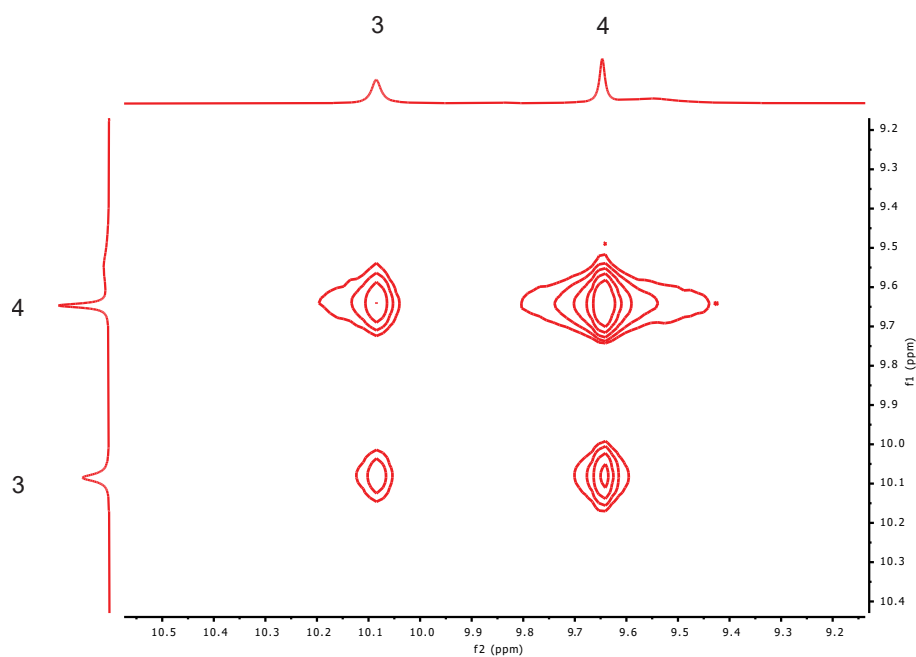


Figure S78. A magnified segment of the 2D NOESY ^1H -NMR spectrum of **3** in d_6 -DMSO, showing the cross-peak interactions between the signals of the two NH urea protons, H3 and H4 ($\delta = 10.08$ ppm and $\delta = 9.53$ ppm, respectively).

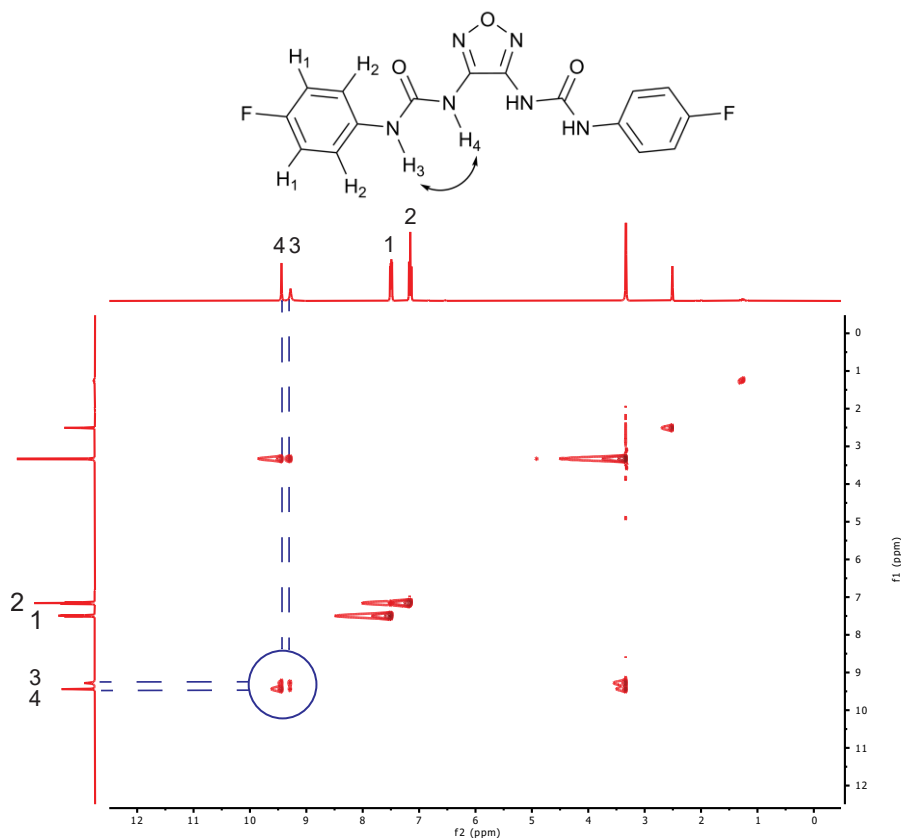


Figure S79. The 2D NOESY ¹H-NMR spectrum of **4** in *d*₆-DMSO.

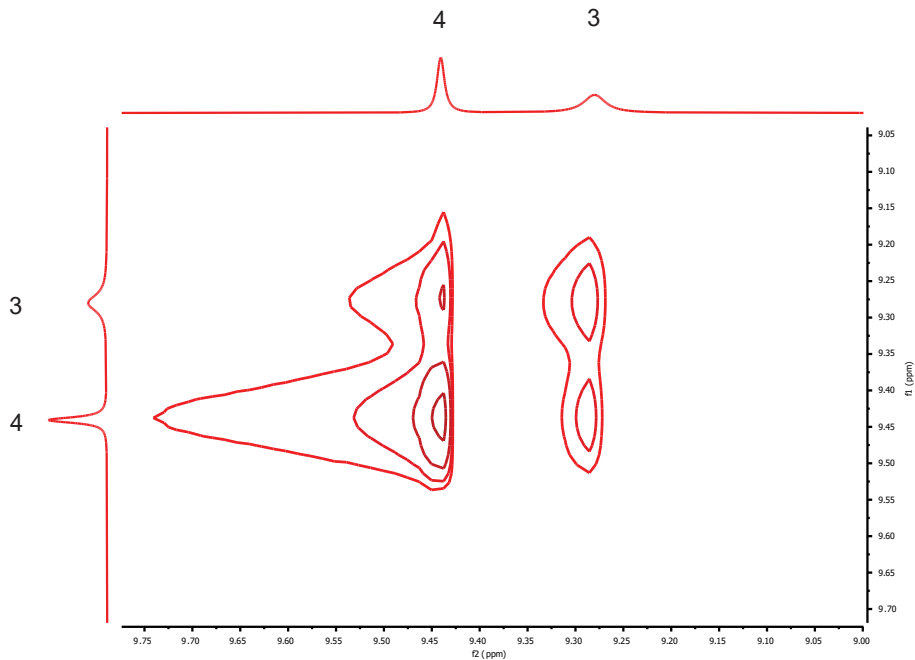


Figure S80. A magnified segment of the 2D NOESY ¹H-NMR spectrum of **4** in *d*₆-DMSO, showing the cross-peak interactions between the signals of the two NH urea protons, H₃ and H₄ ($\delta = 9.42$ ppm and $\delta = 9.30$ ppm, respectively).

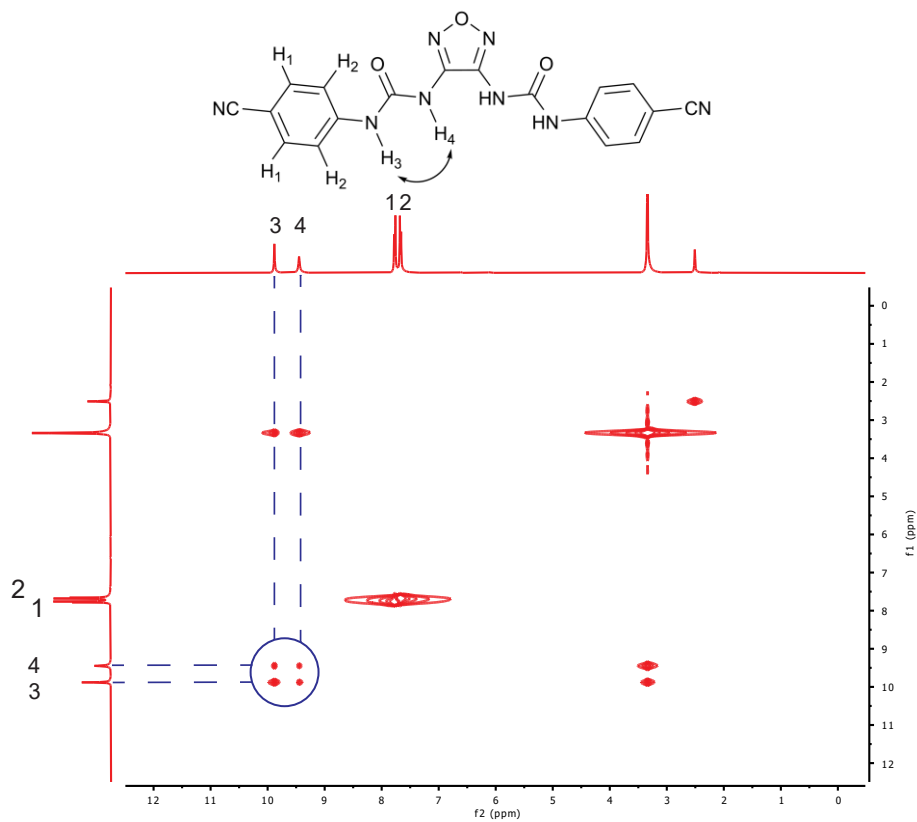


Figure S81. The 2D NOESY ^1H -NMR spectrum of **5** in d_6 -DMSO.

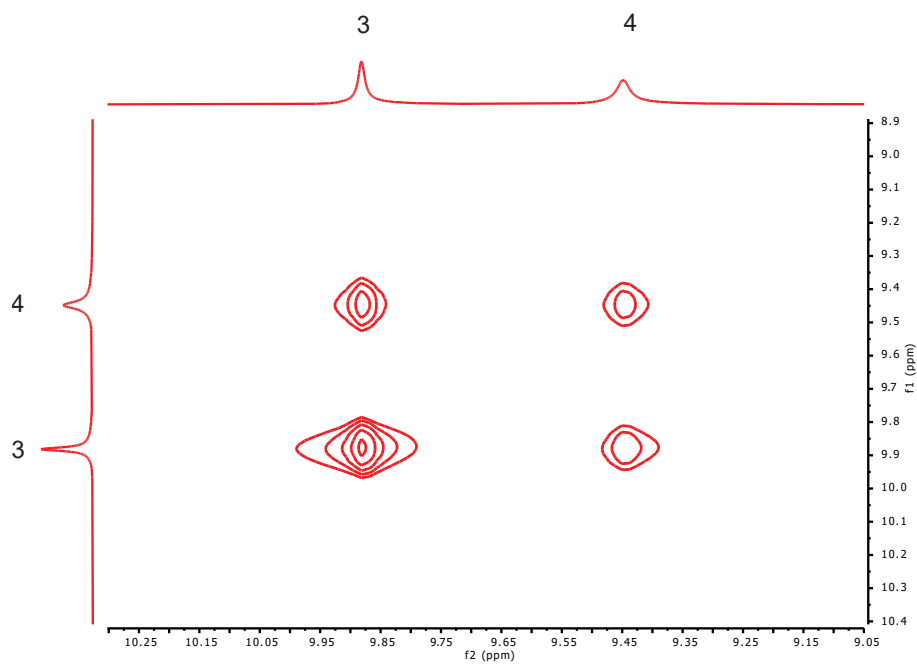


Figure S82. A magnified segment of the 2D NOESY ^1H -NMR spectrum of **5** in d_6 -DMSO, showing the cross-peak interactions between the signals of the two NH urea protons, H3 and H4 ($\delta = 9.87$ ppm and $\delta = 9.45$ ppm, respectively).

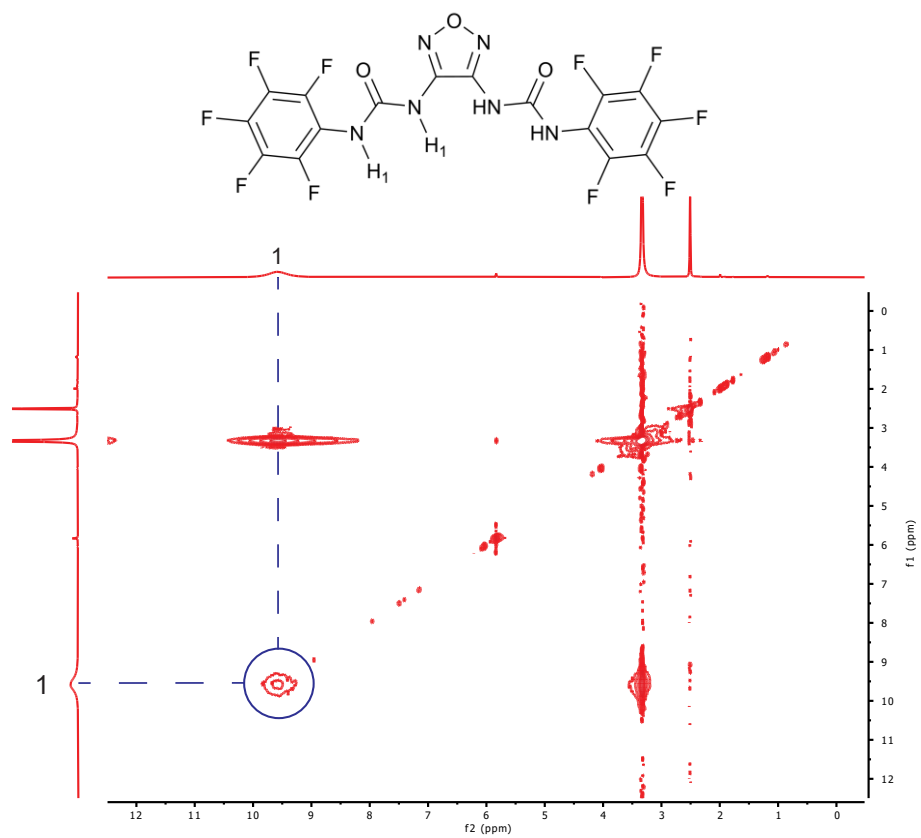


Figure S83. The 2D NOESY ¹H-NMR spectrum of **6** in *d*₆-DMSO.

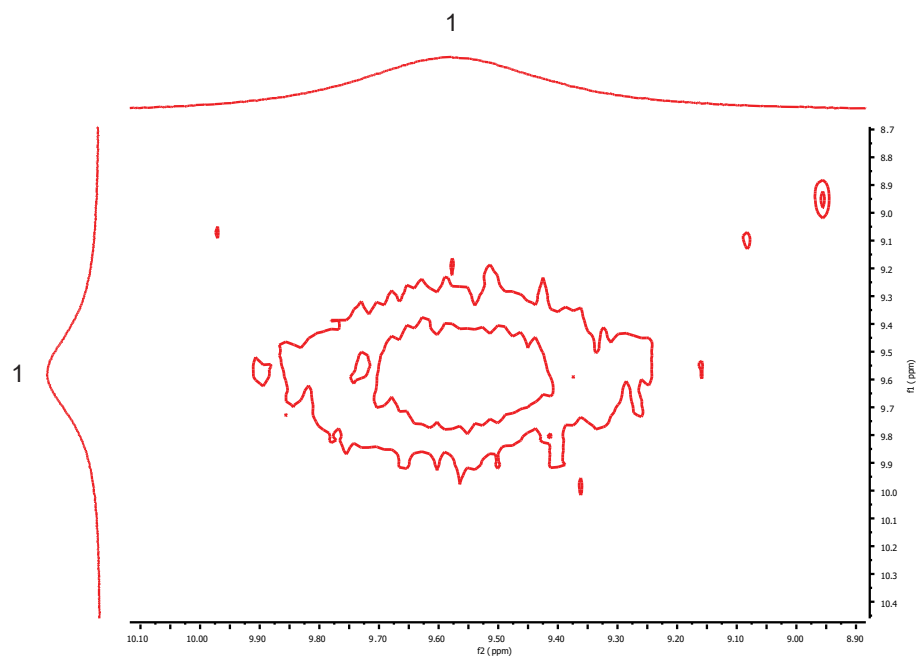


Figure S84. A magnified segment of the 2D NOESY ¹H-NMR spectrum of **6** in *d*₆-DMSO, showing the cross-peak interactions between the signals of the two NH urea protons, H₁ (δ = 9.54 ppm).

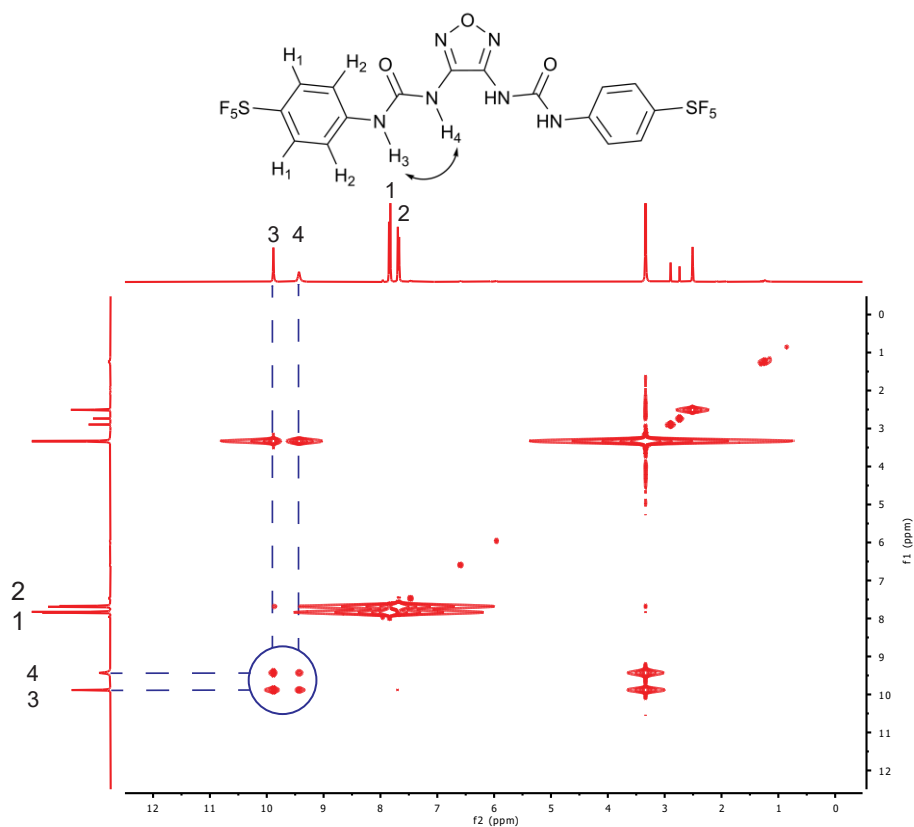


Figure S85. The 2D NOESY ^1H -NMR spectrum of **7** in d_6 -DMSO.

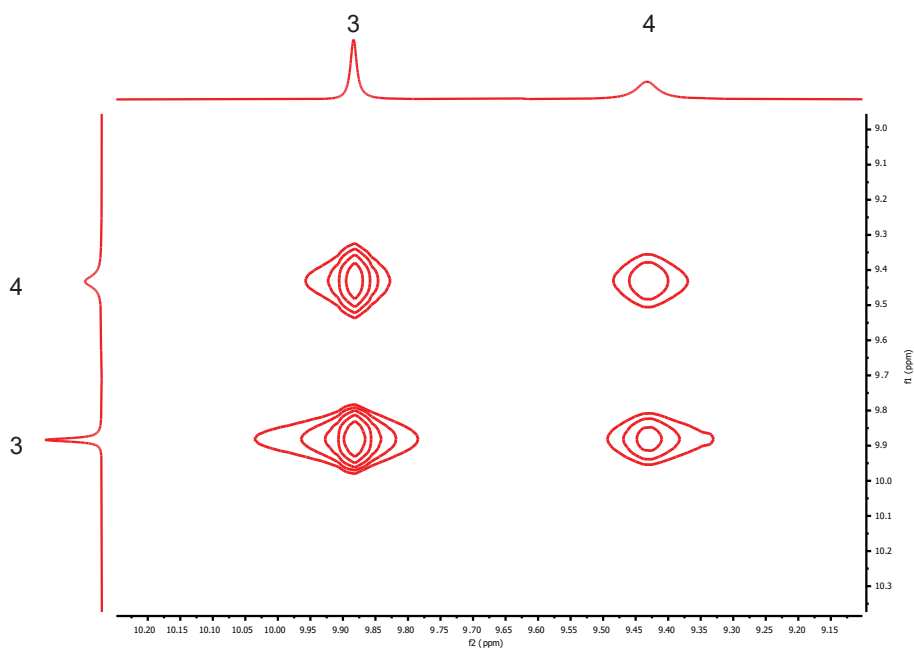


Figure S86. A magnified segment of the 2D NOESY ^1H -NMR spectrum of **7** in d_6 -DMSO, showing the cross-peak interactions between the signals of the two NH urea protons, H3 and H4 ($\delta = 9.87$ ppm and $\delta = 9.42$ ppm, respectively).

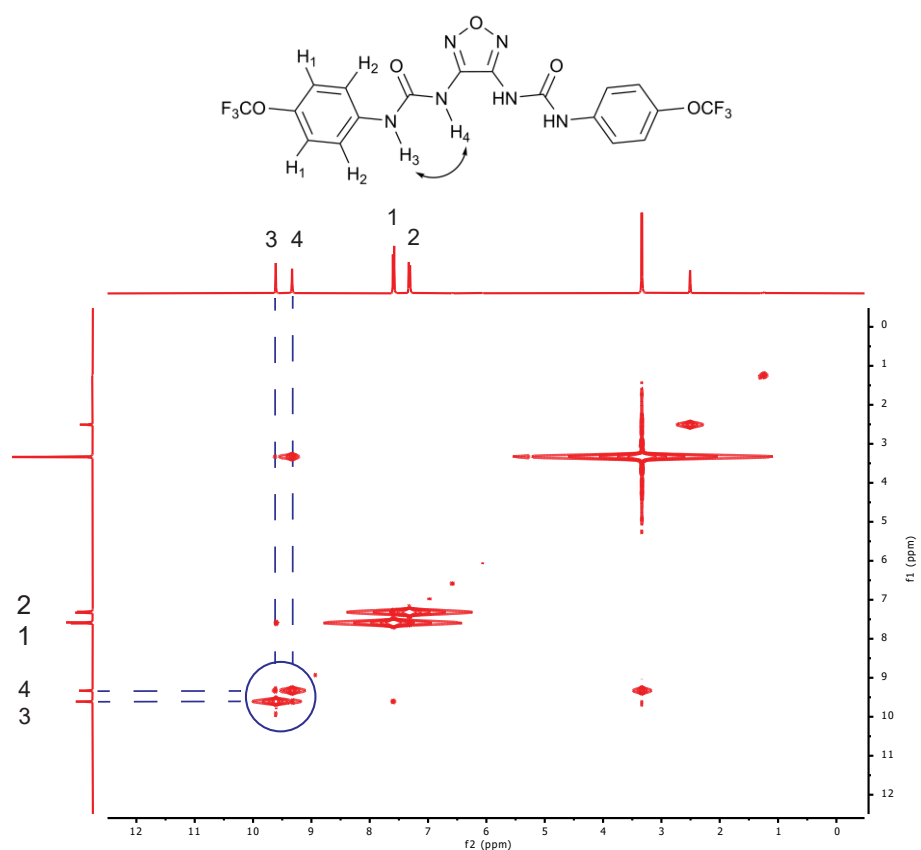


Figure S87. The 2D NOESY ¹H-NMR spectrum of **8** in *d*₆-DMSO.

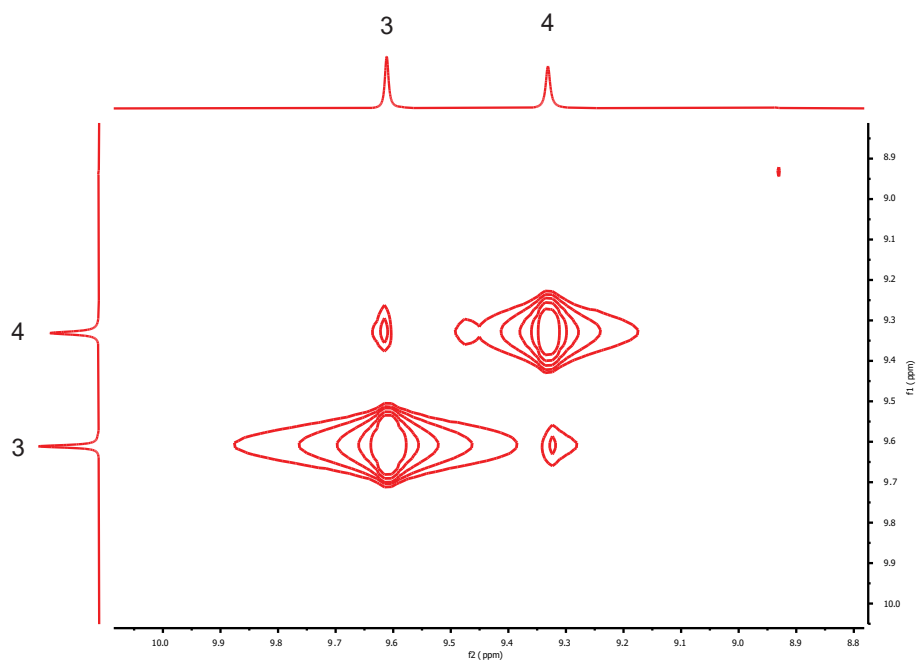


Figure S88. A magnified segment of the 2D NOESY ¹H-NMR spectrum of **8** in *d*₆-DMSO, showing the cross-peak interactions between the signals of the two NH urea protons, H₃ and H₄ ($\delta = 9.60$ ppm and $\delta = 9.32$ ppm, respectively).

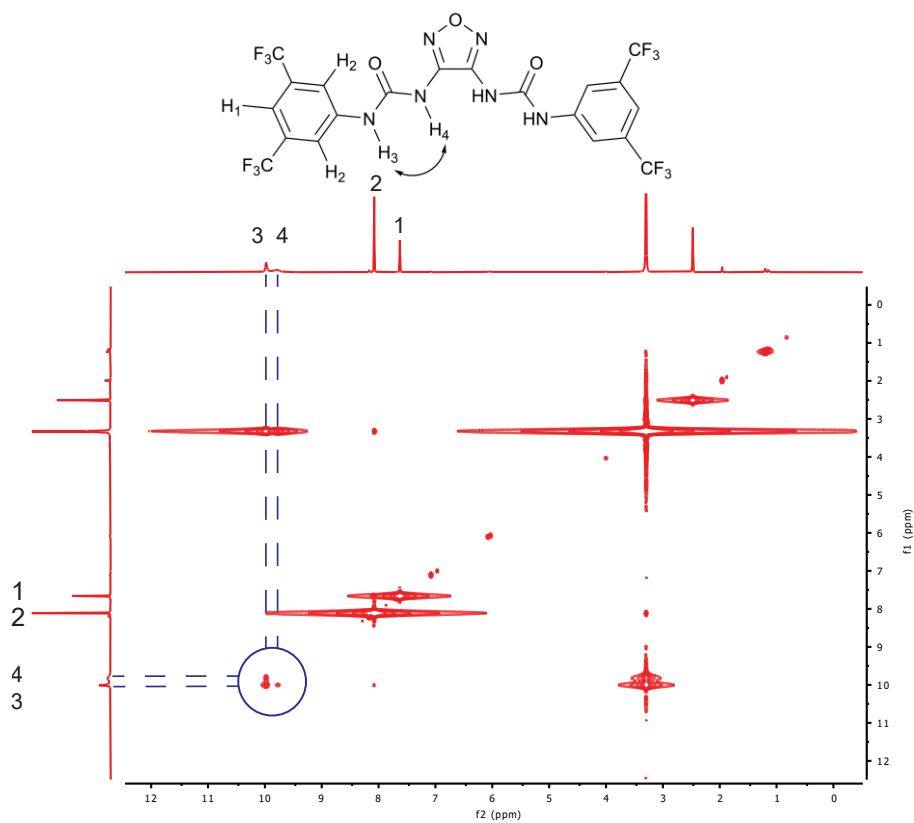


Figure S89. The 2D NOESY ^1H -NMR spectrum of **9** in d_6 -DMSO.

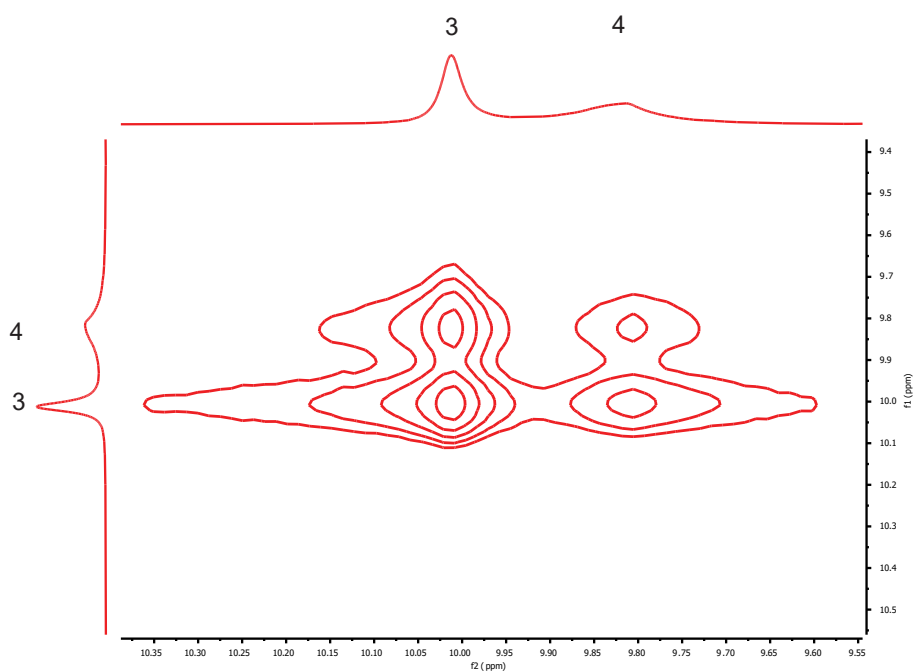


Figure S90. A magnified segment of the 2D NOESY ^1H -NMR spectrum of **9** in d_6 -DMSO, showing the cross-peak interactions between the signals of the two NH urea protons, H3 and H4 ($\delta = 10.00$ ppm and $\delta = 9.81$ ppm, respectively).

References

- [1] L. J. Bourhis, O. V. Dolomanov, R. J. Gildea, J. A. Howard, H. Puschmann, *Acta Crystallogr. Sect. A: Found. Adv.* 2015, **71**, 59-75.
- [2] O. V. Dolomanov, L. J. Bourhis, R. J. Gildea, J. A. Howard, H. Puschmann, *J. Appl. Crystallogr.* 2009, **42**, 339-341.
- [3] G. M. Sheldrick, *Acta Crystallogr. Sect. A: Found. Crystallogr.* 2008, **64**, 112-122.
- [4] L. A. Jowett and P. A. Gale, *Supramol. Chem.*, 2019, **31**, 297-312.